

POLITECNICO DI TORINO

Corso di Laurea Magistrale

in Ingegneria Biomedica

Tesi di Laurea Magistrale

Surface and tribological characterization of dental biomaterials in presence of artificial saliva



Relatore

prof. Silvia Maria Spriano

Candidato

Eva Ravinale

Anno Accademico 2019/2020



Acknowledgements – Ringraziamenti

Il mio primo e più importante ringraziamento è rivolto alla mia famiglia, in particolare ai miei genitori, per il loro sostegno morale ed economico.

Un ringraziamento speciale va al mio compagno di vita Matteo che non ha mai smesso di amarmi, supportarmi e credere in me.

Ringrazio sentitamente anche tutti gli amici che mi hanno accompagnata durante questo percorso, in particolare Angelica, Manu, Max, Fede, Vale, Silvia, Riki, Marta, Lube e Buri.

Infine vorrei ringraziare la mia relatrice, la professoressa Silvia Maria Spriano, Deepak, Angela e Fabio, senza l'aiuto dei quali questo lavoro di tesi non sarebbe stato possibile.



Abstract

Dental implants are used to replace teeth lost due to decay, trauma or periodontal diseases. The most common design for dental implants involves three different unit, a root (or implant) in direct contact with the bone, an abutment across the gingiva and a crown that bears the chewing loads and provides natural appearance to the implant.

Titanium and its alloys are widely used to manufacture implants and abutments due to their low density, excellent biocompatibility, mechanical properties and corrosion resistance. However, titanium abutments can change the appearance of soft tissues, thereby compromising aesthetics. To overcome this limitation, dental implants abutment are usually made of ceramic zirconia because of its white appearance, high strength and biocompatibility.

Although zirconia is 10 times harder than titanium, it causes significantly less damage to the titanium implant compared to the titanium abutments. In fact, the inert nature of zirconia results in low wear volume loss, which is important in minimizing metal ion liberation.

The release of metal ions or material particles, or both, into tissues that surround implanted dental devices can create post-implantation complications. These rare but disturbing events are mainly caused by the mechanical movements of the components of the implant against each other, coupled with the influences of local biochemical and electrochemical factors. Mechanical movement of the components of implants against each other results in friction and wear, the study of which is called tribology. The tribology of an implanted device depends on the patient's activity and is affected by variables such as load, frequency and the surface properties of the components of the implant that are in contact. Local biochemical and electrochemical factors include the ambient pH, and concentrations of protein and oxygen. The effect on local tissues and extracellular fluid can produce biochemical or electrochemical responses to the implant material in the surrounding solution, which is termed corrosion. The combined effect of these mechanical, biochemical, and electrochemical factors is known as tribocorrosion.



The aim of this study was to evaluate the possible different tribological behavior of titanium against zirconia in the presence of two artificial saliva, namely Biotène and BioXtra.

In order to simulate the dental implant-abutment contact, a sphere-plane system was used, where the sphere simulates the abutment and the plane simulates the implant. Disks made of commercially pure titanium (Gr2) and Ti6Al4V alloy (Gr5) were tested against zirconia balls using a tribometer (High Frequency Reciprocating Rig TR-282, Ducom) which imposed a reciprocal movement with a stroke length of 2 mm. The tests were conducted under a normal load of 2 N, a frequency of 30 Hz, a temperature of 37°C and a duration of 60 minutes. The volume of lubricant was 2 ml. At the end of each test, the extent of wear on the disks and balls was evaluated by means of an optical microscope.

Subsequently the surface electric charge of the disks was evaluated by measuring the zeta potential (ζ), after adsorption of artificial saliva on them. Finally, contact angle measurements were performed on the surface of the same samples used to measure the zeta potential to assess their wettability.

The results show that, compared to BioXtra, the Biotène reduces the friction coefficient and therefore the wear between the tested materials (in particular the lower values are reached with the Ti6Al4V alloy) and it allows the formation of a stable adsorbed layer with a highly hydrophilic behavior acting as a good lubricant.

The best performances of the Biotène could be due to the presence in it of some surfactants and polymers that act as organic corrosion inhibitors; moreover, even the absence of fluorides in this saliva could positively influence the corrosion resistance of titanium and its alloys.



Table of contents

Acknowledgements – Ringraziamenti.....	2
Abstract.....	3
Table of contents.....	5
1. Theory references.....	8
1.1 Tribology.....	8
1.1.1 Definition and history of tribology.....	8
1.1.2 Industrial significance of tribology.....	10
1.1.3 Friction.....	12
1.1.3.1 The coefficient of friction.....	13
1.1.4 Lubrication.....	14
1.1.4.1 Lubrication regimes.....	15
1.1.5 Wear.....	17
1.1.5.1 Wear rate.....	19
1.2 Biotribology.....	21
1.2.1 Oral tribology.....	21
1.2.2 Composition and wear of human teeth.....	22
1.2.3 Composition and properties of human saliva.....	24
1.3 Dental implantology.....	27
1.3.1 Overview on dental implants.....	27
1.3.2 Historic background.....	28
1.3.3 Classification of implants.....	30
1.3.4 Implant components.....	34
1.3.5 Criteria to select the proper dental implant.....	35
1.3.6 Biomechanics of dental implants.....	36



1.4	Titanium-zirconia hybrid implants.....	40
1.4.1	Overview on dental implant materials.....	40
1.4.2	Titanium and its alloys.....	41
1.4.3	Zirconia.....	44
1.4.4	Zirconia as dental abutment.....	47
1.4.4.1	Structural design.....	48
1.4.4.2	Manufacturing processes.....	51
1.5	Tribocorrosion in oral environment.....	54
1.5.1	Presence of oral biofilms.....	56
1.5.2	Corrosion of titanium.....	59
1.5.3	Wear processes on dental materials.....	60
1.5.4	Simultaneous degradation of titanium by corrosion and wear interactions.....	61
1.5.5	Interaction of wear debris with surrounding tissues.....	63
1.6	Surface characterization.....	65
1.6.1	Zeta potential.....	65
1.6.2	Wettability.....	76
2.	Materials and methods.....	81
2.1	Tribological tests.....	81
2.1.1	Disk materials.....	81
2.1.2	Ball material.....	82
2.1.3	Composition of artificial saliva.....	83
2.1.4	Sample preparation.....	99
2.1.5	Instrumentation.....	101
2.1.6	Experimental test procedure.....	108
2.2	Zeta potential tests.....	111



2.2.1	Disk materials.....	111
2.2.2	Composition of artificial saliva.....	111
2.2.3	Sample preparation.....	111
2.2.4	Instrumentation.....	114
2.2.5	Experimental test procedure.....	117
2.3	Wettability tests.....	120
3.	Results and discussion.....	122
3.1	Tribological tests.....	122
3.1.1	Friction.....	122
3.1.2	Wear.....	125
3.2	Surface characterization tests.....	134
3.2.1	Zeta potential.....	134
3.2.2	Wettability.....	138
4.	Conclusions.....	140
	Appendix.....	142
	References.....	144

1. Theory references

1.1 Tribology

Tribology is the science and technology of interacting surfaces in relative motion and covers the three subjects of friction, wear and lubrication [36].

1.1.1 Definition and history of tribology

The word tribology was first reported in a landmark report by Jost (1966) [21]. The word is derived from the Greek word “tribos” meaning rubbing, so the literal translation would be “the science of rubbing”. Its popular English language equivalent is friction and wear or lubrication science, alternatively used. The latter term is hardly all-inclusive. Dictionaries define tribology as the science and technology of interacting surfaces in relative motion and of related subjects and practices. Tribology is the art of applying operational analysis to problems of great economic significance, namely, reliability, maintenance and wear of technical equipment, ranging from spacecraft to household appliances. Surface interactions in a tribological interface are highly complex and their understanding requires knowledge of various disciplines, including physics, chemistry, applied mathematics, solid mechanics, fluid mechanics, thermodynamics, heat transfer, materials science, rheology, lubrication, machine design, performance and reliability [4].

Despite the relatively recent naming of the field of tribology, quantitative studies of friction can be traced as far back as 1493, when Leonardo da Vinci first noted the two fundamental ‘laws’ of friction. According to da Vinci, frictional resistance was the same for two different objects of the same weight but making contact over different widths and lengths. He also observed that the force needed to overcome friction doubles as weight doubles [22]. His work had no historical influence, however, because his notebooks (figure 1.1) remained unpublished for hundreds of years [4].

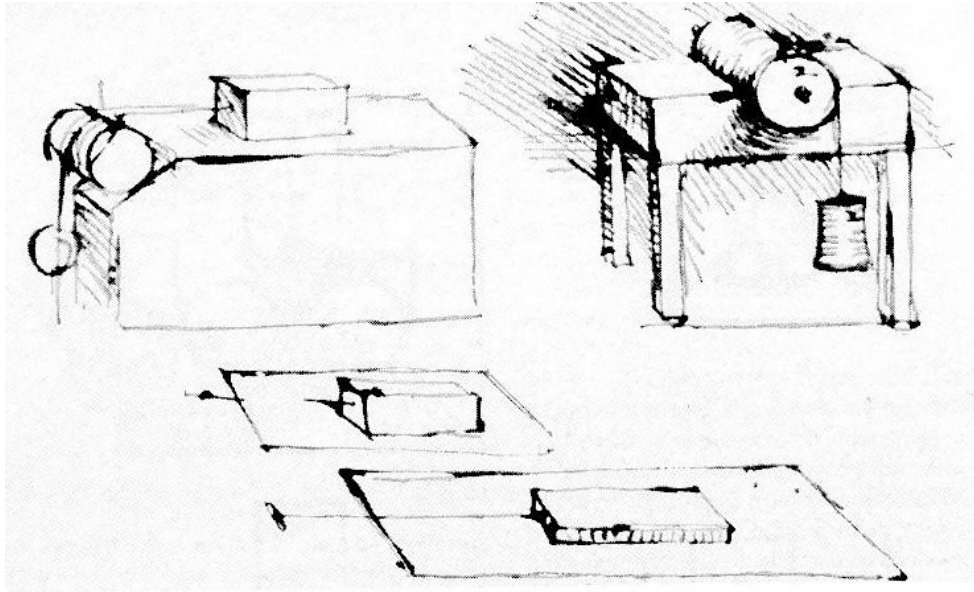


Figure 1.1: Tribological experiments suggested by Leonardo da Vinci [23].

The two fundamental ‘laws’ of friction were first published (in 1699) by Guillaume Amontons [24], with whose name they are now usually associated, they state that:

1. the force of friction acting between two sliding surfaces is proportional to the load pressing the surfaces together;
2. the force of friction is independent of the apparent area of contact between the two surfaces.

Although not universally applicable, these simple statements hold for a surprisingly wide range of systems [25]. These laws were further developed by Charles-Augustin de Coulomb (in 1785) [26], who noticed that static friction force may depend on the contact time and sliding (kinetic) friction may depend on sliding velocity, normal force and contact area [27][28].

In 1798, Charles Hatchett and Henry Cavendish carried out the first reliable test on frictional wear. In a study commissioned by the Privy Council of the UK, they used a simple reciprocating machine to evaluate the wear rate of gold coins. They found that coins with grit between them wore at a faster rate compared to self-mated coins [29]. In 1860, Theodor Reye proposed Reye's hypothesis [30]. In 1953, John Frederick Archard



developed the Archard equation which describes sliding wear and is based on the theory of asperity contact [31].

Other pioneers of tribology research are Australian physicist Frank Philip Bowden [32] and British physicist David Tabor [33], both of Cavendish Laboratory. Together they wrote the seminal textbook “The Friction and Lubrication of Solids” [34] (Part I originally published in 1950 and Part II in 1964). Michael J. Neale was another leader in the field during the mid-to-late 1900's. He specialized in solving problems in machine design by applying his knowledge of tribology. Neale was respected as an educator with a gift for integrating theoretical work with his own practical experience to produce easy-to-understand design guides. The “Tribology Handbook” [35], which he first edited in 1973 and updated in 1995, is still used around the world and forms the basis of numerous training courses for engineering designers.

Duncan Dowson surveyed the history of tribology in his 1997 book “History of Tribology” (2nd edition) [27]. This covers developments from prehistory, through early civilizations (Mesopotamia, ancient Egypt) and highlights the key developments up to the end of the twentieth century [23].

1.1.2 Industrial significance of tribology

Tribology is crucial to modern machinery which uses sliding and rolling surfaces. Examples of productive friction are brakes, clutches, driving wheels on trains and automobiles, bolts and nuts. Examples of productive wear are writing with a pencil, machining, polishing and shaving. Examples of unproductive friction and wear are internal combustion and aircraft engines, gears, cams, bearings and seals [4].

According to some estimates, losses resulting from ignorance of tribology amount in the United States to about 4% of its gross national product (or about 200 billion dollars per year in 1996) and approximately one-third of the world's energy resources in present use appear as friction in one form or another. Thus, the importance of friction reduction and wear control cannot be overemphasized for economic reasons and long-term reliability. According to Jost [21], savings of about 1% of gross national product of an



industrial nation can be realized by better tribological practices. According to recent studies, expected savings are expected to be of the order of 50 times the research costs. The savings are both substantial and significant, and these savings can be obtained without the deployment of large capital investment [4].

The purpose of research in tribology is understandably the minimization and elimination of losses resulting from friction and wear at all levels of technology where the rubbing of surfaces is involved. Research in tribology leads to greater plant efficiency, better performance, fewer breakdowns and significant savings [4].

Tribology is not only important to heavy industry, it also affects our day-to-day life. For example, writing is a tribological process. Writing is accomplished by the controlled transfer of lead (pencil) or ink (pen) to the paper. During writing with a pencil there should be good adhesion between the lead and the paper so that a small quantity of lead transfers to the paper and the lead should have adequate toughness/hardness so that it does not fracture/break. The objective when shaving is to remove hair from the body as efficiently as possible with minimum discomfort to the skin. Shaving cream is used as a lubricant to minimize friction between the razor and the skin. Friction is helpful during walking and driving. Without adequate friction, we would slip and a car would skid. Tribology is also important in sports. For example, a low friction between the skis and the ice is desirable during skiing. Fabric fibers should have low friction when touching human skin [4].

Body joints need to be lubricated for low friction and low wear to avoid osteoarthritis and joint replacement. The surface layer of cartilage present in the joint provides the bearing surface and is lubricated with a joint fluid consisting of lubricin, hyaluronic acid (HA) and lipid. Hair conditioner coats hair in order to repair hair damage and lubricate it. It contains silicone and fatty alcohols. Low friction and adhesion provide a smooth feel in wet and dry environments, reduce friction between hair fibers during shaking and bouncing, and provide easy combing and styling. Skin creams and lotions are used to reduce friction between the fingers and body skin. Saliva and other mucous biofluids lubricate and facilitate the transport of food and soft liquids through the body. The saliva in the mouth interacts with food and influences the taste-mouth feel [4].

1.1.3 Friction

Friction is the force resisting the relative motion between two surfaces in contact. It is commonly divided into dry friction and viscous friction. It may be static, that is the solid bodies have no relative motion, or dynamic, when the solid bodies are moving relative to each other. Dry friction occurs between two dry solid bodies. Viscous friction occurs when the two solid bodies are more or less separated by a fluid, for example a lubricant [36].

1.1.3.1 The coefficient of friction

The coefficient of friction μ is defined as the ratio of the friction force F and the normal force N between the bodies, as shown in Figure 1.2 and expressed by

$$\mu = \frac{F}{N} \quad (1.1)$$

where the normal force is actually the sum of the load of the mass mg and any externally applied load, F_{load} :

$$N = mg + F_{load} \quad (1.2)$$

The normal force always acts perpendicular to the contact area. When sliding the mass, the friction force is the force required to maintain the sliding and it always acts tangential (i.e. parallel) to the contact area.

In tribological contacts external load is often applied to magnitudes making the mass weight negligible, that is $mg \ll F_{load}$, which implies

$$\mu = \frac{F}{F_{load}} \quad (1.3)$$

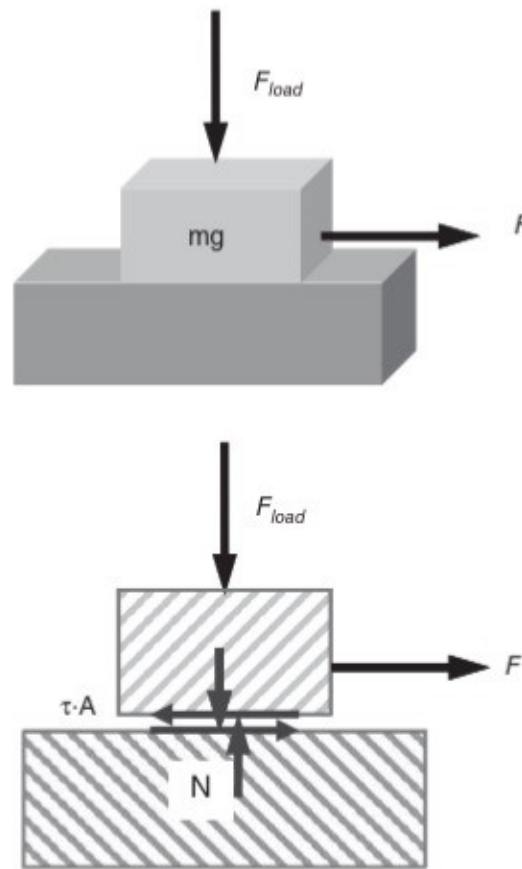


Figure 1.2: Friction visualized as pulling a small box across a flat surface. The set-up (top) and a cross-section view (bottom). The forces at the interface also are shown [36].

The coefficient of friction is obtained from known or measured forces. Both F and F_{load} can be measured with use of, for example, a load cell and may thus be logged as a function of time.

For a contact where the surfaces are fully separated by a lubricant the friction force is commonly expressed by

$$F = \tau A$$

(1.4)

where τ is the shear stress in the lubricant and A is the contact area. The shear stress is determined by the lubricant properties, the velocity of the motion and the distance between the bodies [36]. The forces in the lubricated contact act on both the solid bodies and the fluid, as shown in Figure 1.3.

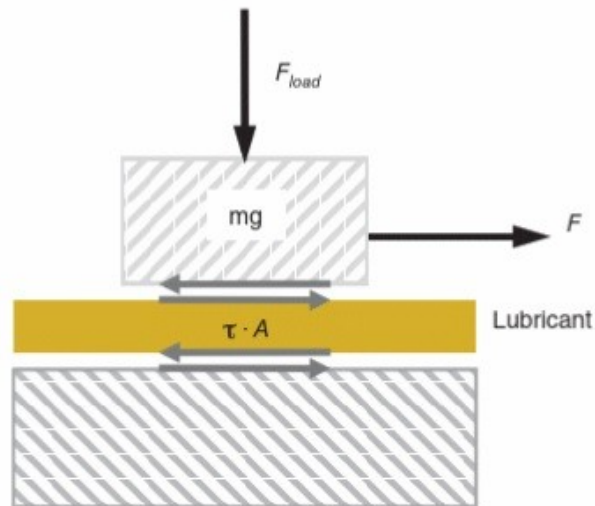


Figure 1.3: Illustration of shear forces between solid bodies and fluid in a lubricated contact [36].

1.1.4 Lubrication

Lubricants can serve several functions in tribological contacts. The overall purpose of it is to control friction and wear. However, the diversity of the lubricant function comprises the following:

- separate moving parts;
- transfer heat;
- transfer power;
- reduce friction;
- protect against wear;
- prevent corrosion;
- carry away contaminants and debris;
- seal for gases;
- reduce noise and vibration.

Lubricants can be solids, liquids (or dispersions of these) and gases.

1.1.4.1 Lubrication regimes

A general description of the friction behavior in a lubricated contact can be seen in Figure 1.4, where the dependence of the coefficient of friction μ versus the film parameter Λ is shown. The film parameter Λ is calculated as

$$\Lambda = \frac{h}{\sqrt{R_{qA}^2 + R_{qB}^2}}$$

(1.5)

where h is the lubricant film thickness and R_{qA} and R_{qB} represent the surface roughness of the two surfaces A and B in contact [36].

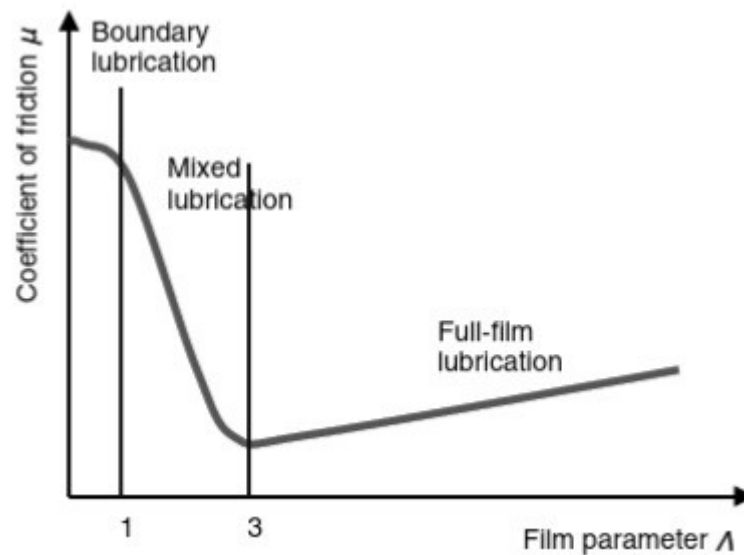


Figure 1.4: Coefficient of friction μ versus film parameter Λ in lubricated sliding contacts [36].

The contact is classified as boundary, mixed or full film lubricated depending on the degree of mechanical contact between the solid surfaces. The curve in Figure 1.4 originates from the Stribeck curve.

Boundary lubrication implies heavy contacting between the asperities with a Λ -value below 1. The load is carried by the solid surfaces in contact (see Figure 1.5). The lubricant is mainly acting as a carrier of additives. The presence of additives is necessary to ensure the performance and build-up of a boundary film. This regime is characterized by high load and low speed.

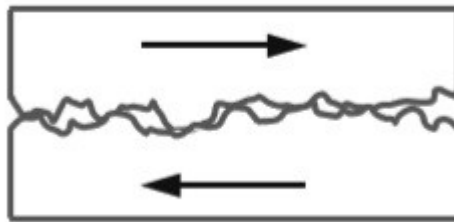


Figure 1.5: Boundary lubrication, where there are always some asperities in contact [36].

In mixed film lubrication the surfaces are less separated than in the full film regime. The surfaces are close enough for asperity contact to occur occasionally. The mixed film lubrication regime is a combination of full film lubrication and boundary lubrication with Λ -values between 1 and 3. Thus, the load is carried partly by a pressure in the fluid film and partly by the asperities in contact, as shown in Figure 1.6. The lubricant will support the contact with necessary additives to reduce wear.

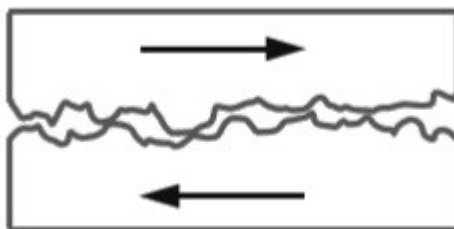


Figure 1.6: Mixed lubrication, where the surface roughness is in the same order of magnitude as the film thickness [36].

In full film lubrication the solid bodies are lubricated by a thick enough lubricant film to ensure full separation of the surfaces (see Figure 1.7). In this regime the coefficient of friction is very low. A Λ -value higher than 3 indicates full film lubrication.

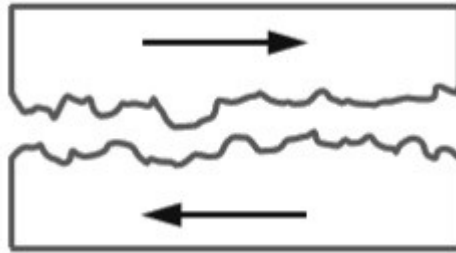


Figure 1.7: Full film lubrication, where the surface roughness is much smaller than the film thickness [36].

The lubricant film thickness h (see Equation (1.5)) is determined by the lubricant properties, the operating conditions, the contact geometry and the solid surface's material properties. In practice, typical lubricant film thicknesses are about 1– 100 μm [36].

1.1.5 Wear

Wear is loss of material from a solid surface. Wear can appear in many ways depending on the material of the interacting contact surfaces, the environment and the operating conditions. At least five principal wear processes can be distinguished: abrasive wear, adhesive wear, surface fatigue and fretting and erosive wear (Figure 1.8). These are briefly described below.

Adhesive wear occurs under sliding conditions where asperities are plastically deformed and welded together by high local pressure and temperature. When the sliding continues, the asperity bonds are broken and the result is removal of material or transfer of material from one surface to the other. Extensive adhesive wear is commonly described as scoring, galling or seizure.

Abrasive wear may occur when a rough hard surface mates a softer material where the asperities of the hard material scratch the softer surface. This process is called two-body abrasive wear. If hard loose wear particles are present between the mating surfaces one

or both surfaces can be worn by scratching. This situation is called three-body abrasive wear.

Surface fatigue occurs when cyclic loading weakens the material and can be the predominant wear mechanism in rolling contacts involving some sliding. This may result in subsurface cracks that may propagate and lead to material losses. Surface fatigue is sometimes also called pitting when small pieces of material break away from the surface, forming pits.

Fretting wear, or fretting, occurs when there is a very small oscillatory relative motion between two surfaces in contact. Often the intention is that the surfaces should be fixed, but due to, for example, vibrations some motion still occurs. The term fretting is often used to denote damage mechanisms such as fretting fatigue, fretting wear and fretting corrosion.

Erosive wear occurs in situations where hard particles impact a solid surface and remove material.

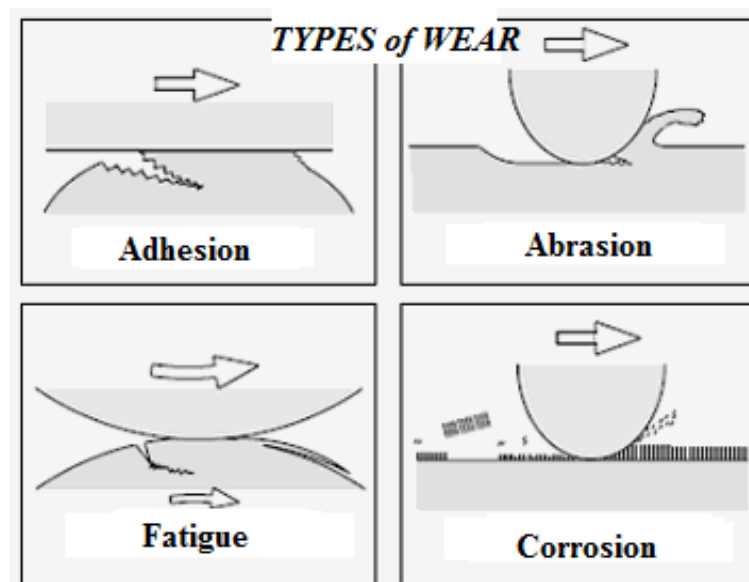


Figure 1.8: Types of wear [62].

Often more than one wear mechanism is active at the same time. For example, small, abrasive particles may be generated due to adhesive wear or surface fatigue, which may

also lead to abrasive wear. In addition, tribochemical wear can occur, which involves chemical reactions between the solid surfaces and surrounding lubricant or environment. The chemical reactions, such as corrosion, can weaken the surface layer, which will enhance the effect of other wear mechanisms.

1.1.5.1 Wear rate

Wear is often classified as mild or severe from an engineering point of view. Mild wear often results in a surface that is smoother than the original surface. On the other hand, severe wear often results in a surface that is rougher than the original surface. Wear is an ongoing process between two mating contacts that has to be controlled. Typical wear behavior is shown in Figure 1.9. Starting with newly manufactured surfaces, the process starts with a running-in period, followed by, if correctly designed, a mild wear period. The life of the components ends if the wear rate significantly increases and causes failure.

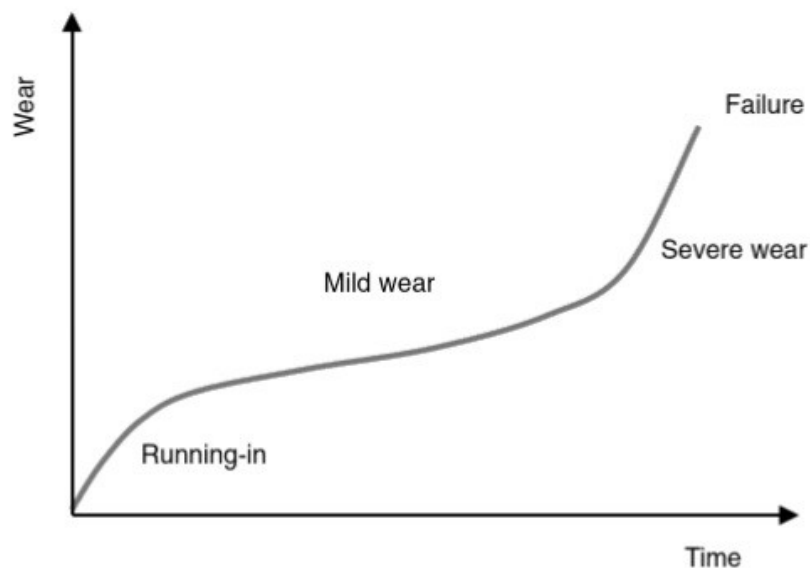


Figure 1.9: The wear process depends on time with periods of running-in, mild wear, severe wear and failure [36].



A severe wear situation is not acceptable in most cases. Mild wear is what the engineers strive for. It can be obtained by proper shape and surface roughness of the contact surfaces together with proper materials. However, often lubrication of the surfaces is necessary to secure mild wear. Wear can be expressed as wear volume or wear rate. The wear rate is commonly expressed by Archard's wear model

$$\frac{V}{s} = k_w N \tag{1.6}$$

where V is the volume removed from the surface, s is the sliding distance, k_w is the specific wear number and N is the normal load. The result is a ratio often called the wear rate, given as a number in units of mm^3/m [36].

1.2 Biotribology

The word “biotribology” was firstly used and defined by Dowson in 1970 as “those aspects of tribology concerned with biological systems” [37]. However, many investigations and practices were reported on friction, wear and lubrication of bio-systems long before the concept of biotribology was introduced [5].

The term biotribology is widely used to refer to tribological phenomena occurring in either the human body or in animals, and possibly plants. There are two distinct themes in biotribology:

- tribological processes naturally occurring in or on the tissues and organs of living organisms, and
- tribological processes that may occur after implantation of an artificial device in the living human body.

An example of the former is the wear of skin and its replenishment by new skin cells or the lubricated sliding of eyelids over the eye. An example of the latter is the wear of orthopedic implants (e.g., artificial hips and knees), which releases alien debris into the body [6].

1.2.1 Oral tribology

Oral tribology concerns all aspects of tribology related to oral systems. Human oral cavity is composed of palate, chin, teeth, tongue, mucosa and glands. The temporomandibular joint (TMJ) connects palate to chin. Friction and wear in the mouth is normally related to the processing of various foods, oral hygiene and orthodontics and thus is unavoidable. Generally, oral tribology involves the studies on teeth, saliva, TMJ and soft tissues of oral cavity [5].

Tooth wear can be a clinical problem that is increasingly important in ageing population. It is estimated that around 7% of the population shows pathological wear requiring treatment [38].



There are four main categories of wear that contribute to the destruction of natural teeth [38]. Physiologic wear is related to the vital functions of human mouth, i.e. mastication. It results in the slow reduction of the convexity of tooth cusps. Pathological wear, caused by diseases and abnormal conditions, can cause excessive deterioration of teeth and restorations. Prophylactic wear is caused for preventive purposes, mainly tooth-brushing. Finishing procedure wear results from cutting, polishing and finishing of both teeth and restorations.

1.2.2 Composition and wear of human teeth

Human teeth (Figure 1.10) are composed of enamel, dentine-enamel junction, dentine and pulp. Enamel composed of 92-96% inorganic substances, 1-2% organic materials and 3-4% water by weight, is the hardest tissue in human body, with a hardness of about 360 HV50g in human body. It is made of tightly-packed, fiber-like hydroxyapatite, built up in rods or prisms. Dentine (about 60 HV50g) is a hydrated biological composite composed of 70% inorganic material, 18% organic matrix and 12% water by weight, which is considered to be elastic and soft. Between the enamel and dentine is dentine-enamel junction, a biological interface. Generally the enamel is exposed at the occlusal surface to the oral chemical environment [5].

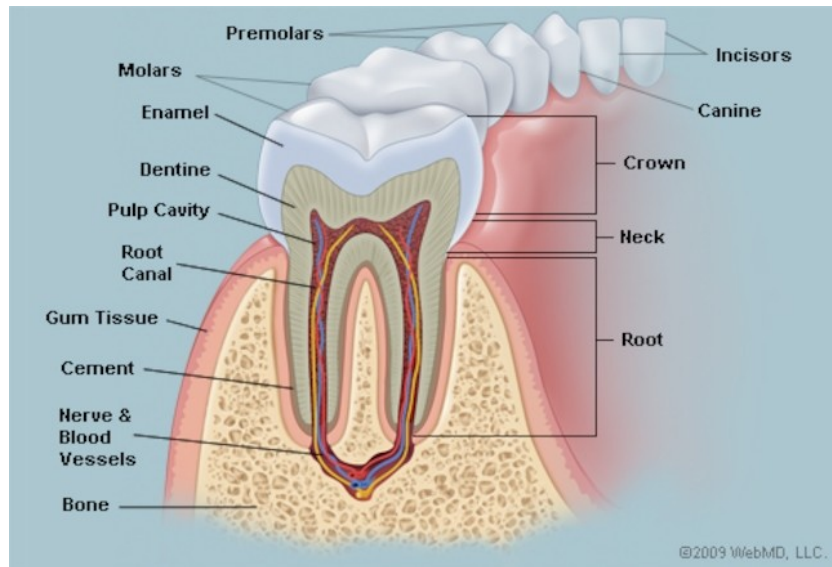


Figure 1.10: Picture of human tooth [63].

Wear of teeth, either natural or artificial, mainly results from mastication. Mastication is the action of chewing food, which involves open phase and closed phase. No occlusal forces are involved in open phase, and then no or very minor tooth wear occurs, while during closed phase occlusal load is applied to the foods and the hard particles in foods are dragged across opposing surfaces, causing occlusal surface wear [5]. During mastication, tooth wear generally occurs with the lubrication of saliva or food slurry [38].

Thegosis and bruxism also can cause tooth wear. Thegosis is the action of sliding teeth into lateral positions, which is considered a genetically determined habit to sharpen teeth. Bruxism, a response to stress and treated clinically as pathologic behavior, is the action of grinding teeth without the presence of food. During thegosis and bruxism, occlusal forces are applied, and then tooth friction and wear occur in direct tooth-tooth contact.

Furthermore, nowadays, chemical effects play an increasingly important role in tooth wear, mainly as a result of large consumption of acid drinks [5]. Eroded enamel is more susceptible to abrasion than the native enamel, because of the decreased hardness and elastic modulus caused by the acidic environment [38].

Additionally, tooth wear can also result from tooth cleaning such as tooth-brushing, and habits such as pipe smoking and pencil chewing. The relationship of movement and tooth wear is shown in Figure 1.11.

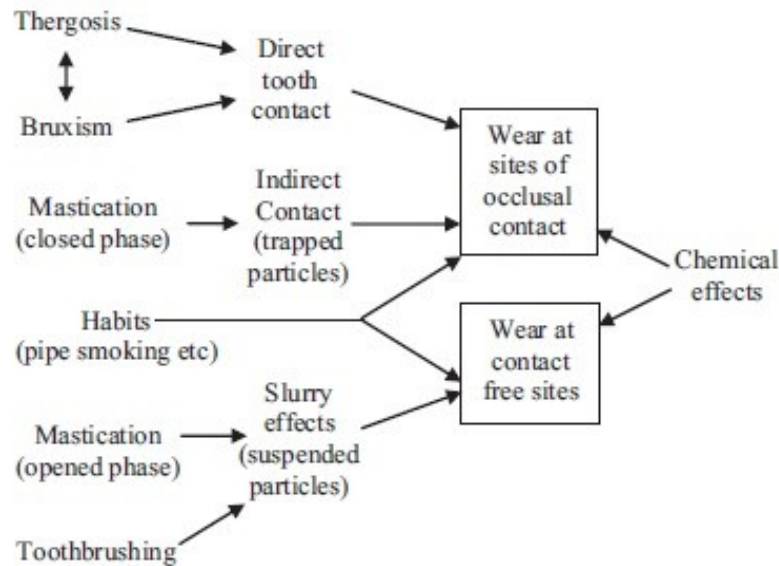


Figure 1.11: Relation between movement and wear of teeth [5].

Limited tooth wear has no clinical or aesthetical relevance, whereas excessive wear can lead to a damage to the occluding surfaces, alteration of mastication, hypersensitivity and pulpal pathologies [5].

1.2.3 Composition and properties of human saliva

Human saliva consists of a mixture of fluids produced from parotid, submaxillary, and submandibular glands as well as by oral mucosal glands (labial, lingual, palatal, and vestibular glands) at a pH between 6 and 7. The composition of saliva, which includes organic, inorganic compounds and 99% water, is also dependent on external factors that can be present in the oral cavity. Surfaces inside oral cavities are regularly reached by saliva at a pH altered, between 3 and 8, by external factors such as dietary, presence of acidic substances, and microbial metabolites. Additionally, the composition and

properties of saliva can be modified by internal factors associated to salivary gland dysfunctions or to the time of the day.

The role of saliva has been considered in the maintenance of the oral health of the human body due to the presence of numerous organic and inorganic compounds. Proteins (e.g., albumin, proline-rich proteins, statherin, histatin), glycoproteins (e.g., mucin) and aminoacids (e.g., leucine, glycine, glutamate, aspartate) are the main organic constituents of the saliva and valuable for microorganisms. Even though some organic constituents are important for microbial metabolism and growth, other constituents such as antibodies (IgAs, IgM, IgG) and enzymes (lysozyme, lactoferrin, lactoperoxidase) act as regulators of microbial colonization. Additionally, carbohydrates (glucose, galactosis and sialic acid) and lipids (phospholipids, triglycerides and cholesterol) are also organic constituents present in the saliva.

In the oral cavity, the viscous property of the saliva provided by glycoproteins (e.g., mucin) present in the acquired pellicle can protect the dental surfaces against wear. The friction recorded on titanium surfaces under sliding against an alumina ball can be reduced in the presence of water, lipids and glycoproteins (e.g., mucin). That can be compared to the effect of commercial lubricant agents.

The inorganic fraction is basically represented by ions such as Ca^{2+} , PO_4^{3-} , Na^+ , K^+ , and HCO_3^- . Bicarbonate (HCO_3^-) and phosphate (PO_4^{3-}) ions act as a buffer to maintain the pH of the saliva between 6 and 7. Acting as the main buffering agent, HCO_3^- binds to H^+ to form H_2CO_3 , H_2O and CO_2 , increasing the pH which leads to the prevention of tooth demineralization and corrosion of dental materials. However, the buffering mechanism can be limited by a high density of microbial cells or by a low salivary flow rate.

The salivary glands produce 1–1.5 L of saliva per day which is responsible for the mechanical removal of microorganisms and food stuffs. The masticatory process and the muscular movements increase the salivary output, optimizing the oral cleaning. However, the salivary flow rate decreases during sleep facilitating the increase in the number of microorganisms in the oral cavity and consequently the lowering of the pH.



In fact, the increase of lactic acid-producing bacteria metabolism is a critical factor for the lowering of the pH [16].

1.3 Dental implantology

1.3.1 Overview on dental implants

The restoration and replacement of missing teeth are important aspects of modern dentistry. As teeth are lost to decay, disease and trauma, there is a demand for improvement of esthetics and restoration of function.

Conventional methods of restoration include a removable complete denture, a removable partial denture, a fixed prosthesis, or combinations of these approaches.

There are different indications for each method, with associated advantages and disadvantages. Removable dentures have long been considered problematic because of their varying mobility/stability over time and the inconvenience of removing them each day. Also, many removable dentures were bulky, others complicated chewing and some were not adequately esthetic. Fixed prostheses were considered more esthetic and comfortable for the patient, but they involved the preparation of adjacent teeth and they were associated with problems such as secondary decay or irreversible pulpitis. If the adjacent teeth did not have restorations, the decision to prepare them for a fixed prosthesis was difficult because two or more natural teeth would have to be surgically altered to provide retention for one or more artificial teeth (a bridge).

For centuries people have attempted to replace missing teeth by implanting synthetic and natural substances. “Implantation” has been defined as the insertion of any object or material, such as an alloplastic substance or other tissue, either partially or completely, into the body for therapeutic, diagnostic, prosthetic or experimental purposes.

Implantation is usually differentiated from other, similar procedures such as replantation and transplantation. Replantation refers to the reinsertion of a tooth back into its jaw socket after its accidental or intentional removal, whereas transplantation is the transfer of a body part (homogeneous or heterogeneous) from one host to another [8].

1.3.2 Historic background

Implant designs are traceable to early Egyptians and South Central American cultures and have evolved into the present implant designs that are now experiencing explosive popularity. The earliest dental implants were of stone and ivory cited in archeological records of China and Egypt before the Common Era. Gold and Ivory dental implant were used in the 16th and 17th centuries. Metal implant devices of Gold, Lead Iridium, Tantalum, Stainless Steel and Cobalt alloys were developed in the early 20th century [55].

Ancient Egyptians in 2500 B.C. attempted to stabilize periodontally compromised teeth with the use of gold ligature wire. Implanted animal teeth carved of ivory cited in ancient Egyptian writings are the oldest examples of primitive implantology. Dating to approximately 500 B.C. the Etruscan population utilized soldered golden bands incorporating animal teeth to restore masticatory efficiency. The Phoenician population in the same era utilized gold wire to stabilize periodontally compromised teeth [56].

Sea shells were used in place of teeth in 600 AD evidence of which was found in Honduras (Figure 1.12), and tooth restorations made of Jade and Turquoise, were found in Mayan skulls. Albucasis de Condue (936-1013) of France used ox bone to replace missing teeth; this was one of the early documented placement of implant [8].



Figure 1.12: This mandible, dated 800 A.D., was found in Honduras. It shows three implanted incisors made of carved seashells. Calculus formation on these three implants indicates that they were not made solely for a burial display but served as fixed, functional, and esthetic tooth replacements [8].

In 1700's John Hunter [67] suggested the possibility of transplanting teeth of one human to another. Towards the 18th century, Pierre Fauchard and John Hunter further documented tooth transportation with conditions for its success [8].

In 1809, Maggiolo fabricated gold roots that were fixed to teeth by means of a spring. These single, tooth size gold implant were placed without a crown to heal passively in a fresh extraction site just above the gingival (that were not truly submerged into bone). The crown was added after healing. The insertion of such roots of gold was in exitable followed by intense pain and gingival inflammation [8].

Harris followed in 1887 with the implantation of a platinum post coated with lead. The post was shaped like a tooth root and the lead was roughened for retention in the socket. Bonwell in 1895 used gold and iridium tubes implanted into bone to restore a single tooth as to support complete dentures. Payne, in 1898 implanted a silver capsule as a foundation for a porcelain crown that was cemented several weeks later. Scholl in 1905 demonstrated a porcelain corrugated root implant. The implant was successful for two years and was anchored to adjacent teeth and fillings through the use of pins [8].

Greenfields in 1913 introduced and patented hollow 'basket' implant made of mesh work of 24 gauge iridium-platinum wires soldered with 24 karat gold. This was used to support single implant as well as fixed dental prosthesis comprising as many as eight implants [8].

After 1925 modern era started with advancement in implant biomaterials. In 1937 Venable et al. analyzed the interactions of cobalt alloy and other available metals and alloys with bone. They concluded that certain metals produced a galvanic reaction, which led to corrosion when these metals contacted tissue fluids [58]. Strock in 1939 described a method of placing a vitallium screw to provide anchorage for placement of a missing tooth [58].

Formigini in 1947 developed a single helix wire spiral implant made from tantalum or stainless steel. At the same time, Raphael Chercheve designed a double delinked spiral implants made of a chrome-cobalt alloy. In 1948 Goldberg and Gershkoff reported insertion of first viable sub-periosteal implant. In 1952 Branemark developed a threaded

implant design made of pure titanium that increased the popularity of implants to new levels. Branemark studied every aspect of implant design, including biological, mechanical, physiological and functional phenomena relative to success of endosteal implant. His studies utilized unalloyed titanium, a root form design and very controlled conditions for surgery, restoration and maintenance. In 1963 Linkow designed and introduced the hollow basket design with vents and screws threads [7].

1.3.3 Classification of implants

Implants can be classified according to anatomic location, device design, implant properties, or implant attachment mechanism. In a broad context, there are four implant design types that can be classified by anatomic location and they have evolved over centuries of development [8].

The first and most commonly used type of design is the “endosteal” (called endosseous) implant (Figure 1.13), a device placed into an alveolar and/or basal bone of the mandible or maxilla that usually transected only one cortical plate. These implants were formed in many different shapes, such as root-form cylindrical cones or screws or thin plates called plate or blade forms, and they were used in all areas of the mouth [8].

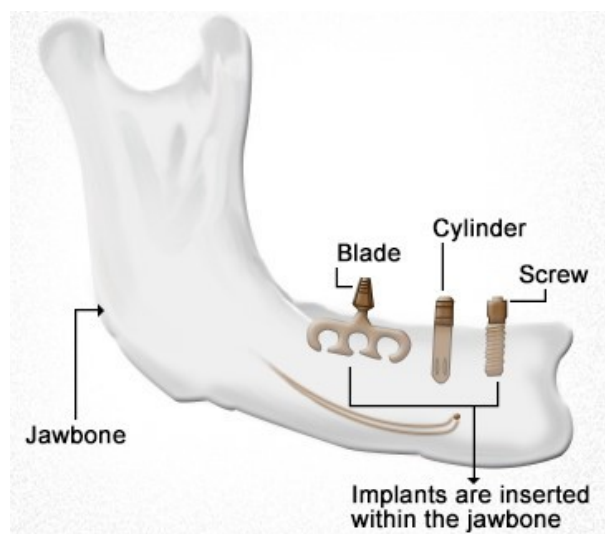


Figure 1.13: Endosteal implant [57].

The most popular endosteal implant has been the root-form, which was designed initially to mimic the shape of tooth roots for directional load distribution as well as for positioning in bone.

The second implant design was the “subperiosteal” implant (Figure 1.14), which employed an implant substructure and superstructure. The custom-cast frame was placed directly beneath the periosteum overlying and fitting along the bony cortex [8].

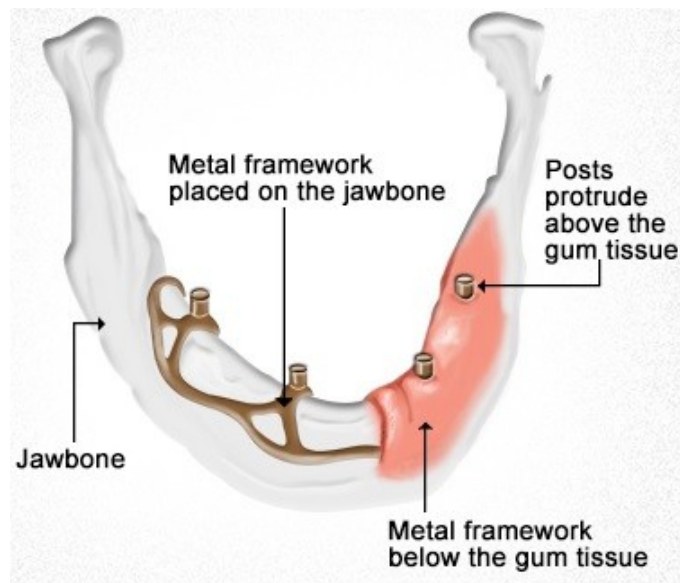


Figure 1.14: Subperiosteal implant [59].

The third design was the “transosteal” implant (Figure 1.15), which combined subperiosteal and endosteal components. This type of implant penetrated both cortical plates and passes through the full thickness of the alveolar bone. Use of the transosteal implant has been restricted to the anterior area of the mandible and provides support for tissue-borne overdentures [8].

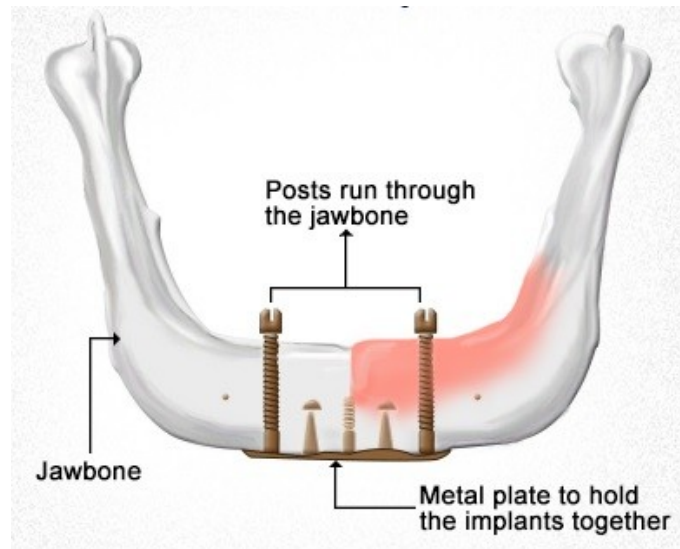


Figure 1.15: Transosteal implant [60].

The fourth implant design was the “epithelial” implant (Figure 1.16), which was inserted into the oral mucosa. This type was associated with a simple surgical technique where the mucosa was used as an attachment site for metal inserts placed into an acrylic denture [8].

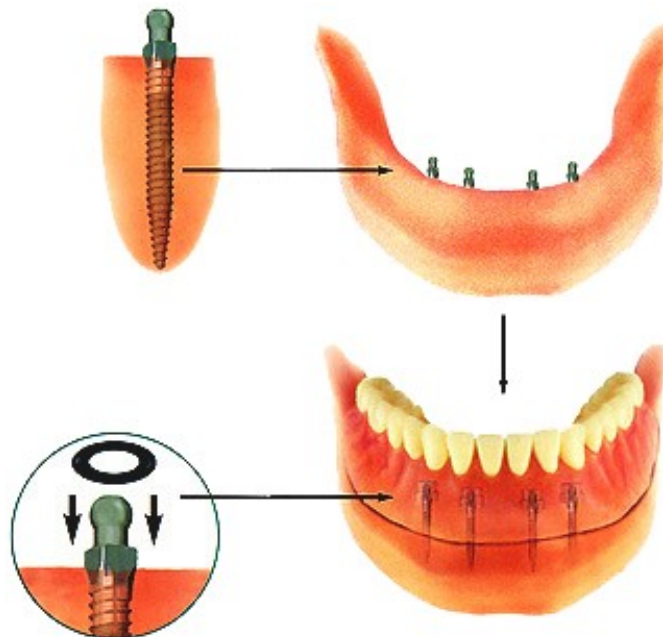


Figure 1.16: Epithelial or intramucosal implant [61].



Implant biomaterials can also be classified according to their composition and their physical, mechanical, chemical, electrical, and biological properties. These classifications often include ranked comparisons of properties such as elastic moduli, tensile strength, and ductility to determine optimal clinical applications (see chapter 3). These properties are used to aid in the design and fabrication of the prosthesis [8].

Another way of classifying implants is through interactions at the implant-to-tissue interface. Periodontal structures, which attach teeth to bone, consist of highly differentiated fibrous tissue. These fibers are replete with numerous cells and nerve endings that allow for functional force transfer, sensory function, bone formation, and tooth movements. Although this is the ideal form of integration, there are no known implant biomaterials or designs at present that can stimulate the growth of these fibers and fully mimic the function of the periodontal ligament and a natural tooth.

Historically, implant interactions occurred through fibrous connective tissue, and this was accepted as a measure of successful implant function (the pseudoligament concept). This type of interaction was reported to be very susceptible to acute or chronic inflammatory responses, which were accompanied by pain and eventual loss of the implant. Such an implant has also been called a pseudoperiodontium.

The implant-to-bone interaction (called osseointegration) is characterized by direct contact between bone and the surface of a functional implant after one year. This central theme of the Brånemark group was called “direct anchorage to bone” and has become a major attribute of dental implants. This mode is described as the direct adaptation of bone to implants without any other intermediate nonbony tissue and has been described by some as similar to tooth ankylosis, where no periodontal ligament or fibrous tissue exists. The strength of this contact has been shown to be stable, which is advantageous compared with the soft tissue interface described previously.

This type of osseous interface has been described extensively and includes a process wherein bone-producing cells migrate along the implant surface through the connective tissue scaffolding that forms adjacent to the implant surface. Integration at the implant interface is highly dependent on the implant surface’s chemistry and design. Bone apposition has been reported at higher rates when microscopic surface ridges are

present. Osseous integration has also been achieved through the use of bioactive materials that stimulate the formation of bone along the surface of the implant. Another way of achieving osseous integration involves de novo bone formation, wherein a mineralized interfacial matrix and/or active growth factors are deposited along the implant's surface. Once again, the implant's surface topography influences the strength of its attachment to bone [8].

1.3.4 Implant components

To understand the material characteristics and function of an implant, one must first be knowledgeable about its numerous component parts. Although each implant system varies, the parts are basically consistent.

The body of the implant (called a “fixture” for the Branemark system) (Figure 1.17, A) is the implant component that engages with bone. Depending on the implant system, the body section can have different surfaces threading, grooved, perforated, plasma-sprayed, or coated. These characteristics are often classified as subtraction (acid etch) or addition (coating) types. Each surface type is meant to serve a particular purpose—for example, increased surface area enhances bone integration, and better cortex engagement plays an important role in immediate and long-term bone anchorage. The coated or plasma-sprayed biomaterials are used to enhance attachment to bone.

There are variations in the overall shape of the implant: screw-type and cylinder-form implants. The first one is the most used and includes “tapered root-form implants” and “straight (parallel-walled) implants”. It can be placed in smaller sockets and transmit biting force efficiently to the bone. The cylinder-form implant has a cylindrical shape without screw threads and can be placed easily in the jawbone. However, it does not show sufficient primary stability because the surface area is smaller than that of screw-type implants [73].

The second component (figure 1.17, B) is the transmucosal “abutment”, which provides the connection between the implant body and the intraoral prosthesis to be fabricated (Figure 1.17, C) which will provide intraoral function.

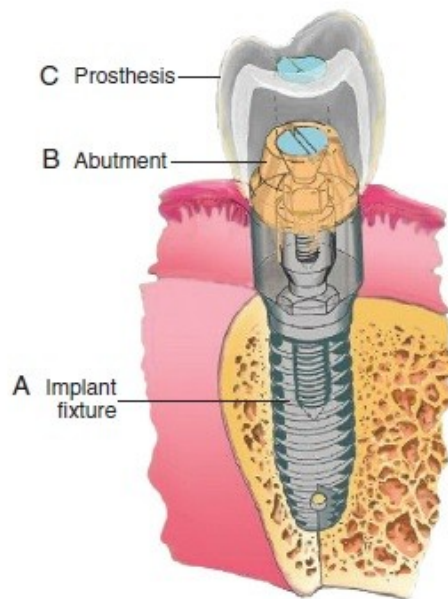


Figure 1.17: Diagram of implant components. A, The implant fixture (endosteal root form). B, Transmucosal abutment serving as the attachment between fixture and the actual prosthesis. C, The actual prosthesis, which can either be cemented, screwed, or swaged [8].

The abutment is usually connected to the implant body by means of a screw; however, it can also be cemented or connected by a Morse taper-type design. Abutments can become engaged to the implant body either by an internal or external geometry (initially a hexagon) within the implant body, which also serves as an anti-rotation device and is particularly important for single-unit restorations.

The last part of an implant is the “prosthesis”. This can be attached to the abutments through the use of screws, cement, precision attachments, magnets, or other designs, such as those used for removable implant overdentures [8].

1.3.5 Criteria to select the proper dental implant

The choice of the proper dental implant relies on two factors: the strength of the implant biomaterial and the type of bone in which the implant will be placed.

The other factors to consider are the implant design, abutment choices, abutment availability, surface finish and biomechanical considerations of restorative treatments [8].

The needed strength is related to the zone where the restoration has to be placed. In the anterior zone, the forces are relatively lower (95-250 N), and the implant has to be placed in a narrower space (diameter of 3.25 mm or less); in the posterior area, on the contrary, is subjected to higher force transfer (180-850 N) and the available space is bigger, allowing the placement of implants with a bigger diameter (7-8 mm).

The type of bone influences the mechanical coupling of the implant with the bone itself. The bone in which the implant will be placed is classified in 4 types that highlight the different ratios between compact and trabecular bone as well as the density of the trabecular bone. Type I consists of mostly homogeneous compact bone, type II consists of a thick layer of compact bone surrounding a core of dense trabecular bone, type III is a thin layer of cortical bone surrounding a core of dense trabecular bone and type IV is composed of a thin layer of cortical bone with a core of low-density trabecular bone. Type IV bone is by far the most compromised bone environment for implant stability because of its inadequate quality and quantity [8].

1.3.6 Biomechanics of dental implants

The integration of bone with implants serves as the basis for the biomechanical analyses performed for dental implants. Close approximation of bone-integrated conditions with the surface of an implant permits the transfer of forces and site-specific stresses with elastic displacement of the bone and implant. The stresses that are generated are highly affected by four main considerations:

1. masticatory factors (frequency, bite force and mandibular movements);
2. support for the prosthesis (implant-supported, implant-tissue-supported, implant-tooth-supported);

3. the mechanical properties of the materials involved in the implant restoration (elastic modulus, ductility, fracture strength, etc.);
4. the design of the implant body and the associated intraoral prostheses.

One of the most important variables affecting the close apposition of bone to the implant surface is the relative movement or micro-motion. In fact, early-stage failures are most commonly associated with the inability to achieve primary stability and proper osseointegration. According to the conventional approach [64], it is necessary to wait 4-6 months before loading the implant after surgery because the micro-movements above 150 μm prevent the formation of bone and encourage soft tissue deposition and eventual encapsulation of the implant body with fibrous tissue. But success has been reported [65] with immediate loading of dental implants depending on bone quality, patient selection and short-term controls of intraoral function. This technique eliminates the need for a second surgery and allows the implant to be used immediately to support a temporary or permanent prosthesis. The problem with immediately loading implants is that micro-movement can occur and jeopardize the bone formation around the implant body. However, research has shown that there is a range of allowable micro-movement from 30 to 150 μm , where bone deposition is not hindered. The key issue is control of implant-to-tissue micro-motion during the initial healing of bone.

The relationships for the response of bone to the types of biomechanical stresses and strains and their magnitudes have been defined and the results have been summarized as the “Frost paradigm,” (figure 1.18) where micro-strain magnitudes are correlated with bone conditions of disuse atrophy (less than 500 $\mu\epsilon$), normal function (500 to 1500 $\mu\epsilon$), and micro-trauma (more than 500 $\mu\epsilon$). This paradigm affords opportunities to evaluate implant and construct designs on a relative basis using finite element models and analyses (FEM/FEA).

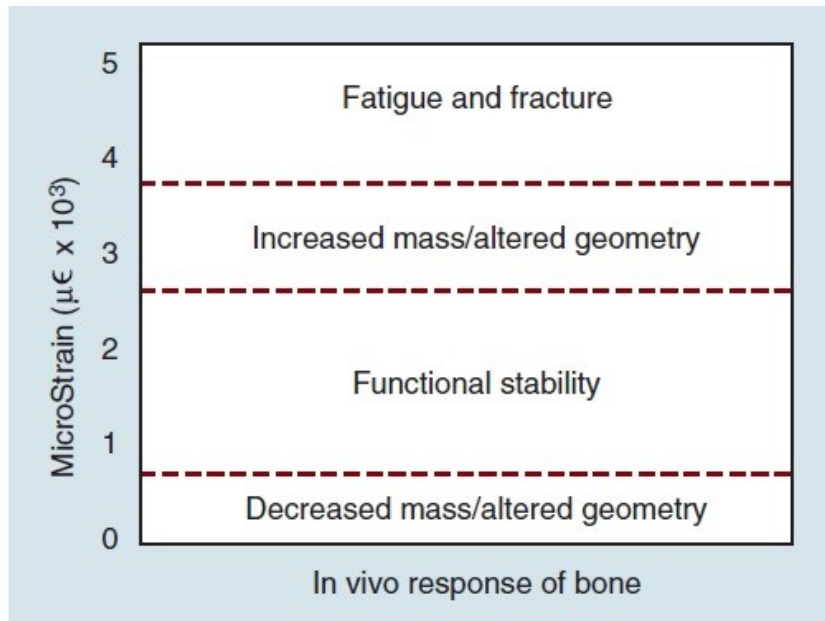


Figure 1.18: Schematic diagram of Frost paradigm [8].

Moreover, late-stage failures occur after loading or placement of a prosthesis and can be the result of complications stemming from uncontrolled periodontal disease or overloading of the implant. Overloading can be due to lateral or oblique forces exerted on the prosthesis from improper occlusal loading or parafunctional habits. Bone is susceptible to micro-fractures or fatigue fractures, depending on the type and amount of occlusal load being exerted. Once the bone reaches the tolerance limit for the occlusal loads, these fractures can occur and can lead to implant failure. Excessive bone deformation has been shown to occur between 2000 and 3000 $\mu\epsilon$ and pathological overloading can be seen at over 4000 $\mu\epsilon$. A delicate balance must be achieved in load transfer from implant to bone to maintain proper bone health. Excessive occlusal forces lead to overloading of the bone surrounding the implant, which can, in turn, lead to bone resorption and micro-fracture. Conversely, minimal load transfer to bone can lead to bone atrophy from disuse. Rough surfaces along the implant are typically conducive to transferring more load to the bone due to the increased surface area contact. This reduction in localized stress decreases the strain around the implants. On the other hand, smooth-surfaced implants have the opposite effect, as evidenced by resorption along the marginal areas, where there is a smooth transition from the implant to bone. Also the material of the implant body influences the transfer of strain across the implant-tissue

interface. In fact, the greater the elastic modulus of the implant compared to the elastic modulus of the bone (cortical bone: 17-28 GPa; cancellous bone: 0.5-3 GPa) [66], the greater the stress in the implant, therefore the lower the stress transferred to the bone. Thus, an implant whose elastic modulus is comparable with the one of the bone would be preferable.

Two main types of loading conditions can occur at an implant site. These are represented by axial forces and bending moments caused by non-centric loading conditions. A bending moment can best be demonstrated by visualizing a cantilever beam design in which the maximum bending moment is located at the fixed base of support and is calculated as force (perpendicular to the beam) times the length of the lever arm. The type of prosthesis used can also have an effect on how the forces are transferred along the implants. Prosthesis design should minimize long cantilever arms so as to avoid offset loads or high bending moments on the implants. Lateral forces are not tolerated as well as direct axial loading. Cement-retained prostheses have been found to be more favorable in maintaining proper axial loading as opposed to screw-retained restorations. The absence of a screw hole allows proper occlusal design for the prosthesis to adequately direct loading to the implant. Conversely, the presence of a screw hole will redirect occlusal forces and introduce bending moments to the implant.

Another important factor to consider is the fit of the prosthesis on the implant. An inaccurate fit will lead to a non-uniform distribution of load, with the unit closest to the load bearing most of the forces [8].

Failures in dental implant systems have been attributed not only to biomechanical overloads, but also to corrosion and wear synergy along with the cyclic loading mechanism of the masticatory process [16] (see Chapter 1.5).

1.4 Titanium-zirconia hybrid implants

1.4.1 Overview on dental implant materials

A broad assortment of materials was used in the past to restore or repair teeth, including metals, seashells, ivory, animal and human teeth [8].

Current dental materials include metals, ceramics, polymers and composites. Dental biomaterials can be further divided in three categories, according to their application in dentistry, namely restorative, auxiliary and preventive materials [8]. Restorative materials are intended to replace a missing a malfunctioning tooth structure; these materials are contemplated for temporary, short-term or long-term operation. Auxiliary materials facilitate or are necessary to the fabrication of prostheses, but are not meant to be part of it at the end of the process. Preventive materials aim for inhibiting the tooth degeneration or even preventing it; these materials are most represented by sealants used in pits and fissures and materials that release fluorides or antibacterial agents.

Pure metals are infrequently used for applications in dentistry, apart from pure titanium and pure gold. Indeed, pure titanium can be used to make dental implants, as well as inlays, crowns and bridges; pure gold is used to make restoration directly on teeth, but this procedure is less and less used nowadays [8]. Metal alloys are used for implants, orthodontic wires and brackets, frameworks, crown and bridges.

Ceramics are used for implants, crowns, inlays, veneers and porcelain restoration. To comply with the need for both high fracture resistance and aesthetic appeal, ceramic parts are often manufactured with several layers (a tough core underneath one or more layers of a not as tough but translucent ceramics). Alumina (Al_2O_3) and zirconia (ZrO_2) are the most used ceramic materials in implant dentistry [8].

Polymeric materials are widely used for both preventive and restorative purposes [8]. The main applications of polymers in dentistry are cements and orthodontic appliances.

Dental composite materials are made of a monomer resin matrix that embeds inorganic or filler particles [8].

1.4.2 Titanium and its alloys

The most popular implant biomaterials in use today are titanium and titanium alloy. Titanium exists in nature as a pure element with an atomic number of 22. With an atomic weight of 47.9, titanium makes up about 0.6% of the earth's crust and is a million times more abundant than gold. This metal exists as rutile (TiO_2) or ilmenite (FeTiO_3) compounds and requires specific extraction methods to be recovered in its elemental state.

Titanium has several favorable physical properties, which include low density of 4.5 g/cm^3 and a relatively high flexure strength comparable to that of cast forms of cobalt and stainless steel alloys. Titanium is also very resistant to corrosion; as a result of this property, it can be passivated by a thin layer of titanium oxide, which is formed instantly on its surface. This metal has the ability to form an oxide layer of nanometer thickness (2-10 nm) within a millisecond, and this oxide reforms if lost because of mechanical removal. If left unchecked, this oxide layer can become thicker over time. Pure titanium has the ability to form several oxides, including TiO , TiO_2 , and Ti_2O_3 . Of these, TiO_2 is considered the most stable and is found after exposure to physiological conditions [8].

The most commonly used titanium products are grades 1 to 4 of unalloyed Ti (cp Ti) which differ in their oxygen content: grade 4 is having the most (0.4%) and grade 1 the least (0.18%) oxygen content. The mechanical differences that exist between the different grades of cp Ti is primarily because of the contaminants that are present in minute quantities [68]. The compositions of these metals in weight percentage are given in Table 1.1.

Table 1.1: Composition of CP Titanium and Alloys (Percent by Weight)* [8].

Titanium	N	C	H	Fe	O	Al	V	Ti
CP grade I	0.03	0.08	0.015	0.20	0.18	—	—	Balance
CP grade II	0.03	0.08	0.015	0.30	0.25	—	—	Balance
CP grade III	0.05	0.08	0.015	0.30	0.35	—	—	Balance
CP grade IV	0.05	0.08	0.015	0.5	0.4	—	—	Balance
Ti-6Al-4 V alloy	0.05	0.08	0.015	0.3	0.2	5.50–6.75	3.50–4.50	Balance
Ti-6Al-4 V (ELI alloy)	0.05	0.08	0.012	0.25	0.13	5.50–6.50	3.50–4.50	Balance

*ASTM Standard: minimum values.

By far the most widely used of the Cp Ti grades is grade 2. From this base, the other grades have been developed for better formability or higher strength levels, significantly increasing corrosion resistance at higher temperatures, and/or improving corrosion resistance at lower pH (or higher acidity) levels. There is a distinct difference in using Cp Ti between industry and medicine. Among various applications of Cp Ti materials in dental and medical fields, the dental Cp Ti implant is the most frequently and widely employed. Information on Cp Ti grade selection for dental application indicates that, despite the popularity of grade 2 in industry, grades 3 and 4 are equally selected in most of the 20 major dental implant systems. More interesting, however, are their availabilities. Grades 2 and 4 were available without any problems, whereas Cp Ti grade 3 is the least popular and is difficult to obtain. After conducting electrochemical corrosion testing, using 37°C Ringer's solution as an electrolyte, it was found that Cp Ti grade 3 exhibited the least corrosion resistance. Regardless of material availability, this supported the unpopularity of Cp Ti grade 3. Hence, despite the popularity and availability of grade 2 in industries, Cp Ti grade 2 is the least popular, although its corrosion resistance is somewhat superior to grade 3, which is the worst grade in terms of corrosion resistance among the four grades [12].

Titanium alloys, namely, Ti-6Al-4V and Ti-6Al-7Nb, are used in extra-low interstitial (ELI) grades. The ELI contains low levels of oxygen dissolved in interstitial sites in the metal. Lower amounts of oxygen and iron improve the ductility of the ELI titanium alloy, which can be alloyed with different elements to modify its properties. For example, titanium undergoes a transformation from a hexagonal-closepacked alpha phase to a body-centered-cubic beta phase at 883 °C. Alloying elements can be added to stabilize either phase. Ti-6Al-4V is one of the titanium alloys more commonly used in

the United States. Aluminum acts as an alpha stabilizer for the purpose of increasing strength and decreasing density. Vanadium is a beta-phase stabilizer, which is used to minimize the formation of $TiAl_3$ to approximately 6% or less and to decrease the alloy's susceptibility to corrosion. With the exception of pure titanium, the modulus of elasticity of Ti-6Al-4V is closer to that of bone than that of any other widely used metallic implant biomaterial. The strength of cp Ti is less than that of Ti-6Al-4V alloy, although the modulus of elasticity values are comparable. The elastic modulus of a typical Ti alloy (113 GPa) (see Table 1.2) is only slightly higher than that for the CP grade 4 Ti (102 GPa). The yield strength of Ti-6Al-4V ELI and Ti-6Al-4V alloys (795 MPa and 860 MPa, respectively) is 65% to 78% greater than that for cp Ti.

Table 1.2: Mechanical properties and density of metallic and ceramic implant materials [8].

Material	Grade or Condition	Yield Strength (MPa)	Elongation (%)	Modulus of Elasticity (GPa)	Tensile Strength (MPa)	Density (g/cm ³)
CP titanium	1	170	24	102	240	4.5
	2	275	20	102	345	4.5
	3	380	18	102	450	4.5
	4	483	15	104	550	4.5
Ti-6Al-4 V		860	10	113	930	4.4
Ti-6Al-4 V ELI		795	10	113	860	4.4
Co-Cr-Mo	Cast	450	8	240	700	8.0
Stainless steel	Annealed	190	40	200	490	8.0
	Cold-worked	690	12	200	860	8.0
Aluminum oxide	Polycrystalline	400* (500/flexure)	0.1	380	220	3.96
Zirconium oxide	Y ₂ O ₃ (stabilized)	1200 (flexure)	0.1	200	350	6.0
Cortical bone		N/A	1	18	140	0.7
Dentin		N/A	0	18.3	52	2.2
Enamel		N/A	0	84	10	3.0

*ASTM standard: minimum values.

Ti alloys are able to maintain the fine balance between sufficient strength to resist fracture under occlusal forces and to retain a lower modulus of elasticity for more uniform stress distributions across the bone-implant interface [8].

1.4.3 Zirconia

Zirconia was used for dental prosthetic surgery with endosseous implants in early nineties. Cranin and coworkers published first research work on Zirconia in 1975 [69].

Zirconium oxide (ZrO_2) possesses excellent chemical stability and durability, since it does not promptly react with most liquids, gases, alkalis and weak acids [8]. Hence, it is stable over long time periods. Zirconia is highly biocompatible, since no harmful element is released in the body environment. Moreover, the surface roughness of the implant will not increase over time, which would have resulted in an increase in the implant abrasiveness to native tissues and enhanced susceptibility to bacterial adhesion. It has a relatively low thermal conductivity and is free from galvanic effects [8]. It has a very favorable esthetic potential, due to its natural white color and the long-term color stability. Compared to metal biomaterials, zirconia has the great advantage of matching the appearance of natural teeth.

Zirconia holds a unique place amongst oxide ceramics due to its excellent mechanical properties [11]. This crystalline oxide of zirconium exhibit very high and very consistent compression resistance (around 2000 MPa) [70] and good to excellent flexural strength (800-1000 MPa) [11]. Tensile strength is not the best parameter to describe the mechanical behavior of zirconia, because it varies with the size, length and shape of the specimen. Tensile strength is also influenced by loading rate, surface treatments and the environment is calculated, making it not necessarily a bulk property. Fracture toughness is a real material property, that can esteem its resistance to crack propagation. Non-doped monoclinic zirconia has a fracture toughness of $2.06 \text{ MPa}\cdot\text{m}^{1/2}$, that rises to $8-10.3 \text{ MPa}\cdot\text{m}^{1/2}$ in the case of the yttria-stabilized tetragonal zirconia [8].

At ambient pressure, unalloyed zirconia can assume three crystallographic forms, depending on the temperature. At room temperature and upon heating up to $1170 \text{ }^\circ\text{C}$, the structure is monoclinic. It assumes a tetragonal form between 1170 and $2370 \text{ }^\circ\text{C}$ and a cubic structure above $2370 \text{ }^\circ\text{C}$ and up to the melting point. Alloying pure zirconia with stabilizing oxides, such as CaO (calcium oxide), MgO (magnesium oxide), Y_2O_3 (yttrium oxide) or CeO_2 (cerium oxide), allows the retention of the metastable tetragonal structure at room temperature. Dental procedures, such as grinding or

sandblasting, can trigger a tetragonal to monoclinic transformation in the surface region. This transformation is accompanied by a substantial increase in volume (~4.5%) that induces surface compressive stresses, thereby closing the crack tip and enhancing resistance to further propagation. This characteristic, known as transformation toughening (Figure 1.19), increases the fracture strength and fracture toughness of Y-TZP (Tetragonal zirconia polycrystal) ceramics compared with other dental ceramics. On the contrary, increased phase transformation toughening may alter the phase integrity of the material and increases the susceptibility of the material to low-temperature degradation [11].

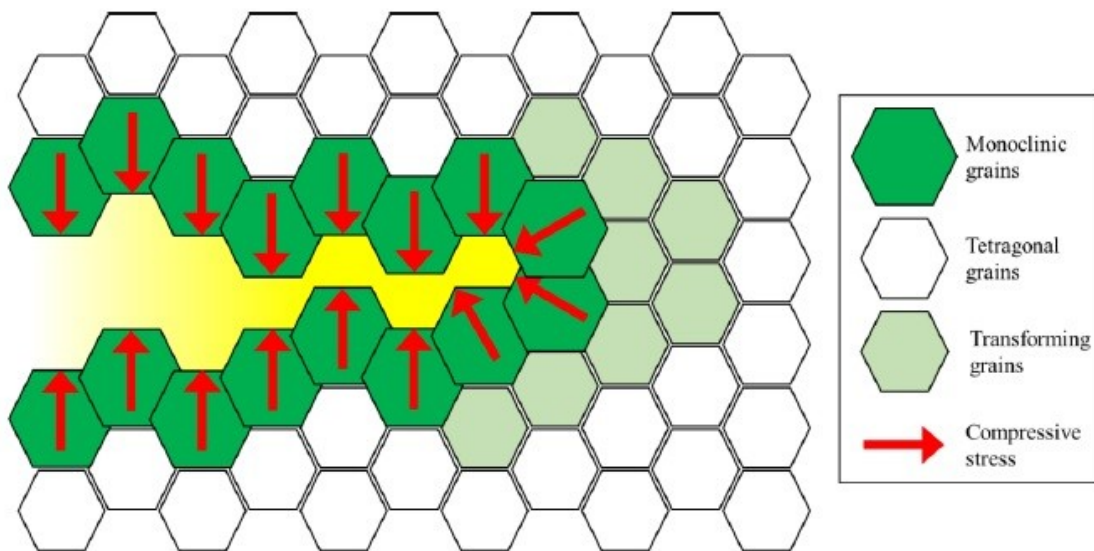


Figure 1.19: Schematics of the transformation toughening mechanism of zirconia [71].

Low-temperature degradation (LTD), also known as “ageing”, occurs by a slow surface transformation of the metastable tetragonal crystals to the stable monoclinic structure in the presence of water or water vapour. As previously mentioned, a certain degree of surface tetragonal-monoclinic transformation can actually improve the mechanical properties of Y-TZP. However, a narrow range exists between improvement and destruction of mechanical properties, as further ageing results in property deterioration. Transformation starts first within isolated grains on the surface by a stress corrosion mechanism. The transformation of one grain leads to a volume increase, thereby stressing the neighbouring grains and generating micro-cracking, which enables further

water penetration, crack propagation and phase destabilization (Figure 1.20).

Experimental observations have shown that the degradation proceeds most rapidly at temperatures between 200 and 300 °C and is time dependent.

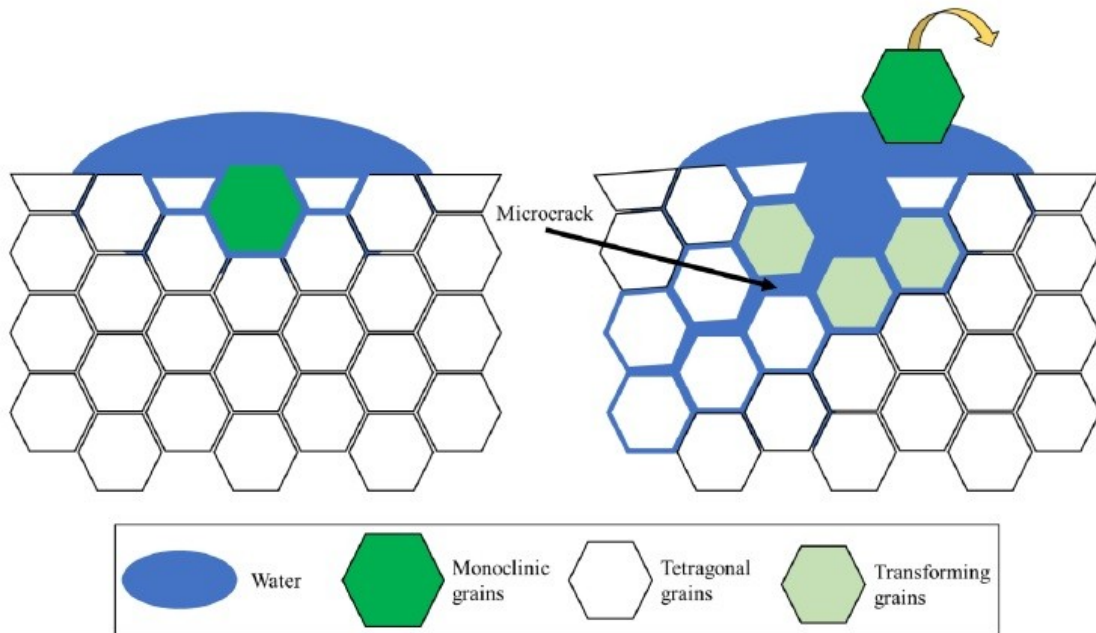


Figure 1.20: Schematics of low thermal degradation mechanism of zirconia [72].

The ageing process depends on several microstructure features, such as porosity, residual stresses, grain size and the stabilizer content of the processed material. A decrease in grain size and an increase in stabilizer content were found to retard the transformation process. The critical grain size reported in the literature ranges from 0.2 to 1 μm depending on the Y_2O_3 content.

LTD results in an adverse cascade reaction involving Y-TZP grain pull out, roughening of the surface, increased wear and micro-cracking. When the micro-cracked and damaged zone reaches the critical size for slow crack growth to proceed, degradation in mechanical properties of the material will occur.

Attempts to minimize LTD of 3Y-TZP (Yttrium-Stabilized Tetragonal Zirconia Polycrystals) systems include the addition of small amounts of silica, the use of yttria-coated rather than co-precipitated powder, the reduction of the grain size, an increase of

the stabilizer content or even the formation of composites with aluminium oxide (Al_2O_3). The addition of alumina to zirconia clearly hinders ageing or at least drastically reduces its kinetics, as it changes the grain-boundary chemistry and limits the tetragonal grain growth during sintering which results in a more stable structure [11].

1.4.4 Zirconia as dental abutment

Replacing a missing tooth by a single implant-supported crown has increasingly gained popularity by both the clinicians and the patients [74]. Long-term clinical studies have shown excellent survival rates of single implant tooth replacement [75][76]. However, the success of an implant treatment does not only depend on the successful osseointegration of the implant, but also the prosthetic supra-construction i.e. implant-abutment-crown complex has to naturally blend with the surrounding peri-implant tissue and the rest of the dental arch [77][78].

In spite of the continuous updates in the manufacturing and designs of metal abutments, the problem of visibility of the gray metal component might still compromise the esthetic outcomes of the treatment [79][80]. A related factor of the grayish appearance of the gingiva overlying the metal abutment (Figure 1.21) is the thin biotype nature of the gingiva, which in its turn is unable to block the reflected light from the metal surface [81]. In order to redeem or enhance the esthetic appearance of a single implant restoration, the use of an all-ceramic abutment has been suggested [82].



Figure 1.21: Aesthetic problems caused by titanium implants. (a) Gingiva appears greyish when the titanium implant is covered by relatively thin soft tissue. (b) Greyish implant is exposed after gingival recession [9].

Compared to metal abutments, ceramic abutments overcome the risk of having a gray discoloration of the gingiva by facilitating light transmission through its physical nature [83].

Zirconia has recently attracted significant interest because of its superior fracture resistance compared to alumina, its superior esthetic properties and its improved biocompatibility compared to metal abutments [84].



Figure 1.22: Labial view of customized zirconia implant abutment on right maxillary central incisor [10].

1.4.4.1 Structural design

Zirconia abutments are available in two basic designs. The first is a one-piece abutment (Figure 1.23), in which all parts are made of zirconia in a unit and the abutment is connected to the implant directly. The other design is the two-piece abutment introduced by Brodbeck [86] (Figure 1.24), which includes a secondary metallic component (usually titanium or titanium alloy) as the connecting part. The zirconia structure is adhered to the metallic component and then mounted onto the implant. Many studies [88][89][90] have verified that the fracture strength of two-piece abutments is higher than that of the one-piece design. The fracture of the one-piece zirconia abutments always occurs under relatively low loads and before damage or plastic deformation of the screw or implant [84][89]. In an 11-year follow-up study, no one-piece zirconia abutment fractured, but two screws loosened [91]. This was considered as a drawback of the external hexagon implant system.

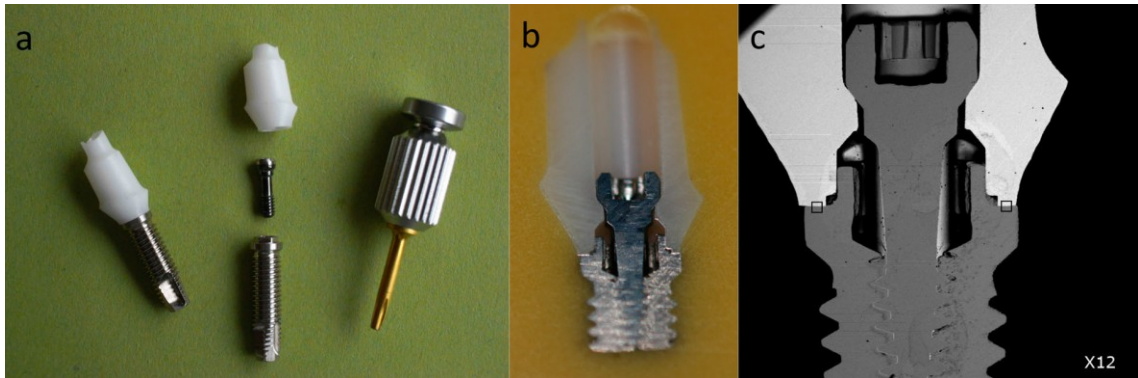


Figure 1.23: One-piece zirconia abutment for titanium implants. (a) All components have a direct connection via a tightening screw of the one-piece zirconia abutment to the titanium implant. (b) (c) A photograph and an SEM image of the cross-section of the one-piece zirconia abutment/titanium implant system connected by a central screw. Misfit at the interface between the zirconia abutment and the titanium implant is evident [9].

Meanwhile, severe wear between a zirconia abutment and titanium implant could induce loosening of the abutment connection, which could further increase the wear between the abutment and implant. Furthermore, the titanium wear debris may induce peri-implant gingivitis, gingival discoloration, or marginal bone adsorption. Metal has a higher ductility than zirconia and can withstand higher tensile forces through elastic deformation. Therefore, deformation of the metallic parts, sometimes followed by abutment fracture and screw loosening, is the main fracture mode of two-piece abutments [89]. Meanwhile, a metallic part will protect the interface between the abutment and implant from serious wear, especially when micro-motion is present [92]. For two-piece abutments, the interface between the zirconia and metallic parts is the weak link. Gehrke et al. [93] noted that complete adhesive failure was the main failure mode of a two-piece abutment, leaving the detached zirconia coping and the titanium insert undamaged. Although this finding has not been frequently verified in a clinical context, it indicates that the resin cement should be carefully chosen and adhesion optimized under laboratory conditions [94].

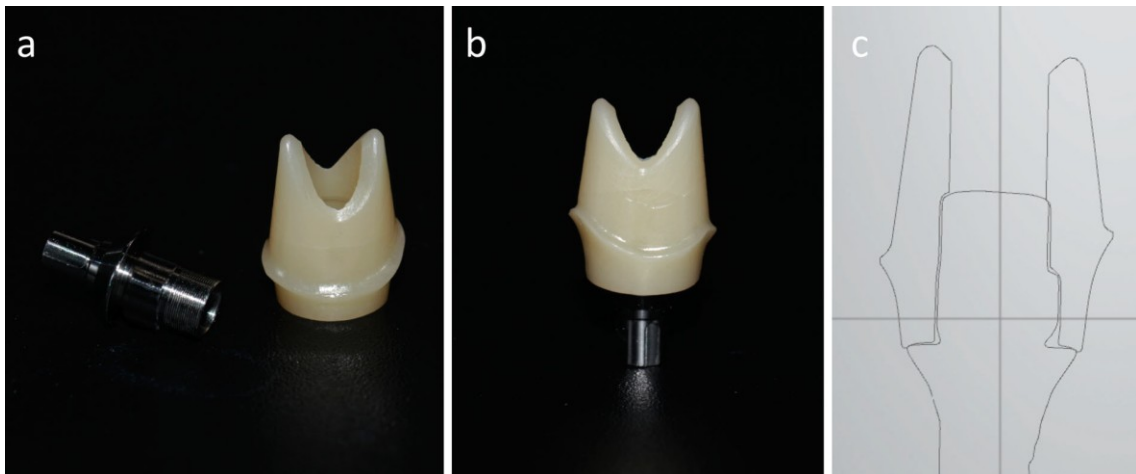


Figure 1.24: Two-piece zirconia abutment for titanium implants. (a) The two components of the two-piece zirconia abutment: the metallic titanium base and the zirconia superstructure. (b) The two components were glued together as a unit, which is then connected to the titanium implant with a central screw. (c) Computer-aided design of a customised two-piece zirconia abutment [9].

Rosentritt et al. [94] believed that the weakest point is not the bonding connection but rather the design of the connecting parts. Generally, the type of connection can be divided into the external connection and the internal connection. With the external connection system, there is an external anti-rotation mechanical structure on the implant shoulder for connecting the abutment. With the internal connection system, the connection formed through inserting the extending part of the abutment into the interior of the implant. The internal connection is more popular than the external one because it better distributes the load and thereby provides higher fracture strength [89][95]. In the internal connection system, the abutment connector can have various geometries, including hexagonal, octagonal and conical (Morse taper) shapes. Although there was no significant difference among them in terms of implant success and survival rate in in vivo studies, several advantages have been found for the conical design. Conical connection systems seem to be good at bacterial sealing, inhibiting micro-motion, resisting torque loss, and reducing abutment screw stresses and load distribution. A 12-year follow-up study of zirconia abutments with different connection designs showed that both survival and success rates of standard platform abutments were higher than those of platform switching abutments [96]. For the platform switching design, there is abutment fracture risk because the thickness of the abutment is reduced [9]. The concept of platform switching consists in the use of small diameter abutments

positioned on larger diameter implants. In this way a step is created between the most coronal portion of the implant and the initial part of the prosthetic pillar. According to Lazzara [97] with platform switching the diameter of the prosthetic connection is reduced by concentrating the inflammatory infiltrate above the implant platform and not laterally, thus reducing peri-implant bone remodeling. The advantages of this solution in traditional titanium dental implants are functional, since the bone level is maintained, but also aesthetic, since good peri-implant soft tissue maintenance is achieved [98]. The reduced transmucous volume of the abutment allows an increase in the volume of peri-implant soft tissues, constituting an effective barrier effect against bacterial penetration and apical migration of the sulcus epithelium, which lead to bone resorption.

1.4.4.2 Manufacturing processes

Two kinds of one-piece zirconia abutment, the prefabricated ones (Figure 1.25, d) and the custom-made ones (Figure 1.25, a), are available. The former designs are uniform and standardised, but if the position or angulation of the fixture is not appropriate or if the height of the surrounding soft tissue is insufficient, this fully dense abutment is difficult to grind. Material loss and defect generation will further reduce the fracture strength [99]. Custom-made zirconia abutments are fabricated according to individual models. The model or implant fixture in the mouth is digitised and the abutment is digitally designed to take into account the occlusion/angulation/emergence profile and provide room for the final aesthetic restoration.

Both customised and prefabricated standard zirconia abutments have comparable fracture strengths [100]. The strength is sufficiently high to restore anterior teeth, but more attention should be paid when the abutment is located in the posterior area [101].

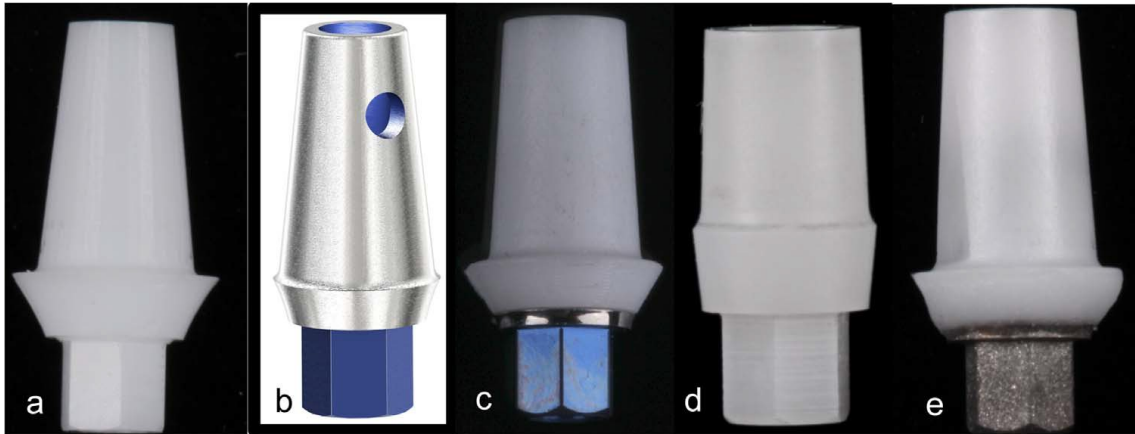


Figure 1.25: (a) CAD/CAM produced all-zirconia abutment. (b) Titanium abutment. (c) Zirconia abutments adhesively luted to a titanium base. (d) Prefabricated all-zirconia abutments. (e) Zirconia abutments glass soldered to a titanium base [87].

Park et al. [102] found that the abutment/implant interface was the weakest area of one-piece zirconia abutments. A microgap (Figure 1.26) in this region cannot always be completely avoided. An irregular or large microgap can lead to mechanical and biological injury, such as screw loosening or fracture, bacterial accumulation, and peri-implant bone deficiency [103]. Several studies reported that the dimensional accuracy of customized abutments is inferior to that of prefabricated ones [100][102][104]. Microgap at the customised abutment-implant interface is larger than that at the prefabricated abutment-implant interface. Although a microgap is clinically acceptable, the precision of the design and processing should be further improved to strengthen this weak region. For the customised two-piece zirconia abutment, the misfit problem is less obvious because the connecting metallic part is prefabricated.

Abdelhamed et al. [105] reported a clear correlation between torque and microleakage for zirconia abutments. Higher applied torque can effectively reduce the microgap between the zirconia abutment and the implant and thereby reduce the risk of microleakage and inflammation [105][106][107]. Rosentritt et al. [94] suggested that sufficiently high torque moments and early re-screwing in a clinical context be used to reduce the microgap and risk of screw loosening. More attention should be paid when tightening a zirconia abutment than a titanium one; Carrillo reported two zirconia abutments that fractured when tightened at the required torque [108].

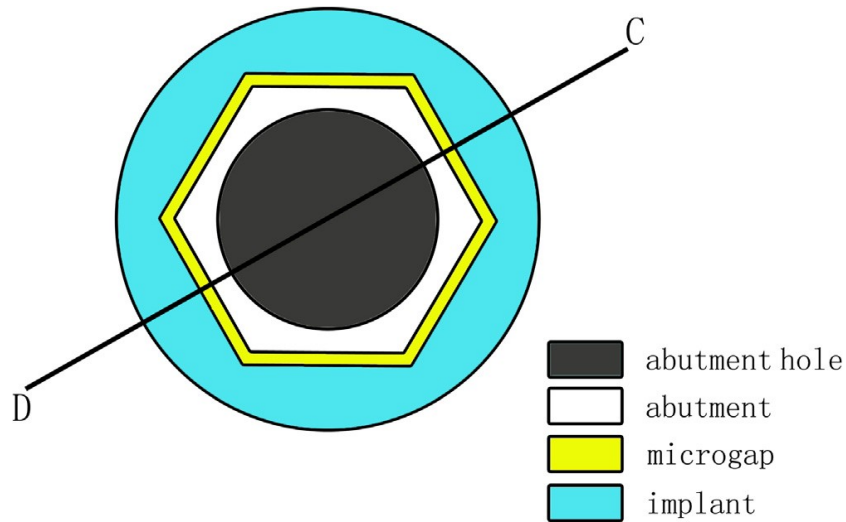


Figure 1.26: The cross section of internal hexagon in abutment–
implant interface [85].

Zirconia abutments are typically manufactured by manual copy-milling and computer-aided milling. The raw material can be pre-sintered blocks or green bodies. Injection moulding has also been used to obtain parts having excellent strength. Yang et al. [109] produced one-piece zirconia abutments by this technique and loaded them with forces from different angles to simulate the real fracture risk of anterior teeth. They found that zirconia abutments with titanium implants are sufficiently strong for clinical application.

1.5 Tribocorrosion in oral environment

The reasons for implant failure can be categorized according to patient-related, biological and mechanical factors (Figure 1.27). Patient-related factors such as smoking, metabolic diseases (diabetes mellitus) and disorders (anorexia nervosa) increases the risk of implant failure when compared to healthy individuals. Other factors that lead to implant failure include infection/peri-implantitis, aseptic loosening, osteomyelitis and improper bone-bonding due to overload.

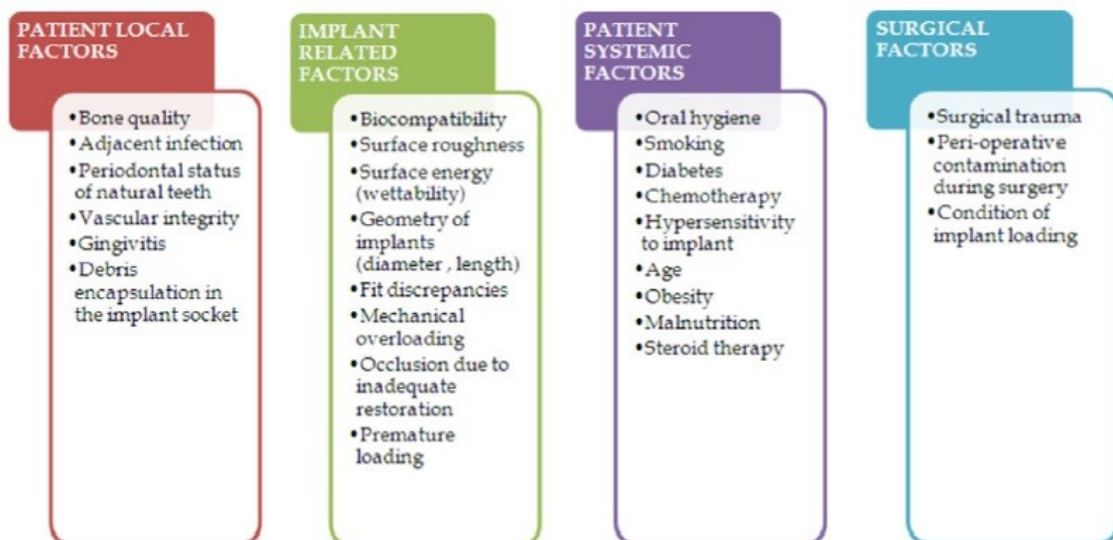


Figure 1.27: Factors affecting dental implant stability [14].

In addition, there are certain electrochemical and tribological factors such as corrosion and wear that accelerates the aforementioned reasons thereby, leading to implant-failure.

As described previously, the presence of protective oxide layer keeps the current flow and the release of corrosion products at very low level. However, no metallic material is completely resistant to corrosion or ionization within living tissues. Mechanical disruption of the oxide layer leads to deterioration of metal surface by processes such corrosion and wear. Many types of electrochemical corrosion are possible in the oral



environment because saliva contains aggressive anions such as chlorides which causes dissolution of the oxide layer and leads to release of metal ions into the surrounding tissues. The electrochemical behavior of Ti-based implants is dependent on various factors such as composition, concentration of anions, pH, buffering capacity and surface-related properties of the implant.

Wear refers to the deformation of the surface of materials as a result of mechanical interaction between two opposite surfaces. The wear resistance of artificial dental materials is essential for long-term stability of the implant. Generally, wear resistance is dependent upon the hardness, roughness, fracture toughness and the Young's modulus of the interacting materials. As wear measurements in vivo is highly complex and time-consuming, wear analysis is usually performed in simulators in the presence of artificial saliva.

Fretting corrosion is another degradation mechanism which refers to the small oscillating movements between two interacting materials (bone-implant, plates-screws) in presence of corrosive oral environment [14].

Simultaneous action of electrochemical and mechanical interaction occurring on materials subjected to relative movement, i.e. wear and corrosion occurring simultaneously is referred to as “tribocorrosion”.

Above mentioned degradation mechanism (wear, corrosion, tribocorrosion) causes the release of metal ions/debris into the peri-implant region. Metal debris activates a cascade of signaling molecules that result in the activation and differentiation of osteoclast cells and leads to bone resorption/osteolysis of the peri-implant region. As a result, the bonding between the bone and implant is lost and results in implant loosening. Also, it has been found that the titanium implanted region turns black. This is because the surface of titanium undergoes repassivation when the oxide layer is disrupted. In certain conditions, the repassivation process forms so much TiO_2 oxide layer that the region turns blacker. This process is referred to as metallosis and has been considered to be harmful [14].

1.5.1 Presence of oral biofilms

The effect of biofilm on the tribocorrosion in the oral cavity concerns the following factors:

- biofilm composition,
- biofilm adhesion process,
- role of microorganisms,
- biofilm metabolites,
- restorative surface characteristics.

The oral cavity is a complex environment that gathers several substances from food and saliva to microorganisms and their metabolites. Along time, several areas in the oral cavity can be covered by a complex microbial community embedded in an extracellular matrix composed of polysaccharides, proteins, nucleic acids, and water, known as “oral biofilm” [16]. As a result, the pH in the oral cavity is frequently altered reaching low values after the intake of acidic substances and/or acids release from oral microbial metabolism. Moreover, the biofilm composition is influenced by the local pH values, considering the release and tolerance of bacteria to acids. The temperature also varies temporarily during the intake of warm or cold foods. Therefore, there is a variation of oxygen in the oral cavity, as for example the low presence or absence of oxygen concentration in the areas below gingival margin. As a consequence, the microbial colonization in the mouth follows the variation of oxygen which promotes the preferential growth of aerobic or anaerobic microorganisms. Finally, the oral cavity habitat must not be considered as uniform since there are different micro-areas depending on the saliva composition, nutrient accumulation, tissue and restorative surfaces, and resident microorganisms. The topography of dental restorative systems is of major importance for microbial colonization taking into account that rough surfaces are more susceptible to be colonized by microorganisms than smooth ones.

In the oral cavity, microbial adhesion can take place in both soft tissues and hard structures represented by tooth and restorative structures. These surfaces are usually coated with a conditioning film (0.1–10 μm) (Figure 1.28, A) that is composed of glycoproteins, ions (e.g., Ca^{2+} , Mg^{2+}), and water. The conditioning film or enamel

acquired pellicle, such as often known when covering tooth enamel, protects the oral surfaces against wear originated from masticatory contacts [16] and assists in modulating the initial adhesion and colonisation of microorganisms and shapes the composition of the resident oral microbiota [110]. The acquired enamel pellicle is formed by the sequential adhesion of salivary proteins to the enamel, where a layer with larger molecule aggregates is formed with time, providing an environment that may be protective to the enamel mineral. The acquired enamel pellicle also provides colonising bacteria with nutrients through breakdown of dietary starch, lipids and proteins and bacterial metabolism of salivary components, for example glycoproteins [110].

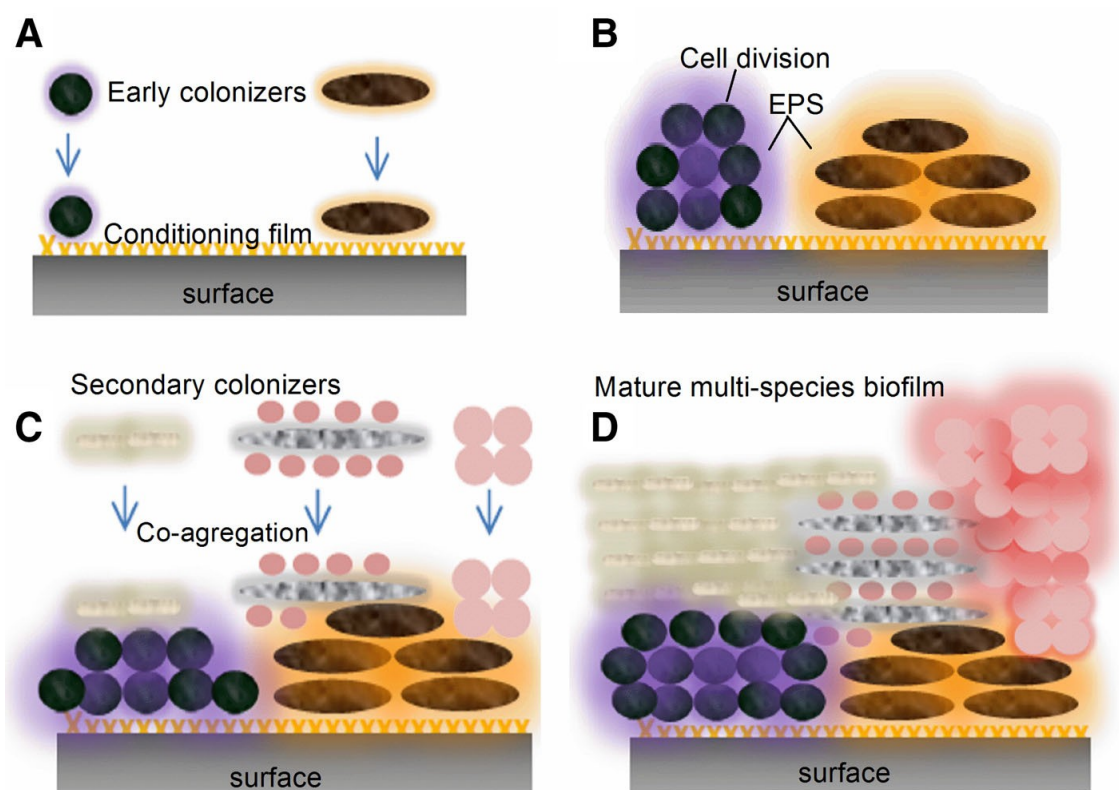


Figure 1.28: Schematic biofilm formation and co-aggregation of multi-species biofilms. (A) Initial biofilm formation by primary colonizers on a substratum covered with a conditioning film; (B) cell growth, division, and production of extracellular matrix (EPS); (C) coaggregation of single cells; (D) maturation and the formation of the multispecies biofilms [16].

However, the primary microorganism colonizers present protein macromolecules on their surfaces named adhesins that bind to receptors present on glycoproteins (e.g., mucin) in the conditioning film at oral surfaces. This is a specific mechanism of microbial colonization that allows microbial cells to bind selectively to surfaces (Figure 1.28). The multilayered biomass composed of glycoproteins, water, nucleic acids, and polysaccharides chains acts as viscoelastic material which can support considerable elastic deformation under shear stresses and is able to distribute loads, thereby decreasing the contact pressure at the surface. Since there is a modification of the environment associated to the presence of early colonizers, secondary or late colonizers can co-aggregate with previous species forming multi-species biofilms, as shown in figure 1.28, C-D. Finally, the cell growth and division in a complex microbial community follows nutritional and environmental conditions in the oral cavity [16].

The microbiota present at peri-implant seems to depend on the same factors related to microbiota of natural tooth surfaces. The highest concentration of microorganisms (70%) is represented by Gram-positive coccus and facultative anaerobic bacillus. Therefore, the commensal microbiota present in the oral cavity influences the microbial colonization of dental implant systems and prostheses.

In a dental implant-supported fixed prosthesis, the microbial colonization begins at prosthetic areas exposed to the oral environment taking into account that biofilm formation depends on the prosthetic design, surface conditions and on the oral microbiota. After implantation, a part of the margin area of implant fixture is in contact with connective and epithelial tissues, while another part is in contact with abutment and oral fluids. In literature, a mean interfacial discrepancy of about 2.5–60 μm in implant fixture-abutment gaps was reported. As the diameter of microorganisms is less than 10 μm , the prosthetic gaps can be effortlessly colonized by several microorganism. Hence, the penetration of microorganisms in implant internal connections can be caused by microbial leakage at the implant-abutment joints.

The presence of oral fluids and biofilms in the implant internal connection and prosthetic micro-gaps can be one of the factors responsible for a loss of mechanical integrity of the abutment screw by unscrewing. Thus, biofilms generated an ultra-low



friction on titanium under sliding. On the other hand, as a result of biofilm growth, there is a release of acidic substances from carbohydrates metabolism that alters pH and the oxygen content of the local environment. Specifically, lactic acid-producing bacteria such as *S. mutans* perform fermentation of carbohydrates (e.g., sucrose) releasing lactic acid that decreases the pH to values lower than 5.5 and dissolves the carbonate hydroxyapatite mineral of teeth by a process called demineralization. However, the pH of the oral surfaces surrounding media can be lower than the ones reported that could promote a localized corrosion of titanium.

The localized corrosion of titanium caused by biofilm colonization has been revealed by previous studies [111][112]. In fact, the pH of the medium in which biofilms grow decreased in the presence of microorganisms probably due to the release of acidic substances that reduced the corrosion resistance of titanium. The exposure of structural materials to oral fluids, including acidic substances produced by bacterial metabolism, is associated to the corrosion of the implant fixture-abutment joint. In addition, fluorides can be accumulated in biofilms depending on their structure and composition, physico-chemical properties of the solute, and biofilm thickness. Due to the diffusion of F⁻ ions through extracellular matrix, fluorides can also reach oral tissues and other micro-areas in the biofilm. The lowering of pH caused by the release of lactic acid from microbial metabolism in the biofilm can be responsible for a considerable concentration of HF that can corrode titanium and feldspar-based porcelain surfaces of dental implant-supported prostheses [16].

1.5.2 Corrosion of titanium

Titanium is known as a material with a very high corrosion resistance in physiological solutions and has an excellent biocompatibility due to the formation of a protective titanium oxide film, like TiO₂, when in contact with the surrounding environment. Nevertheless, the protective TiO₂ film can degrade in the oral cavity in the presence of corrosive substances such as fluorides, lactic acid, carbamide peroxide (urea peroxide) and hydrogen peroxide. The breakdown of the titanium passive film leads to a localized corrosion failure such as intergranular attack, pitting or corrosion fatigue.



The degradation of titanium-based surfaces at high fluoride concentrations was found in previous studies [113][114][115] revealing the occurrence of a localized corrosion process, namely pitting corrosion. The occurrence of pitting corrosion was described as resulting from the formation of hydrated Ti oxides as $\text{Ti}(\text{OH})_2\text{F}^+$, and salts as $[\text{TiF}_6]^{2-}$, TiH_2 , $\text{Na}_3\text{Ti}_3\text{F}_{14}$, TiF_4 $[\text{TiF}_6]^{3-}$ in the presence of HF. Such previous studies have revealed that a minimum concentration of 30 ppm HF is enough to promote a localized corrosion of titanium in fluoride solutions. In fact, the corrosion in fluoride solutions depends on the pH and the formation of HF produced by the dissociation of NaF when it is present at high concentrations, or in low pH solutions due to the bonding between H^+ and F^- ions [16].

1.5.3 Wear processes on dental materials

During chewing process, abrasion of restorative surfaces including titanium can be caused by frictional surface interactions with opposing surfaces, toothbrush and paste, food bolus, and hard particles originated from dietary. A two-body abrasion has been reported when two surfaces were rubbed away from each other by direct contact with their asperities. In the oral cavity, two-body abrasion takes place during a “non-masticatory tooth movement” although it can occur in the prosthetic dental joint surface during masticatory tooth movement. Moreover, the presence of “intervening slurry of abrasive particles” in the tribological contact originates in the three-body abrasion. Under high or low stresses, this kind of mechanism occurs during the masticatory process due to the presence of abrasive particles in the food bolus or it can occur during the wear process of dental surfaces with material loss and debris formation. Then, abrasive particles move along the surfaces in tribological contacts scratching away the antagonist surface. If the prosthetic dental joints act as a closed tribological system, the material loss will be higher than the loss in open systems where the abrasive particles move away from the tribological contact [16].

1.5.4 Simultaneous degradation of titanium by corrosion and wear interactions

Friction on titanium during mastication can destroy the TiO_2 film that leads to a material loss and possible failures of dental implants and prostheses. As a result from corrosion and wear processes, metallic ions are released, and wear particles originating from titanium were found in the surrounding tissues and associated to inflammatory reactions.

Different tribocorrosion mechanisms can take place during rubbing between a ductile metal (e.g., titanium) and a hard inert counter-body (alumina or zirconia), as shown in figure 1.29.

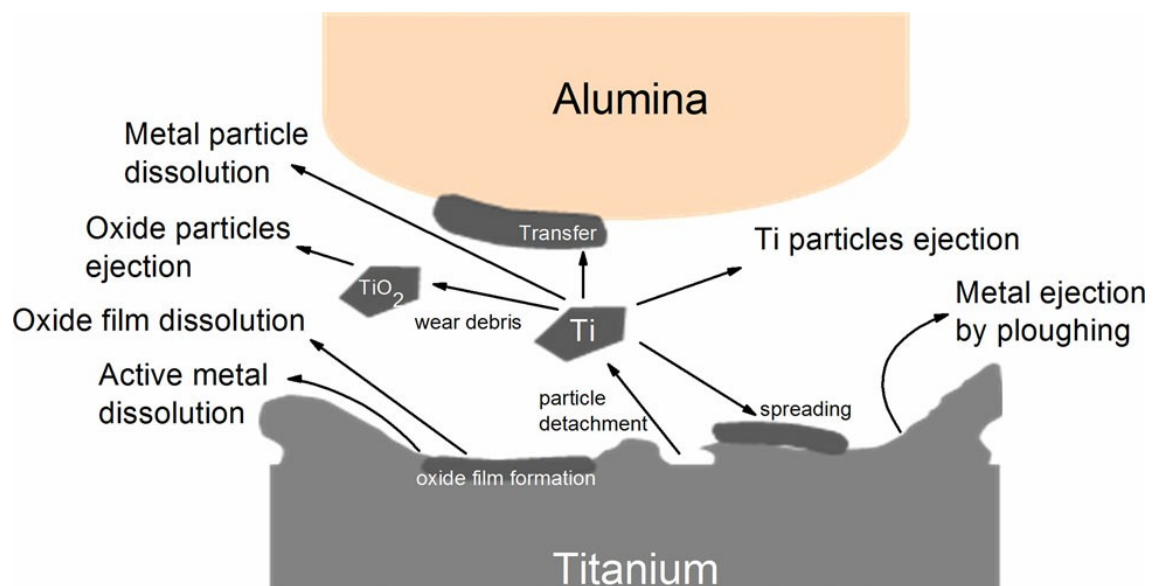


Figure 1.29: Schematic tribocorrosion mechanisms of titanium [16].

Mechanical and electrochemical mechanisms are responsible for the material removal from the hard less materials (first body) during rubbing. As a result, there is plastic flow with metal ejection by plowing and metal detachment forming third bodies (wear particles). The wear particles can be transferred and deposited on the alumina surface or spreading on the titanium surface by adhesive wear forming tribolayers. In contact with environment, the wear particles can be oxidized and form solid oxide that can modify the mechanic of contact. Then, a brittle oxide particle can be formed contributing to a



third-body abrasive mechanism and can extend the mechanical wear of titanium. On the other hand, a solid oxide can chemically dissolve as ions in the environment taking into account that there is also titanium dissolution and an ion release produced by electrochemical reactions between titanium and the environment. The metal detachment exposes a fresh titanium surface that reacts immediately with the environment corresponding to an anodic partial current and a subsequent increase of the corrosion rate due to the high chemical reactivity of bare metal. Then, a galvanic cell is established during the wear process in the electrolyte, where the bare metal (worn area) may act as an anode or a cathode, and its periphery, represented by the passive layer (unworn area), acts as a cathode or an anode, respectively. Consequently, there is a current flowing between anodic and cathodic areas, which induces an electrochemical potential distribution over the surface.

In fact, the chemical and mechanical properties of the titanium passive film influence the surface mechanical response of titanium as well as the third-body behavior. This comprises the repassivation rate of titanium that consists in the formation of a new TiO_2 film immediately after its mechanical destruction (depassivation). Barril et al. [116] studied the fretting corrosion of Ti6Al4V in 0.9% NaCl solution and revealed a strong influence of the electrode potential on the wear rate of titanium alloys. In addition, it was revealed that the oxidation of third-body particles at anodic potentials decreases the mechanical energy involved in the wear process. Considering the presence of fluorides, the wear processes on titanium in high fluoride solutions (12,300 ppm F^-) are quite different compared to the ones noticed in artificial saliva without or containing up to 227 ppm F^- . In fact, the formation of a reaction product layer on titanium at high F^- concentration decreases the coefficient of friction. However, a progressive corrosion of titanium has been detected by surface analysis, as well as by electrochemical measurements, indicating an active state of titanium in artificial saliva at high F^- concentration. The wear rate of titanium in sliding contacts was too fast at high fluoride concentration which could occur in titanium-based structures used in prostheses and dental implants. This last case could be a cause for failures of titanium-based implant systems considering that the material loss can increase microgaps in the prosthetic joints and modify the contact area of structural materials. As a consequence, the distribution

of loads on the implants could be altered promoting over-loads at certain contact areas. Additionally, over-loads can increase the wear rate of prosthetic materials exposed to relative contact motions.

In the presence of biofilms, tribocorrosion tests revealed a low friction on titanium covered with biofilms. The properties of the biofilms were similar to those of the lubricant agents used to decrease the wear rate of materials. However, the lowering of pH promoted by microbial species negatively affected the corrosion resistance of titanium surfaces. A wear-corrosion process that takes place during sliding of titanium-based contacting surfaces in a corrosive environment can be a cause of failure in dental implant-supported systems [16].

1.5.5 Interaction of wear debris with surrounding tissues

In the case of medical implants and prostheses, wear debris and ions release produced due to the loss of material by bio-tribocorrosion of prosthetic surfaces have been related to tissue inflammatory reactions. Additionally, some studies revealed a highly significant relationship between the amount of peri-implant inflammation and the magnitude of alveolar bone loss surrounding implants [117][118] that can be faster than that surrounding natural tooth due to the absence of inflammatory cellular response provided from periodontal ligament.

The presence of metallic ions and particles in human tissues induces the activation of macrophages, neutrophils and T-lymphocytes with elevation of cytokines and metallic proteinases that can promote bone resorption. Coalescence of particles of all classes (including titanium particles) originating from prostheses was often seen in the vesicles of macrophage cytoplasm in the liver (0.1–10 μm in diameter), spleen and para-aortic lymph nodes. In the lymph nodes, titanium particles ranged from 0.1 μm up to 50 μm , while in the liver and spleen the particles ranged from 10 μm .

Hallab et al. [119] investigated the binding of metals such as Ti, Co, Cr, Al (originating from implant wear and corrosion) to serum proteins that can mediate immune reactions.



Even though the long-term biologic effect of circulating metals is not completely known, it could be determined by the detection and characterization of these metal–protein complexes [120]. After wear tests of titanium alloys in vitro, Okazaki et al. [121] verified a low cellular growth in mediums containing Al and V compared to that in free-Al and free-V mediums. This indicates a potential cytotoxic effect of Al and V for human cells.

A significant release of Ti-, Al-, and V-ions has been reported in previous studies [113]. Literature data have revealed the release of Al- and V-ions caused by passive film dissolution, though those alloying elements confer good mechanical properties to Ti-alloys. A corrosion of metallic materials has been classified in three classes based on the ion release [122]: (Class I) $10 \mu\text{g}/\text{cm}^2$ week or less; (Class II) $10\text{--}100 \mu\text{g}/\text{cm}^2$ week or less; (Class III) $100\text{--}1000 \mu\text{g}/\text{cm}^2$ week. Based on Manaranche and Hornberger's [122] study, alloys of class III could stimulate an adverse biological response in patients due the high release of ions. In that respect, cp titanium and Ti6Al4V alloy could induce adverse biological reactions when in contact with high fluoride concentrations [113]. The release of aluminum ions may, however, be considered as a toxic element, while vanadium ions as a mutagenic agent.

An association between ultrafine TiO_2 (UF- TiO_2) (<100 nm in diameter) particles and adverse biologic effect has been reported in the literature [123][124]. Recent studies [122] in cultured human cells have also shown genotoxicity and cytotoxicity effects of UF- TiO_2 . However, the precise pathways of chromosomal changes, apoptosis formation, and inhibition of cell division by UF- TiO_2 are unclear. These findings led us to consider the possible adverse biological effect of TiO_2 particles (<100 nm in diameter) produced during bio-tribocorrosion mechanisms of titanium in the human body [16].

1.6 Surface characterization

In this section the main techniques used in this thesis work will be presented in a brief and simple way to evaluate the surface properties of the titanium samples. The greater emphasis will be given in illustrating the general physical principle that allows to exploit the potential of a certain technique, making reference and underlining the peculiar aspects of the analytical method and trying to give a complete and synthetic description.

1.6.1 Zeta potential

The definition and measurement of potential ζ is, typically, linked to the field of colloidal systems such as particle dispersions or emulsions. References to this property of systems are rarely found outside the context of colloid stability analysis. In the context of this thesis work, on the contrary, the potential ζ is used as a parameter for the analysis of the surface of solid samples.

Although the theoretical bases on which the potential is defined are the same, regardless of whether the technique is applied for the characterization of colloids or solid surfaces, a different approach is needed to understand the potential ζ in the field of solid surface analysis. To introduce the concept of potential ζ , it is considered necessary, first of all, to give a definition as clear as possible for the dispersions, and then go into detail to learn more about what the potential measure for solid surfaces consists of.

For the dispersions we start from the assumption that a particle dispersed in an electrolytic liquid generally has superficial electrostatic charges (for example, produced during the pulverization) that determine an electric field responsible for the redistribution of the ions present in the space that surrounds the particle itself. A distribution of this type involves an increase in the concentration of counterions (charge ions opposite to those of the particle) near the interface surface between the particle and the liquid that surrounds it [125]. The layer of liquid with the ions surrounding the particle, in particular, is characterized by the peculiarity of allowing the distinction of two zones: one internal and closer to the surface of the particle, called stationary layer

(of Stern), where ions are collected which undergo more strongly the influence of the surface charge of the dispersed particle; an external one, called the diffuse layer (of Gouy-Chapman), where the interactions are weaker and there are ions that suffer a weaker influence from the charged particle. The two zones constitute a double electric or electrochemical layer (EDL) around each particle. Within the diffuse layer (much thicker than the Stern layer) the ions form metastable structures: when the particle moves in the liquid, the ions move with it; in particular, the ions beyond the defined cutting plane are replaced and are continuously replaced by the free ions present in the liquid so that the dimensions of the EDL remain constant [125]. The diagram in Figure 1.30 shows, for a generic charged particle, the variation of the electric potential as a function of the distance from its surface: it can be seen how this decreases rapidly inside the stationary layer, more slowly inside the diffuse layer and then even more slowly, until it nullifies itself, by definition, to infinity. This model of charge behavior at the solid-liquid interface is usually indicated with the terminology of the EDL model.

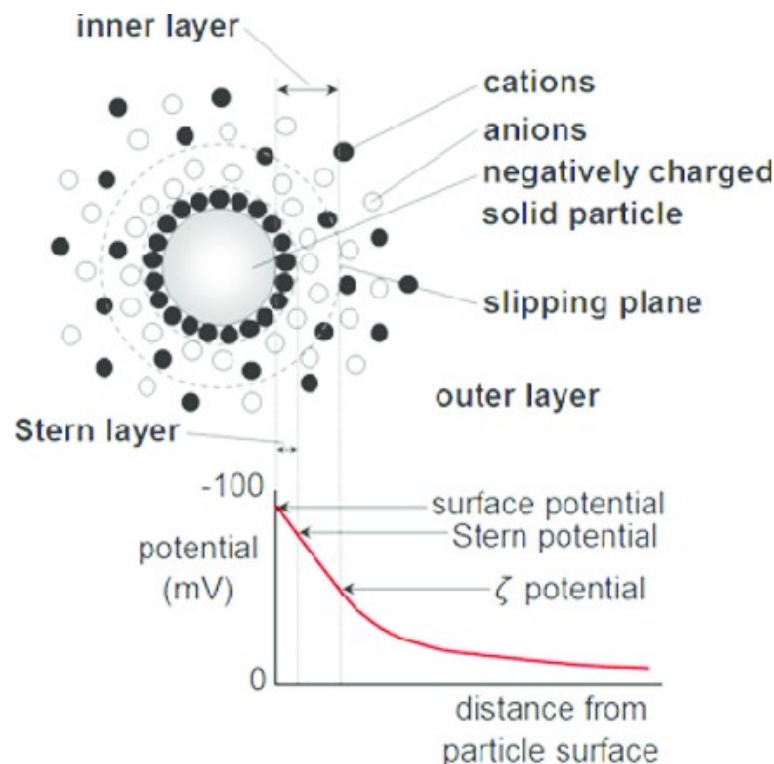


Figure 1.30: Definition of the potential ζ for dispersion particles [126].

Interesting considerations that derive from this theory are: the fact that the intrinsic charge present on the surface of a particle is shielded by the charges of the stationary layer; the fact that the interactions between particles of the same dispersion are regulated based both on the surface charge of the particles of the dispersion and on the shielding given by the presence of the stationary layer. Another important aspect to underline, which derives from the hypothesis of an EDL model, is the possibility of introducing the electrokinetic potential or potential ζ , a property associated with the studied particles. Imagining to move away gradually from the surface of the particle being schematized (Figure 1.30) along the curve in evidence in red, we arrive at a certain point to a plane defined as the cutting plane “slipping or shear plane” at which the potential is measured ζ . This potential value is very important for dispersed systems, because it can help define their behavior.

For solid surfaces, the concept of potential ζ is proposed in a similar way to the case of dispersions, even if, in this case, this value is indicative of the surface charge that is formed on the surface of a massive material placed in contact with an electrolytic aqueous system. The behavior of the charges at the solid-liquid interface of a massive material is also explained using the EDL model, according to which, due to the charge that the solid takes in aqueous environment, a stationary layer and a diffuse mobile layer of counterions are formed in the liquid phase which compensate the surface charge [127]. The potential ζ , also in the case of solid surfaces, is defined in correspondence of the shear plane, the cutting plane, ie the sliding zone between the mobile liquid phase and the stationary phase. The concept of EDL is illustrated schematically in a very simple way to understand in Figure 1.31 for the situation in which a certain surface has a uniformly distributed charge that is simply balanced by the total opposite charge given by the accumulation of the counterions in the electric double layer.

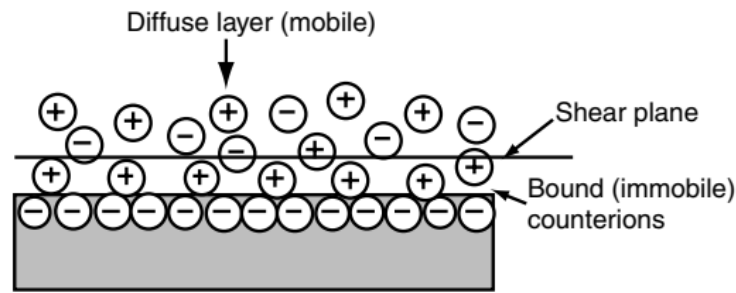


Figure 1.31: Definition of potential ζ for a flat surface [127].

There are several theories that allow us to give a mathematical description of the EDL: the simplest, and by now outdated, is Helmholtz's theory. This theory, later improved by Gouy-Chapman, has taken its final and most accurate form thanks to Stern's scientific contribution. The illustration of the different theories is presented, schematically, in Figure 1.32.

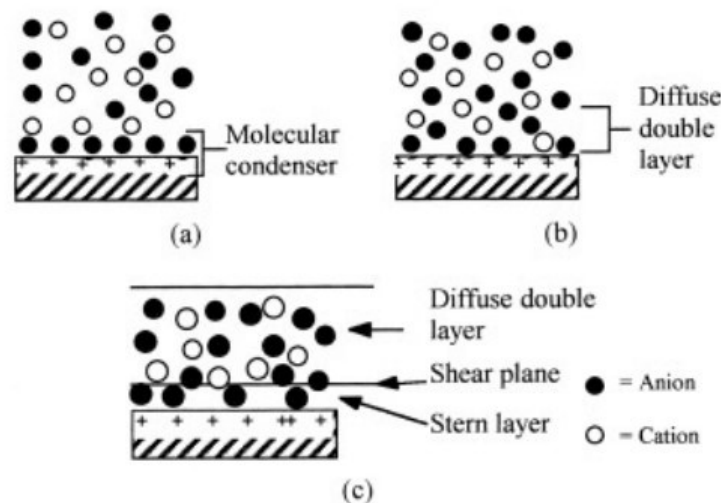


Figure 1.32: Classic models of flat surface-electrolyte interface. (a) Helmholtz model, (b) the Gouy-Chapman model and (c) the Stern model [127].

The idea of the EDL was initially formally proposed by Helmholtz, who developed the concept of a system with charges arranged on two parallel planes as shown in Figure 1.32, a. The Helmholtz model, in essence, is a sort of "molecular" capacitor and is relatively easy to describe mathematically. In reality, of course, the thermal motion of the ions in solution introduces a certain degree of chaoticity which causes the diffusion



of ions in the region of the charged surface, so that the diffuse double layer is formed. In this case, the mathematical description of the electronic environment near the surface is more complex and requires a more detailed analysis. For this reason the more accurate Gouy-Chapman double layer model was developed (Figure 1.32, b). In the approach of these authors, the surface is assimilated to an infinite plane on which a continuous electric charge is distributed in contact with a solution containing point charges of opposite charge. At an infinite distance from the surface the electric potential is identified with that of the solution, while in the vicinity of the surface it gradually changes up to assume the value corresponding to the surface itself. In a better approximation of reality, then, it is necessary to take into account that ions occupy a defined amount of space, so they have certain steric requirements. This last consideration leads to a further refinement of the EDL theory: the Stern model. This author attributes a certain volume to the ions, so that the distance of their centers from the surface cannot be less than the radius; furthermore, in his theory Stern takes into account that at short distances from the surface chemical interactions can take place, associated to the adsorption processes, between the ions and the atoms of the surface itself, interactions that occur when the ions reach a comparable surface distance with binding distances. In essence, the model predicts the existence of the Stern layer, that is a small space that separates the diffuse layer, where the counterions are weakly attracted to the surface, from the steric "wall" present in the stationary state and formed by the most strongly retained counterions, for electrostatic reasons, to the load plane (Figure 1.32, c). The thickness of the Stern layer, shown in Figure 1.32, c, is usually of the order of a few nanometers and reflects the size of those groups of charged ions held by the surface with the opposite charge. In other words, the Stern plane divides the EDL into two separate parts, localizing itself at a distance approximately equal to the radius of the hydrated ion most strongly attracted by the surface charge of the studied object [127].

Given the complexity, the complete mathematical equation for the description of the EDL according to the Stern model is not discussed in the context of this thesis, but the hypotheses and consequences related to the assumption of the Stern model are further discussed below. The knowledge of the potential ζ in fact derives from the measurement

of electrokinetic phenomena, detection in turn connected, as just anticipated, to the determination of the surface charge of a certain sample under investigation.

An important consequence of the existence of electric charges (in a static equilibrium situation) at the interface between solids and electrolytic liquids, leads in fact to introduce the following further considerations. The electrical charges at the interface between solids and electrolytic liquids show certain phenomena under the influence of an applied electric field correlated to the movement of part of the EDL. These phenomena (illustrated schematically in Figure 1.33) collectively defined as electrokinetic phenomena, comprise four main classes: (a) electrophoresis; (b) electroosmosis; (c) flow potential (streaming potential); (d) sedimentation potential.

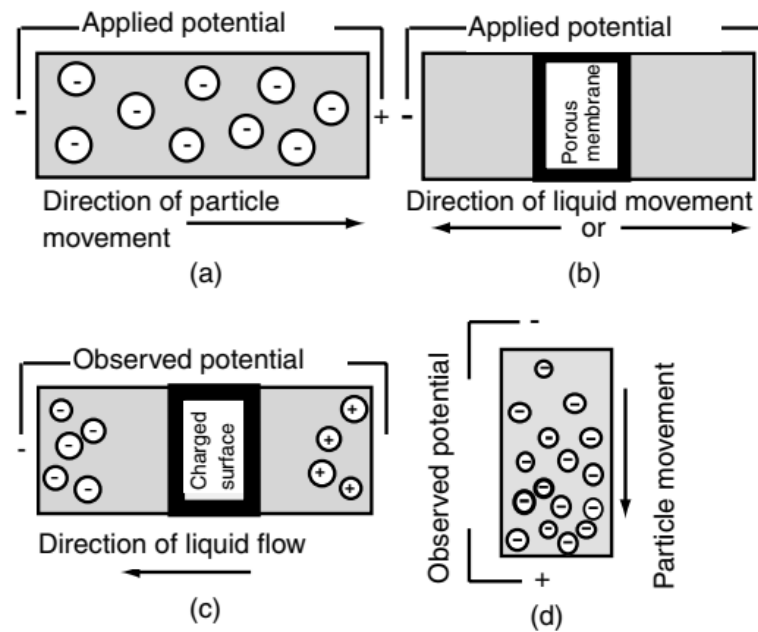


Figure 1.33: Scheme of the four types of electrokinetic phenomena [127].

The electrokinetic phenomena originate from the fact that a liquid, moving tangentially to a surface, does not drag with it the whole double layer; only a part is free to move with it, while a part remains anchored to the solid; this creates a separation of charges parallel to the interphase that gives rise to a potential difference, as in Figure 1.33 (c). If, on the other hand, an electric field is applied, the positive or negative charges that have been created in the diffused zone of the double layer tend to migrate towards the

opposite electrodes, as in Figure 1.33 (d). If the solid is fixed, a displacement of the liquid phase takes place, as occurs in electroosmosis, as in Figure 1.33 (b). If the solid is instead made up of a dispersion of particles, they tend to move, as occurs in electrophoresis, as in Figure 1.33 (a).

In the following discussion, attention is focused only on the flow potential technique (streaming potential), as a method used to measure the potential of the samples produced for the experiments.

When an electrolytic solution is made to flow through a capillary due to a pressure difference, there is the presence of a difference in electrical potential between two electrodes located at the ends of the conduit. If the electrolyte solution flows through a capillary, it is therefore possible, depending on the case, to measure a direct voltage or a direct current. The capillary through which the aqueous solution flows can be irregularly shaped (such as the voids between the particles of a bed of dust or the fibers of a fibrous matrix) or regular (like the channel that is created between two planar surfaces of a material). In any case, when the solution is made to flow in the capillary, shear forces are generated on the counterions present in the mobile part of the EDL that is formed near the surface of the capillary; such counterions begin to move in the direction of the flow. This is how a current potential is generated; its origin is precisely this phenomenon of transport, by the fluid current, of the EDL ions. As a result, a charge separation is generated between the inlet and outlet of the capillary which creates an electrical force that opposes the flow. Thanks to two electrodes placed at the ends of the capillary, the associated flow potential can be detected.

The electrokinetic phenomenon called flow potential is measured in this way. It starts from the assumption that there is a motion relative to the interface between a solid phase and a liquid phase. When an electrolyte solution moves with respect to a charged surface, in fact, the effects of viscosity require that only a certain portion of the EDL (up to the Stern layer, approximately) move. As previously stated, ions in the Stern layer remain relatively firm on the surface, because they are held electrostatically. Thus the presence of the so-called shear plane is outlined, which consists of the boundary line

between the area where there is movement of ions in solution and the area where there are instead fixed ions held by the charged surface [128].

If the Stern layer is assimilated to a condenser of thickness δ , the charge density at the surface can be expressed through the relation

$$\sigma_0 = \frac{\varepsilon}{\delta}(\psi^0 - \psi_\delta) \quad (1)$$

where ψ^0 is the value of the potential at the surface, while ψ_δ is the potential value at the Stern surface, which decays towards zero in the diffuse layer, as it moves away from the charged surface, in accordance with an exponential relationship

$$\psi(z) = \psi^0 e^{-\chi z} \quad (2)$$

The parameter χ is expressed by

$$\chi^2 = \frac{8\pi e^2}{\varepsilon k_B T} \sum_i C_i^0 Z_i^2 \quad (3)$$

where e is the electron charge, ε is the dielectric constant of the liquid, k_B the Boltzmann constant, T the temperature and where C_i^0 indicates the concentration of the i -th ion in the heart of the solution while Z_i is the charge associated with it. Equation (2) is an approximate solution, which gives the dependence of the potential from the coordinate z according to the Debye-Hückel approximation. According to Equation (2) the potential decreases exponentially, and the term $1/\chi$ has the dimensions of a length and represents the thickness in which the double surface layer is essentially located.

Combining the Poisson equation

$$\frac{d^2\psi}{dz^2} = -\frac{4\pi\rho}{\varepsilon} \quad (4)$$

with Equation (2) describing the Debye-Hückel approximation, we obtain the following expression of the charge density as a function of the z coordinate:

$$\rho = -\frac{\varepsilon}{4\pi} \frac{d^2\psi}{dz^2} = -\frac{\varepsilon}{4\pi} \chi^2 \psi^0 e^{-\chi z} \quad (5)$$

from which is obtained, as value of surface electric charge density (ie referred to the unitary area) σ_0 the expression

$$\sigma_0 = -\int_0^\infty \rho(z) dz = \int_0^\infty \frac{\varepsilon}{4\pi} \frac{d^2\psi}{dz^2} dz = -\frac{\varepsilon}{4\pi} \left(\frac{d\psi}{dz} \right)_0 = \frac{\varepsilon \chi \psi^0}{4\pi} \quad (6)$$

from which it can be observed that the surface potential ψ^0 is linked both to the surface charge density and to the ionic composition of the medium. For example, if χ increases, the double layer is compressed and therefore either it must increase σ_0 or it must decrease ψ^0 .

In physical reality, going to measure experimentally directly the value of ψ_δ is impossible; to do this it would be necessary to place an electrode in the plane passing through the center of the first layer of adsorbed atoms. However, it is possible to determine the quantity closest to ψ_δ : the potential ζ , by means of measurements that involve the relative motion of the solid surface with respect to the liquid, ie electrokinetic measurements. If we consider a flat surface lapped by a fluid current in laminar motion, it is in fact possible to define an ideal plane parallel to it, where the shear stress is located and at which a rapid variation in viscosity occurs. In reality, the exact position of this plane, as already mentioned, is not known, also because solvent

molecules must be added to the surface ions. However, it can be reasonably assumed that this plane is placed at a distance just outside the Stern plane, so the potential ζ is marginally lower than ψ_δ . Often it is even assumed that the values of ζ and ψ_δ are identified. The determination of the exact position of the cutting plane is not trivial. The cutting plane, in reality, is a very thin region in which the viscosity effects change rapidly and is therefore difficult to determine by position. The most significant errors, which can occur when measuring the potential at the cutting plan, may be due to: high potentials; high concentrations of electrolytes; presence of massive non-ionic adsorbed species that clutter up and move the cutting plane farther away from the surface. It is usually assumed that this plane lies just outside the Stern layer and, at it, we try to measure the potential ζ .

In conclusion, to understand how in practice we go back to the measurement of potential ζ in the present case study, it is necessary to introduce Equation (7), which is fundamental to correlate the flow potential to the potential ζ :

$$\zeta = \frac{I_{str}}{\Delta p} \frac{\mu}{\varepsilon \varepsilon_0} \frac{l}{A} \quad (7)$$

Equation (7), known as the Helmholtz-Smoluchowski equation, provides a linear relationship between the flow rate of the liquid and the potential ζ and plays an important role in the study of electrokinetic phenomena. Since it does not contain geometric parameters characteristic of the system under examination, this expression offers a tool for tracing directly to the value of the potential ζ from the measured values [129]. Its validity has been confirmed by the experimental results, which show that the intensity of the current is proportional to the volumetric flow rate. However, the application of the Helmholtz-Smoluchowski equation requires an exact knowledge of the flow channel geometry (ie the cell constant l/A). For a thin rectangular cell, for example, the length L and the width W are determined by the size of the solid sample. The height of the distance H is calculated from the flow rate of the measured volume of the liquid passing through the flow channel and from the differential pressure generated.

The measure of potential ζ just described in mathematical terms in the most generic way possible, essentially depends on many different parameters. As reported in Table 1.3 the potential ζ at the solid-liquid interface is influenced by a series of different properties of both the solid material and the liquid phase.

Table 1.3: Solid, liquid and interfacial properties that influence the zeta potential at the liquid solid interface [130].

Liquid properties	Solid properties	Other
pH value	Porosity	Measuring time
Ionic strength	Electronic conductance	Temperature
Additive concentration		Material swelling

In addition, for the flow potential measurements, the aspects of the volumetric flow rate of the solution and the size of the capillary used for the analyzes are of particular importance.

As for the effect of the ionic strength of the electrolyte on the reproducibility of the potential measurement ζ with the current potential method, there are no great uncertainties. The experiments can be conducted by using an aqueous solution of known ionic strength. Typically, an electrolyte with a 1:1 dilution ratio (NaCl, KCl, KNO₃) is used at the ionic strength of 0.001 mol/l. As for the other parameters, the machinery for measuring the ζ potential is designed to have control over every aspect of the investigation.

1.6.2 Wettability

The contact angle is the most commonly used technique in scientific laboratories to determine the wettability of a surface. The principle on which this technique is based is physically described by Young's law, which corresponds to the balance of the total forces acting on a drop of negligible volume deposited on an ideal surface.

$$0 = \gamma_{SV} - \gamma_{SL} - \gamma \cos(\vartheta_c) \quad (8)$$

In equilibrium, in fact, the shape of a drop of liquid (L) falling on the surface of a solid (S) in the presence of a vapor phase (V) is regulated by the balance between three surface tension components (γ_{SL} , γ_{SV} , γ_{LV}). Considering the section of a drop of liquid deposited on a solid, the contact angle is therefore the angle comprised between the direction of the solid-liquid tension and the direction of the liquid-vapor tension, tangent to the external surface of the drop, with the vertex in the three-phase liquid-solid-vapor point (Figure 1.34).

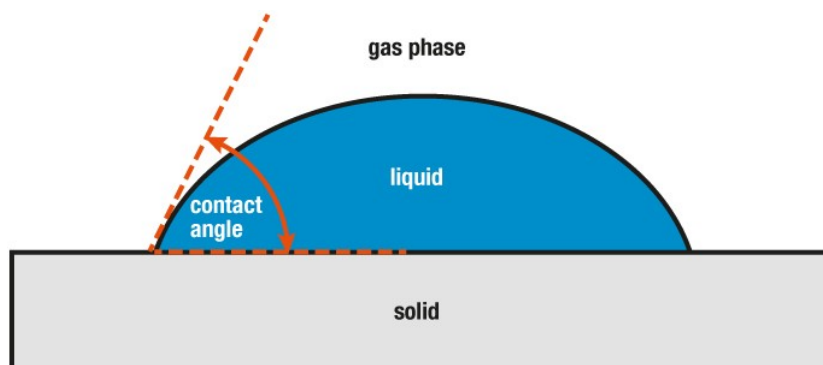


Figure 1.34: Contact angle. Angle between the line tangent to the point of contact and the horizontal line represented by the solid surface under study [131].

In summary, therefore, when a drop of liquid is placed on a solid surface, the liquid has the possibility of behaving in two ways: (i) spreading on the surface to form a thin, approximately uniform film; (ii) distributed to a limited extent but still with a discrete drop shape on the surface (Figure 1.35).

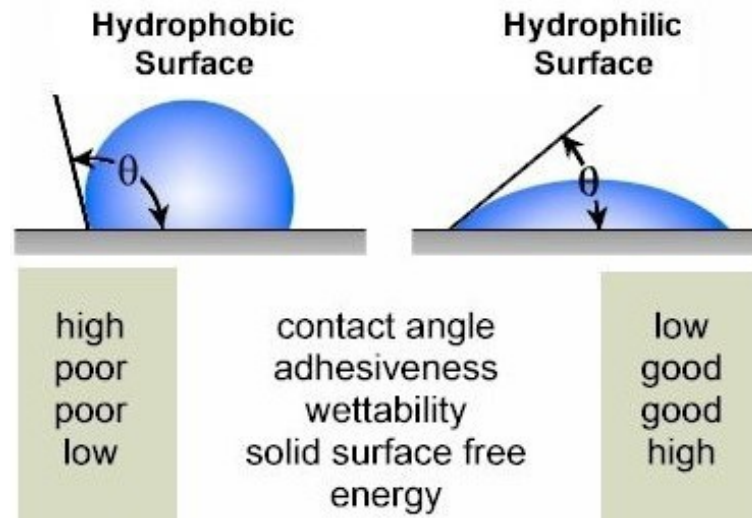


Figure 1.35: Hydrophobic and hydrophilic surface. Properties compared [131].

The final condition of the liquid poured on the surface is considered as an indication of the wettability of the surface by the liquid or, vice versa, of the ability of the liquid to wet the surface, depending on the point of view of the operator performing the analysis. The quantitative measurement of the wetting process is considered as the contact angle. At this point, different scenarios are distinguished. In the case of a liquid that forms a uniform film (ie, where $\theta = 0$), it is said that the solid is completely wetted by the liquid, or that the liquid wets the solid. If, on the contrary, a drop with a contact angle other than zero forms between surface and liquid, there are discussions about how to describe the system. The topic is debated. By convention, in this thesis work, reference will be made to the best known classification used in the academic world, which provides for the definition of hydrophobic surfaces having an angle of contact of equilibrium with water greater than 90 degrees, hydrophilic surfaces with angles less than 90 degrees, as shown schematically in Figure 1.36.

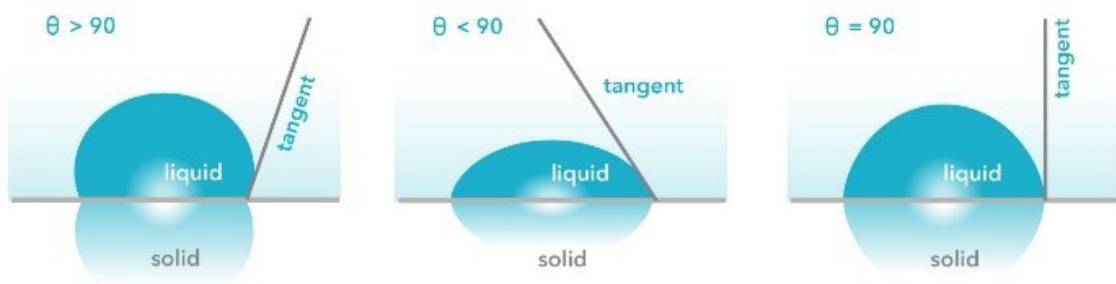


Figure 1.36: Contact angles that define the hydrophilicity/hydrophobicity of a solid surface against a given liquid [131].

Found agreement on the definitions, there are still some aspects of the contact angle measurement which deserves further study. It has been said that the contact angle of a liquid on a solid can be considered a characteristic of the system, but this is true only if the angle is measured under certain conditions of equilibrium, time, temperature, purity of the components and other parameters. The contact angles, therefore, even if they are rather simple measures to carry out and can bring significant information about the surface properties, if not carried out taking the necessary precautions can instead be very misleading. Added to these considerations is the fact that the observation of the physical phenomenon, ie the formation of the drop on a given surface, and the visual evaluation of the image presented to the operator is the only known method (albeit poorly safe and reproducible) to conduct the survey to measure the contact angle. These premises, if taken as a whole, can easily lead to taking note of how the correct interpretation of the contact angle measurement on a real surface is a very complex measure. First of all, the valid surface hypothesis in Young's law decays immediately when dealing with any real surface, whose roughness and heterogeneity, as one can easily guess, is far from ideality. Then, as anticipated, due to the different initial conditions of the system (for example, the ways in which the drop is deposited, the ambient humidity of the room in which the measurement is performed, etc.) the possible onset of different metastable balances must be considered, under whose conditions the shape of the drop can remain constrained and to which correspond different values of contact angles. For this reason it is not always possible to define an equilibrium contact angle value. Then, often, we perform different measures and we go to detect what is



called dynamic contact angle, determining two different angles: one of advancement and one of recession. We speak of a dynamic contact angle in the case of a drop of liquid in motion on the surface of a solid. In the dynamic contact angle measurement, the contact angle varies according to the intersection point between the phases (considered with respect to the direction of motion): the angle with the highest value is called the advance, the lower value is called the recession, and their difference is called the contact angle hysteresis. In fact, the contact angles often have hysteresis and cannot be uniquely defined in some experimental conditions. There are different ways of measuring dynamic contact angles, among which the most common are the Wilhelmy scale and the sessile drop [132]. In the present thesis work only the angle measurement method of equilibrium contact has been exploited for the surface characterization of the samples under analysis. As regards the environmental conditions in which the measurement is carried out, there are no particular precautions to follow. It is sufficient to test the sample you want in contact with small drops of liquids (for example, water or other solvents).

With regard to the information that the equilibrium contact angle measurement allows to obtain, it should be noted that the technique, while being very sensitive to the sample surface chemistry, at the same time provides indirect indications overall. Thanks to the equilibrium contact angle measurement it is in fact possible to obtain information on the surface energy of the material, on the wettability, on the degree of hydrophilicity / hydrophobicity of the surface. It is also possible to investigate the possible presence of polar or apolar components dispersed on the surface, and also to evaluate whether particular superficial rearrangements of the sample can significantly alter the wettability properties.

In conclusion, as shown also in the diagram in Figure 1.37, there is a relationship between wettability and surface energy of the material / surface tension. In materials science surface tension is defined, strictly speaking, as the surface density of binding energy on the interface between a continuous body and a material of another nature (for example a solid, a liquid or a gas). It is therefore clear from this definition that surface tension is a valid parameter to quantify the force necessary for the breakage of the intermolecular bonds that form the surface itself.

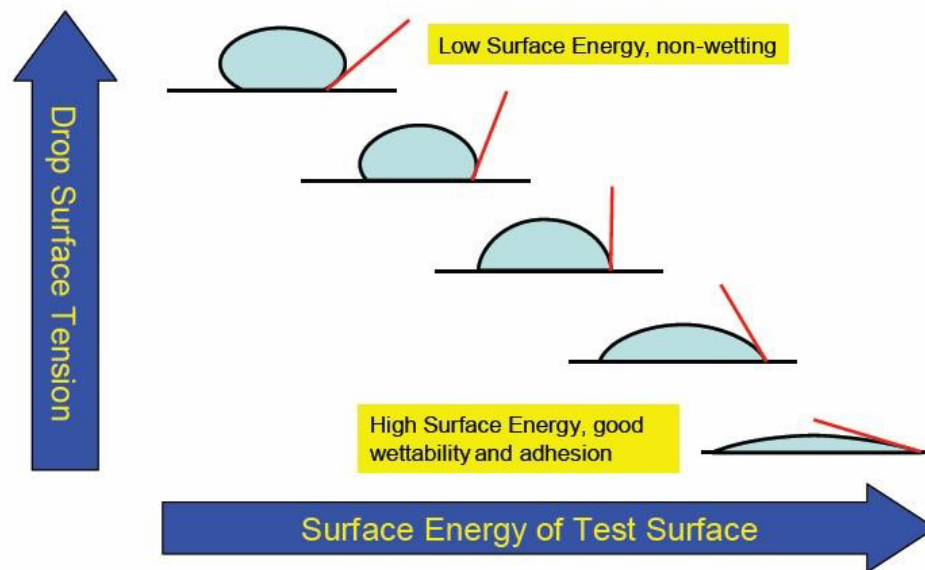


Figure 1.37: Relationship between wettability of a solid surface and surface energy [133].

If for liquids the surface tension coincides with the surface energy, for solids the discourse is different and we must distinguish between high-energy solid surfaces and low-energy solid surfaces. High-energy solid surfaces have strong chemical bonds (ionic, metallic or covalent) between atoms and are completely wetted by most polar liquids. The low-energy solid surfaces are instead made up of atomic species held together by weak bonds (physical interactions of the Van der Waals bond or hydrogen bond) and can be wet completely or partially, depending on the liquid used for the tests of wettability.

From the considerations just explained it is possible to understand how, in the case of solid biomaterials such as titanium, the study of wettability and surface energy is of considerable importance to predict the interaction of the biomaterial itself with the biological environment. The contact angle measurements are able to provide useful hints in the case in which we need to investigate the surface behavior of titanium in contact with solutions of different types.

2. Materials and methods

This chapter is divided into two parts, as the two types of tests carried out evaluate different properties and characteristics.

2.1 Tribological tests

2.1.1 Disk materials

The disks used were made of commercially pure titanium (ASTM B348, Gr2, Titanium Consulting and Trading) (Figure 2.1) and Ti6Al4V alloy (ASTM B348, Gr5, Titanium Consulting and Trading) (Figure 2.2) and they were obtained from cylindrical bars. In particular, the disks had a diameter of 10 mm and a thickness of 2 mm. The chemical composition of the two materials is reported in Table 2.1 and Table 2.2, respectively.



Figure 2.1: Commercially pure titanium (Ti cp) disk.

Table 2.1: Chemical composition of Ti cp disks.

Element	Percent by weight
N	0.03 % max
C	0.10 % max
O	0.25 % max
Fe	0.30 % max
H	0.0155 % max
Ti	Balance
Other	0.4 % max



Figure 2.2: Titanium alloy (Ti6Al4V) disk.

Table 2.2: Chemical composition of Ti6Al4V disks.

Element	Percent by weight
Ti	90 %
Al	6 %
V	4 %
C	< 0.10 %
O	< 0.20 %
N	< 0.05 %
H	< 0.0125 %
Fe	< 0.3 %

2.1.2 Ball material

The balls used were made of zirconium oxide (ZrO_2), also called “zirconia”, partially stabilized with yttrium (Y-TZP) (CERATEC TECHNICAL CERAMICS BV, The Netherlands) (Figure 2.3). Their composition is 94.7 wt% ZrO_2 + 5.3 wt% Y_2O_3 .

The diameter of the balls was 6 mm.



Figure 2.3: Zirconia ball.

2.1.3 Composition of artificial saliva

In this project two different artificial saliva were used, both in the form of oral spray:

- Biotène (Figure 2.4) – Ingredients: aqua, glycerin, xylitol, peg-60 hydrogenated castor oil, vp/va copolymer, aroma, sodium benzoate, xanthan gum, methylparaben, propylparaben, sodium saccharin, cetylpyridinium chloride, limonene. The pH value was measured with a pH meter and is 6.06.



Figure 2.4: Biotène spray, 30 ml, SmithKline Beecham Ltd, EUCH CQ.

- BioXtra (Figure 2.5) – Ingredients: aqua, xylitol, hydrogenated starch hydrolysate, sorbitol, hydroxyethylcellulose, sodium monofluorophosphate, sodium saccharin, potassium chloride, sodium chloride, magnesium chloride, dipotassium phosphate, calcium chloride, colostrum whey, lactoperoxidase, citric acid, sodium benzoate, sodium methylparaben, sodium propylparaben, potassium sorbate.

The pH value was measured with a pH meter and is 7.33.

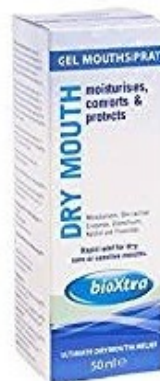


Figure 2.5: BioXtra spray, 50 ml, Lifestream Pharma n.v., s.a.

In these experiments the Biotène and the BioXtra are used in order to simulate the lubricant present in the oral cavity, ie the natural saliva; in fact the purpose of the study is to evaluate any differences in the use of one or the other.

To better understand the differences between the two artificial saliva used, the compounds present in both have been identified and are described below:

- Aqua (water) → is a chemical compound of molecular formula H_2O , in which the two hydrogen atoms are bound to the oxygen atom with polar covalent bond (Figure 2.6). It is a clear, odorless, tasteless liquid and is an excellent solvent for many substances.

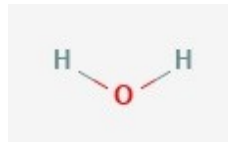


Figure 2.6: Structure formula of water.

- Xylitol → is a pentitol (five-carbon sugar alcohol) having meso-configuration (Figure 2.7), being derived from xylose by reduction of the carbonyl group. It is a colorless or white solid that is soluble in water. The molecular formula is $C_5H_{12}O_5$.

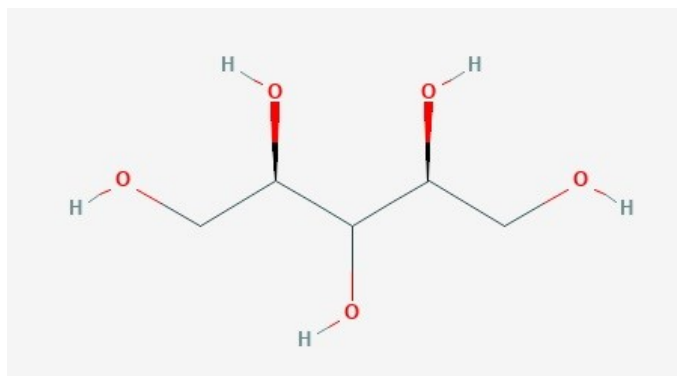


Figure 2.7: Structure formula of xylitol.

- Sodium benzoate → is the sodium salt of benzoic acid (Figure 2.8). At room temperature it appears as an odorless white solid. Its molecular formula is $C_7H_5O_2Na$. It is an organic sodium salt resulting from the replacement of the proton from the carboxy group of benzoic acid by a sodium ion.

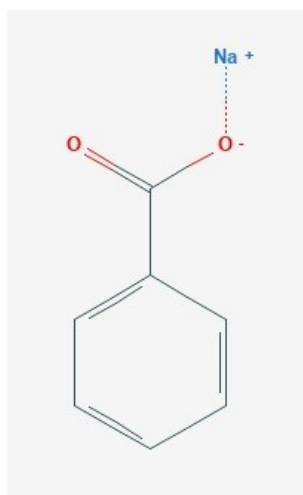


Figure 2.8: Structure formula of sodium benzoate.

- Sodium saccharin → is the sodium salt of saccharin (Figure 2.9), highly soluble in water; flavoring agent and non-nutritive sweetener. The molecular formula is $C_7H_4NNaO_3S$.

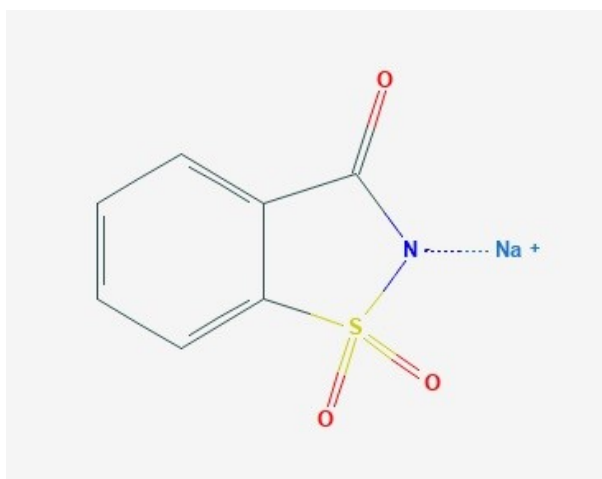


Figure 2.9: Structure formula of sodium saccharin.

The compounds present only in the Biotène are the following:

- Glycerin → also called glycerol (Figure 2.10), is a simple polyol compound. It is a colorless, odorless, viscous liquid that is sweet-tasting and non-toxic. Glycerol has three hydroxyl groups that are responsible for its solubility in water and its hygroscopic nature. The molecular formula is $C_3H_8O_3$.

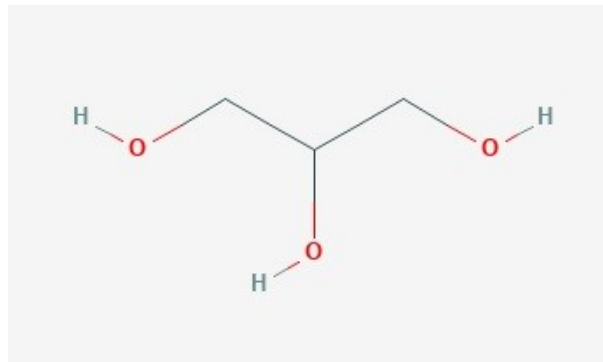


Figure 2.10: Structure formula of glycerol.

- PEG-60 hydrogenated castor oil → is a polyethylene glycol derivative of hydrogenated castor oil with an average of 60 moles of ethylene oxide. Polyethylene glycol (PEG) is produced by the interaction of ethylene oxide with water, ethylene glycol (Figure 2.11). PEG is a flexible, water-soluble polymer. The molecular formula is $(C_2H_4O)_nH_2O$.

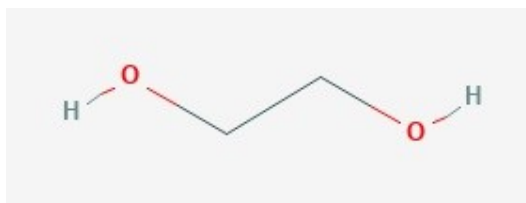


Figure 2.11: Structure formula of ethylene glycol.

- VP/VA copolymer → is a polymer prepared by combining relatively small chemical compounds called monomers into a very large molecule that has very different properties. VP/VA Copolymer (Figure 2.12) is a large molecule made from vinyl pyrrolidone (VP) and vinyl acetate (VA) monomers. The copolymer only contains residual amounts of the original monomers. It is a white, free-flowing powder. The molecular formula is $C_{10}H_{15}NO_3$.

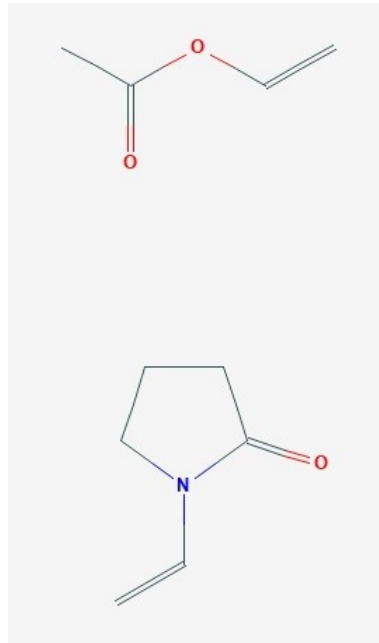


Figure 2.12: Structure formula of VP/VA copolymer.

- Xanthan gum → also called corn sugar gum (Figure 2.13), is a polysaccharide used as a food additive and rheology modifier. It is produced by fermentation of glucose or sucrose by the *Xanthomonas campestris* bacterium. The molecular formula is $C_{36}H_{58}O_{29}P_2$.

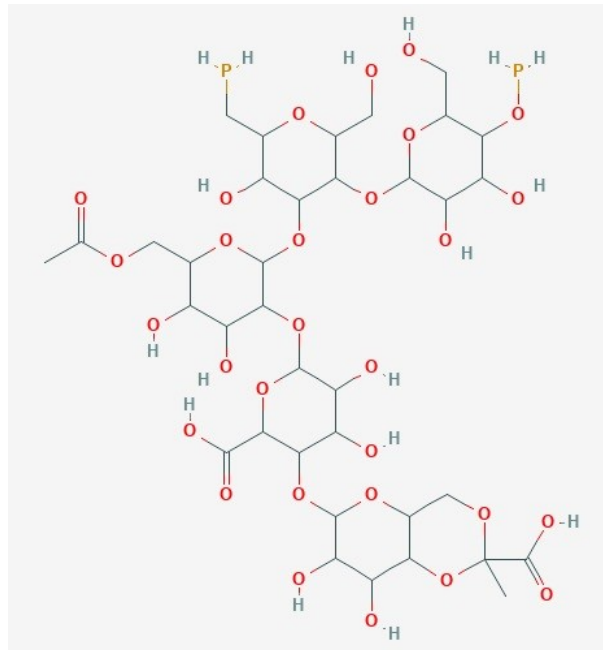


Figure 2.13: Structure formula of corn sugar gum.

- Methylparaben → is a 4-hydroxybenzoate ester resulting from the formal condensation of the carboxy group of 4-hydroxybenzoic acid with methanol (Figure 2.14). It is a Standardized Chemical Allergen. The molecular formula is $C_8H_8O_3$.

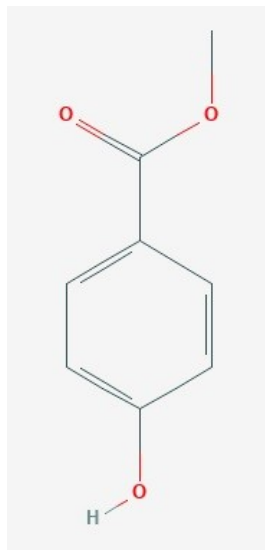


Figure 2.14: Structure formula of methylparaben.

- Propylparaben (Figure 2.15) → colorless crystals or white powder or chunky white solid, is an antimicrobial agent, preservative, flavouring agent. It is a Standardized Chemical Allergen. The molecular formula is $C_{10}H_{12}O_3$.

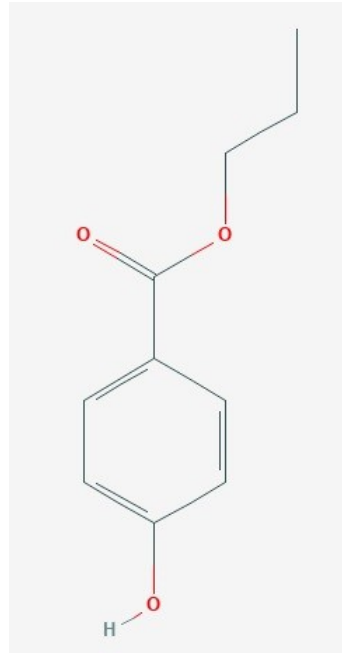


Figure 2.15: Structure formula of propylparaben.

- Cetylpyridinium chloride → is a pyridinium salt that has N-hexadecylpyridinium as the cation and chloride as the anion (Figure 2.16). It has a role as an antiseptic drug and a surfactant. It is a chloride salt and an organic chloride salt. It contains a cetylpyridinium. The molecular formula is $C_{21}H_{38}ClN$.

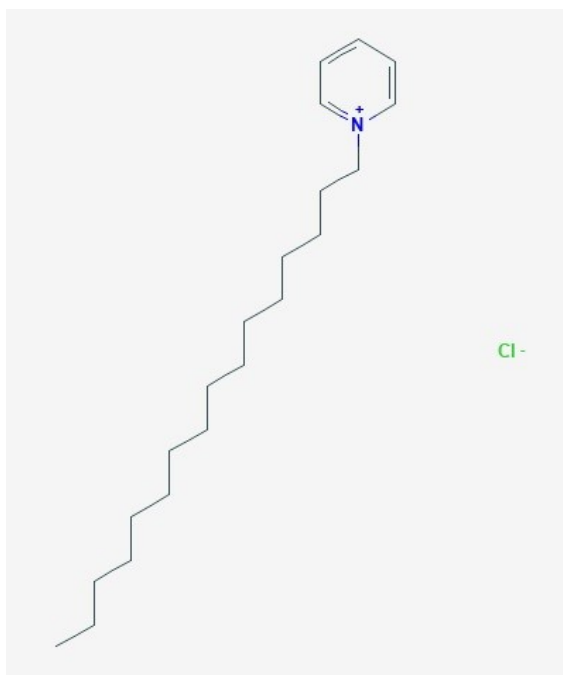


Figure 2.16: Structure formula of cetylpyridinium chloride.

- Limonene → is a monoterpene (Figure 2.17) with a clear colourless liquid at room temperature, a naturally occurring chemical which is the major component in oil of oranges. Limonene is widely used as a flavor and fragrance and is listed to be generally recognized as safe in food by the Food and Drug Administration (FDA). It is a botanical (plant-derived) solvent of low toxicity. The molecular formula is $C_{10}H_{16}$.

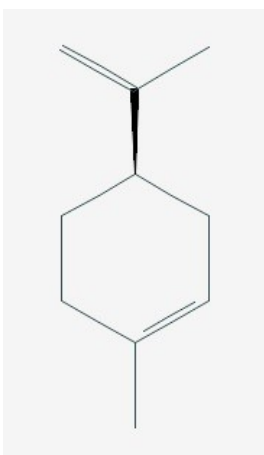


Figure 2.17: Structure formula of limonene.

The compounds present only in the BioXtra are the following:

- Hydrogenated starch hydrolysates (HSHs) → are mixtures of several sugar alcohols (a type of sugar substitute). The molecular formula is $C_{18}H_{34}O_{16}$. They are produced by the partial hydrolysis of starch – most often corn starch, but also potato starch or wheat starch. This creates dextrans (glucose and short glucose chains). The hydrolyzed starch (dextrin) then undergoes hydrogenation to convert the dextrans to sugar alcohols. They are similar to sorbitol: if the starch is completely hydrolyzed so that only single glucose molecules remain, then after hydrogenation the result is sorbitol. Because in HSHs the starch is not completely hydrolyzed, a mixture of sorbitol, maltitol, and longer chain hydrogenated saccharides (such as maltotriitol) is produced. When no single polyol is dominant in the mix, the generic name hydrogenated starch hydrolysates (Figure 2.18) is used.

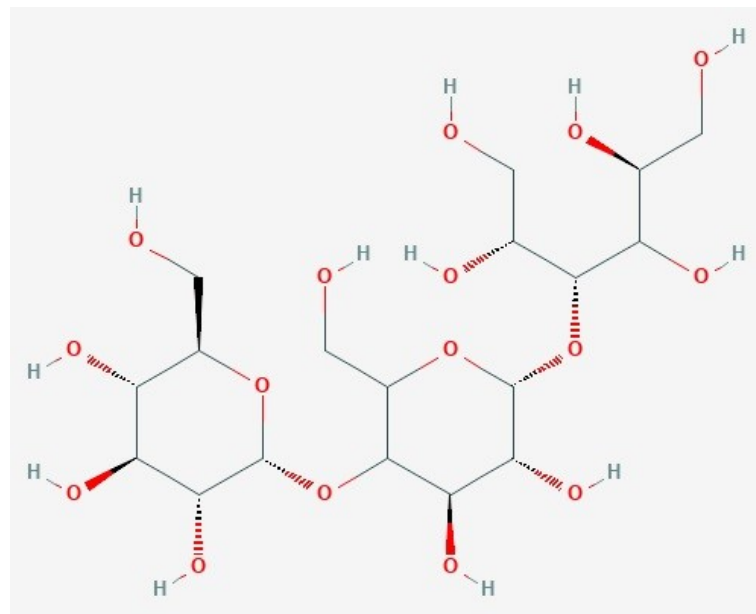


Figure 2.18: Structure formula of HSHs.

- Sorbitol → is a polyhydric alcohol with about half the sweetness of sucrose. It occurs naturally and is also produced synthetically from glucose. The molecular formula is $C_6H_{14}O_6$.

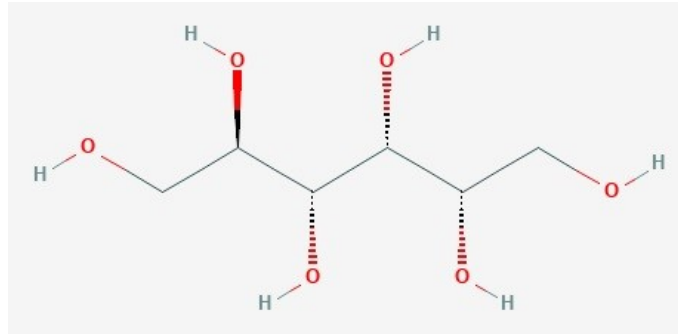


Figure 2.19: Structure formula of sorbitol.

- Hydroxyethylcellulose (Figure 2.20) → is a polysaccharide derivative with gel thickening, emulsifying, bubble-forming, water-retaining and stabilizing properties. It is used as a key ingredient in many household cleaning products, lubricants and cosmetics due to its non-ionic and water-soluble nature. It is often used as an ingredient in ophthalmic pharmaceutical preparations such as artificial tear solutions and adjunct agent in topical drug formulations to facilitate the delivery of drugs with hydrophobic character. The molecular formula is $C_{36}H_{70}O_{19}$.

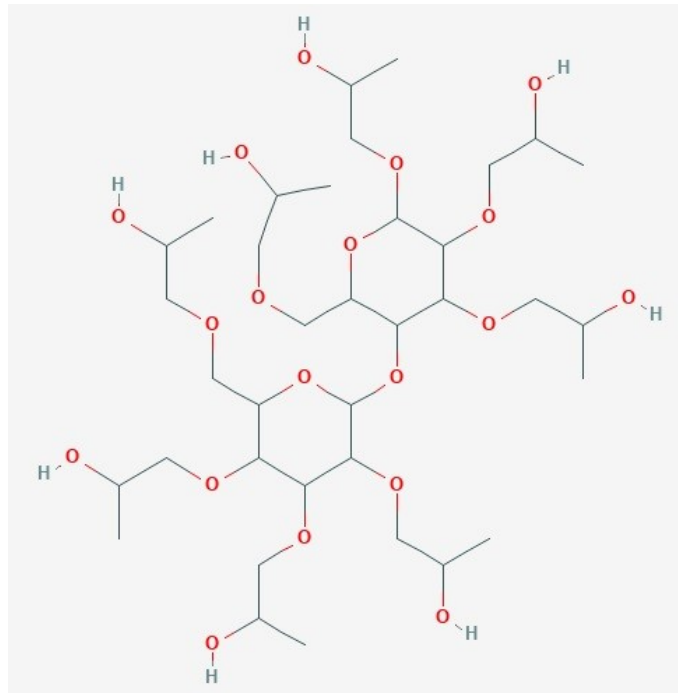


Figure 2.20: Structure formula of hydroxyethylcellulose.

- Sodium monofluorophosphate → is sodium fluorophosphate, commonly abbreviated MFP (Figure 2.21), is an inorganic compound with the chemical formula $\text{Na}_2\text{PO}_3\text{F}$. Typical for a salt, MFP is odourless, colourless, and water-soluble. It has a role as an antibacterial agent. It is an inorganic sodium salt and an inorganic phosphate.

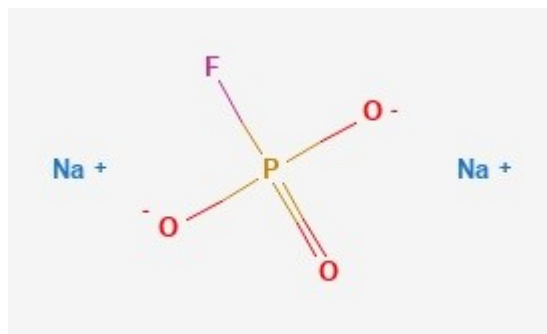


Figure 2.21: Structure formula of sodium monofluorophosphate.

- Potassium chloride → is a metal halide composed of potassium and chloride (Figure 2.22). It is a white crystal or crystalline powder. The chemical formula is KCl.



Figure 2.22: Structure formula of potassium chloride.

- Sodium chloride → is a metal halide composed of sodium and chloride with sodium and chloride replacement capabilities (Figure 2.23). It is a white crystalline solid. The chemical formula is NaCl.



Figure 2.23: Structure formula of sodium chloride.

- Magnesium chloride → is a magnesium salt comprising of two chlorine atoms bound to a magnesium atom (Figure 2.24). It is a magnesium salt, an inorganic chloride and a magnesium halide. The chemical formula is MgCl₂.

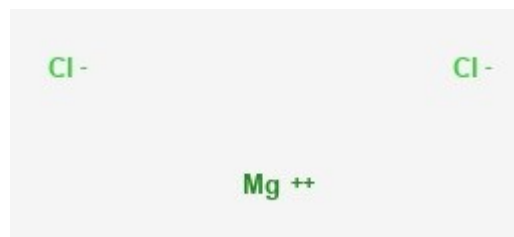


Figure 2.24: Structure formula of magnesium chloride.

- Dipotassium phosphate → is a potassium salt that is the dipotassium salt of phosphoric acid (Figure 2.25). The molecular formula is K_2HPO_4 .

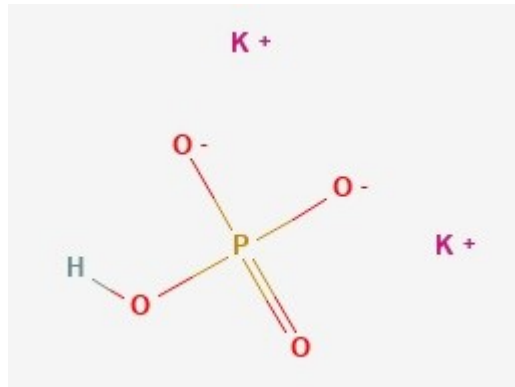


Figure 2.25: Structure formula of dipotassium chloride.

- Calcium chloride → is an ionic compound of calcium and chlorine (Figure 2.26). It is highly soluble in water and it is deliquescent. It is a salt that is solid at room temperature, and it behaves as a typical ionic halide. It is a white to off-white solid. The chemical formula is $CaCl_2$.

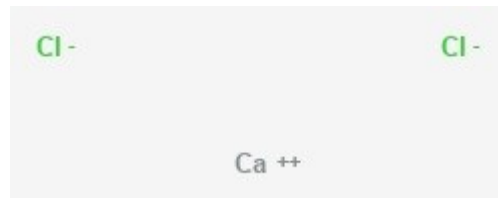


Figure 2.26: Structure formula of calcium chloride.

- Colostrum whey → comes from cows and is usually produced two to four days after they have given birth. This fluid contains a rich store of antibodies and other substances that help protect calves from infection, enhance their immune function and promote growth.

- Lactoperoxidase → is a peroxidase enzyme secreted from mammary, salivary, and other mucosal glands that functions as a natural antibacterial agent. It is a member of the heme peroxidase family of enzymes. Lactoperoxidase catalyzes the oxidation of a number of inorganic and organic substrates by hydrogen peroxide. The oxidized products produced through the action of this enzyme have potent bactericidal activities.
- Citric acid (Figure 2.27) → is a weak organic acid that has the chemical formula $C_6H_8O_7$. It is an acid compound found in citrus fruits.

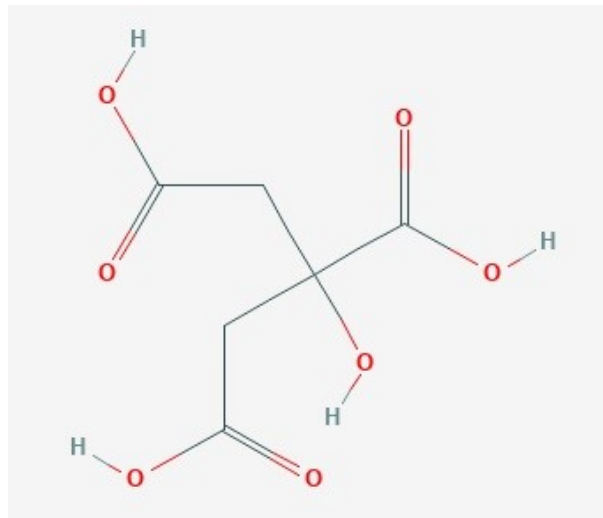


Figure 2.27: Structure formula of citric acid.

- Sodium methylparaben → is the sodium salt of methylparaben (Figure 2.28) with chemical formula $C_8H_7NaO_3$. At room temperature it appears as a white solid almost odorless.

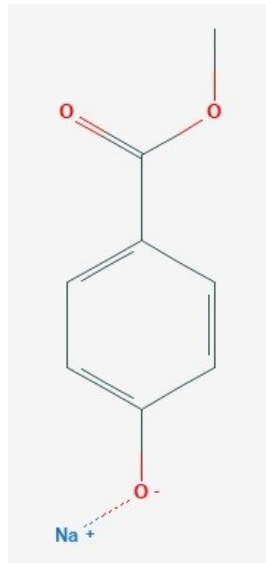


Figure 2.28: Structure formula of sodium methylparaben.

- Sodium propylparaben → is the sodium salt of the 4-hydroxybenzoic acid and 1-propanol ester (Figure 2.29) with chemical formula $C_{10}H_{11}NaO_3$. At room temperature it appears as a white solid almost odorless.

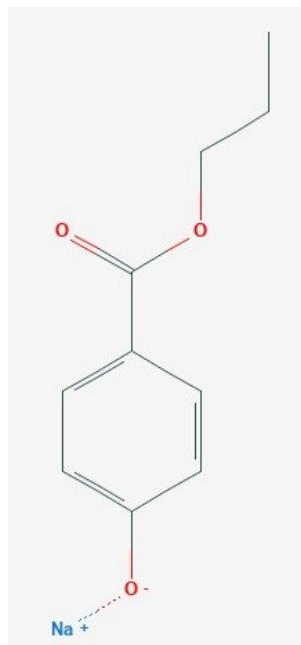


Figure 2.29: Structure formula of sodium propylparaben.

- Potassium sorbate → is the potassium salt of sorbic acid (Figure 2.30) with chemical formula $C_6H_7KO_2$. It is a white salt that is very soluble in water.

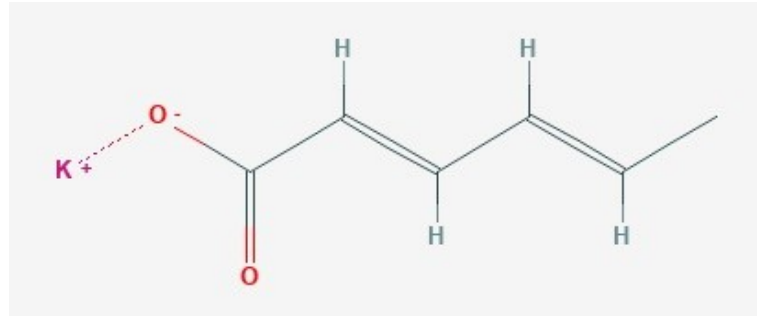


Figure 2.30: Structure formula of potassium sorbate.

2.1.4 Sample preparation

Prior to the tests, the disks have been polished (Figure 2.31) using abrasive paper with different roughness, in particular, increasing grit values have been used (320, 360, 500, 1000, 2000).



Figure 2.31: Polishing machine, Knuth-Rotor 2, Struers.

In order to facilitate polishing, the samples were hot-glued on a cylindrical metal support (Figure 2.32).



Figure 2.32: Support used to polish disks.

After the polishing phase, the samples (both the balls and the disks) were ultrasonically cleaned, separately, in ethanol for 10 minutes twice (Figure 2.33) and then dried with compressed air.



Figure 2.33: Ultrasonic cleaner, Branson 2510.

2.1.5 Instrumentation

Tribological experiments were performed using a tribometer (High Frequency Reciprocating Rig TR-282, Ducom). Ducom HFRR is a ball on disc type tribometer (Figure 2.34). The ball is driven by a motor and cam system to achieve a fixed stroke length of 1 mm and at variable reciprocating frequency. The disc is fixed inside a fluid cell which is heated externally by a pair of resistive heaters. The fluid cell is connected to a flexure carrying a piezoelectric sensor, that is used to measure the friction force generated at the ball on disk interface. Ball is loaded on the disc using the dead weights. This entire unit is enclosed in an environment chamber with a humidity control system.

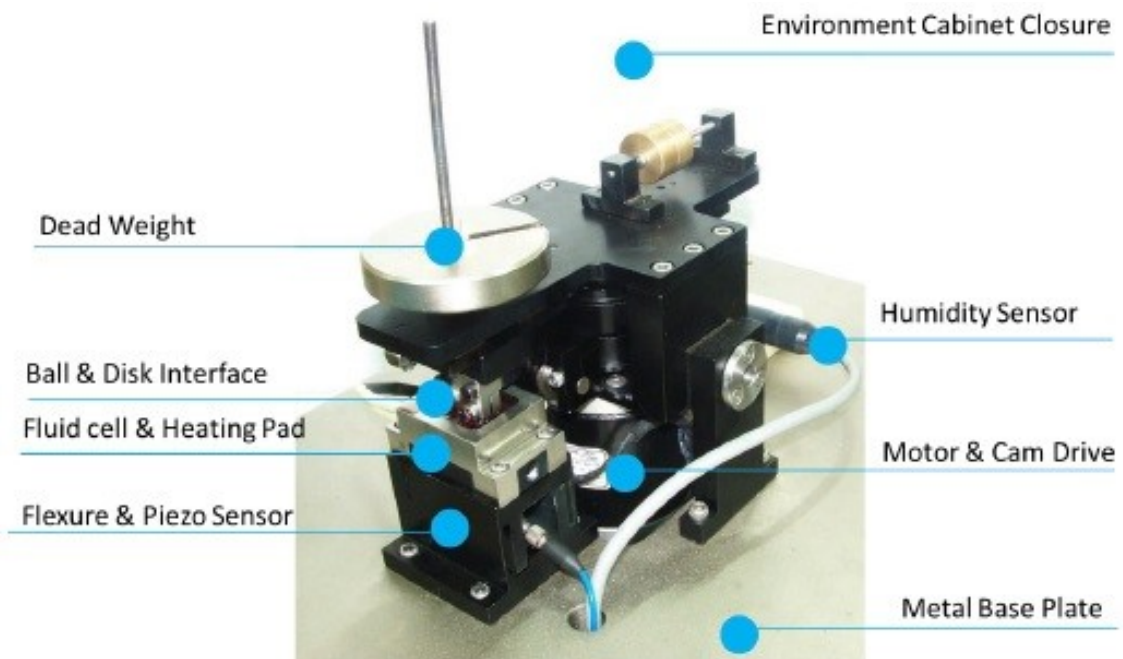


Figure 2.34: Description of Ducom HFRR.

Table 2.3 shows the technical specifications of the machinery.

Table 2.3: Technical specifications of Ducom HFRR.

Parameter	Unit	Range	Remarks
Load	N	1 to 10	Manual loading
Stroke length	mm	1	
Temperature	deg C	RT to 100	Software controlled
Humidity	% RH	35 to 80	Software controlled
Frequency	Hz	10 to 60	Software controlled
Ball holder	mm	6	
Disc holder	mm	10 x 3	
Fluid reservoir	ml	2	

The operating parameters in Ducom HFRR is controlled by a labview based WinDucom software (see Figure 2.35). It acquires and displays the friction force, friction coefficient, temperature and humidity. Operating frequency and load has to be manually entered into the software. Results of different tests can be superimposed for comparative viewing. Data can be exported to other file formats including excel CSV.

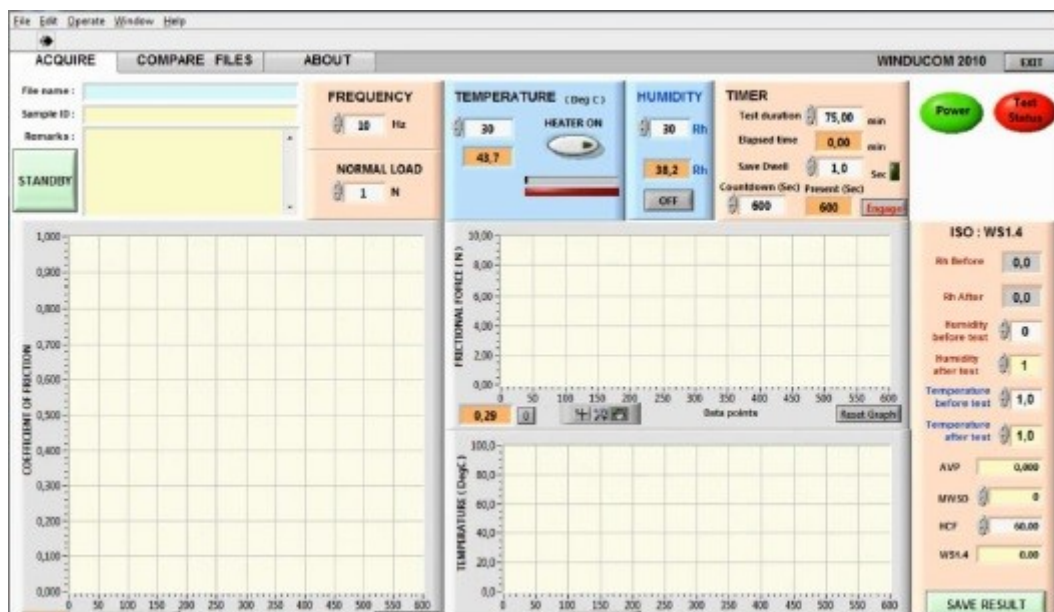


Figure 2.35: WinDucom software screen for Ducom HFRR.



The main features of this test rig are mentioned below.

- The moving specimen is mounted in a holder; it is reciprocated mechanically against fixed lower specimen. The mechanical drive comprises a motor driving an eccentric Cam assembly, providing pure sinusoidal motion. The moving specimen is pressed against the fixed specimen by dead weight.
- The fixed specimen (bottom specimen) is clamped on the heater block above Flexure, flexures are stiff in vertical (loading) direction, but offer limited resistance to horizontal forces. Movement in the horizontal direction is restrained by a piezoelectric force transducer, which measures frictional force in the reciprocating contact. The heater holder and piezoelectric transducer are mounted on a common surface, this not only provides seismic isolation from machine vibrations at high frequencies, but also permits other assemblies to be fitted to extend the operating range of the machine.
- The piezoelectric transducer used to measure friction force as output range to match expected friction level in the contact. The maximum friction level ± 40 N. The charge amplifier converts the measured force to proportional voltage. This is followed by low pass filter, which fixes the upper part cut off frequency of measuring system. This serves to suppress the resonance. Final scaling of the signal for voltage output takes place in 2nd stage amplifier.
- Since the top and bottom specimens are completely immersed in lubricant, the reciprocating motion produce only minimum frictional heating, the temperature measured by RTD sensor is due to only conduction from heater body.
- This rig has PC based sequence programmable control and data acquisition by integrating through NI card and WINDUCOM 2010 software; software is compatible on operating system WINDOWS 2007 and installed on PC, the acquired Data are stored to hard disc in standard spread sheet of compatible file formats.
- Tests are defined by a sequence of steps, each step containing set point, recording rates and alarm levels information. Set points may be adjusted by step change or ramp. The rest sequence is followed unless interrupted by the operator or an alarm. Set point may also be adjusted manually using on screen toggles.



All mechanical assemblies are mounted over a thick base plate, the reciprocating motion is by the rotation of a dc motor, the motor is freely suspended on bearings fitted to two housings; the arms of these housings are connected 180° apart to LM guide to reciprocate on either side. Inner dia of eccentric cam is tightened to motor shaft and its outer dia passes through bearings inside housings. The cam outer body has 0.5 mm eccentricity for 12 mm long on either ends, offset at 180°, the bearing of one housing fits into lower portion of cam and bearing of other housing fits into the top portion of cam. As motor rotates the eccentricity on cam pushes the top and bottom housing out of center by 0.5 mm, to prevent complete rotation the arms of housings are connected to LM guides through reciprocating supports locked by cylindrical pins. The cylindrical pin ensures easy disassembly during repair or for rework.

Two LM guides are fixed on either ends to the base of a top plate, top plate is pivoted to base plate through two cylindrical pins supported on pillars, the base of pillars are lined with hylam sheet. The pivot is at the center of top plate it provides a friction less free oscillatory movement to top plate. When motor rotates the eccentric cam fixed on motor shaft drives the two housings, since the arm of housing is connected to LM guide, the housing does not rotate but moves forward and backward by 0.5 mm on either direction to complete 1 mm stroke length. Corresponding action is performed by the other housing but at 180° apart, during one-half of revolution of motor the cam is designed to simultaneously push both housings outwards to reciprocate on LM guides, and to reciprocate inwards during the other half of rotation. Thus for one rotation of motor, one reciprocating cycle is completed, = 1 forward + 1 backward motion = 2 mm movement by top specimen over bottom specimen. Since it is single station, only one bottom specimen holder (Figure 2.36) is mounted for conducting tests, the other side of reciprocation is only for balancing the motion.



Figure 2.36: Bottom specimen holder.

The top specimen holder (Figure 2.37) is screwed to the reciprocatory support fixed on the sliding portion of LM Guide, the arm of housing is locked to this reciprocatory support by a cylindrical pin, as motor rotates the support reciprocates on LM guide. The top specimen usually spherical ball is tightened between two hardened jaws to retain position without skidding during reciprocation, one of the hardened jaw is permanently tightened to reciprocating support, for changing specimen, unscrew two screws visible in the front to loosen the front jaw to remove ball.



Figure 2.37: Top specimen holder.

The bottom specimen holder clamps disc specimen and holds 2 ml of fluid for test, it is in rectangular shape with inner surface having cavity to fix bottom specimen (disc) at middle with screws and topping with 2 ml lubricant to immerse the specimen completely. The base of specimen holder is tightened to flexure top face; the flexure is

positioned over base plate for the top specimen to be at the middle the bottom specimen. A heater block is placed above Flexure to heat sample oil, the specimen holder bottom face rests on the top face of heater block, transferring heat to oil bath. For heating two cartridge heaters are imbedded inside block and a RTD Sensor is fixed to base of holder to measure oil temperature. The measured oil temperature is the feedback device used for controlling heating.

The flexure works on the principle of parallel beam, it is stiff in vertical (loading) direction, but offer limited resistance to horizontal forces. Movement in the horizontal direction is restrained by a piezo electric force transducer, which measures frictional force in the reciprocating contact. The piezo electric transducer is mounted on vertical limb to provide seismic isolation from machine vibrations at high frequencies.

Normal load is applied by top specimen by dead weight (Figure 2.38) placed over the loading pin fixed on oscillating top plate, the loading pin center passes through the top specimen center, the top plate is balanced with an adjustable counter balance with thimble nut, for the top plate with specimen not to exert any initial load on bottom specimen.

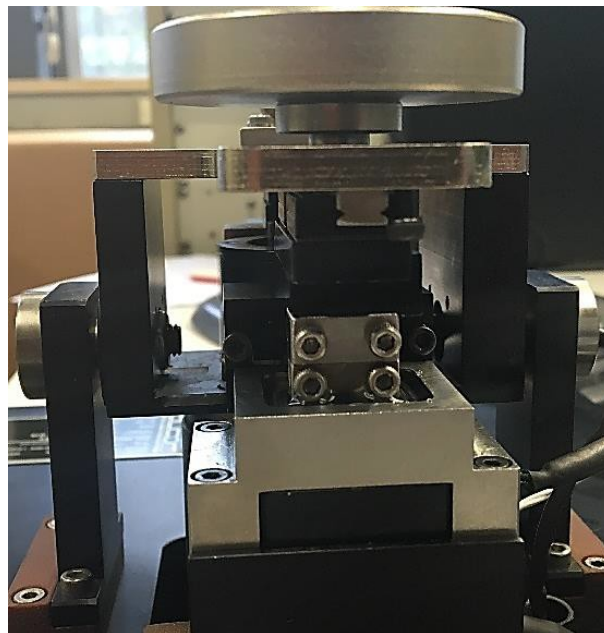


Figure 2.38: Manual loading system or dead weight.

A schematic representation of the test setup is reported in Figure 2.39.

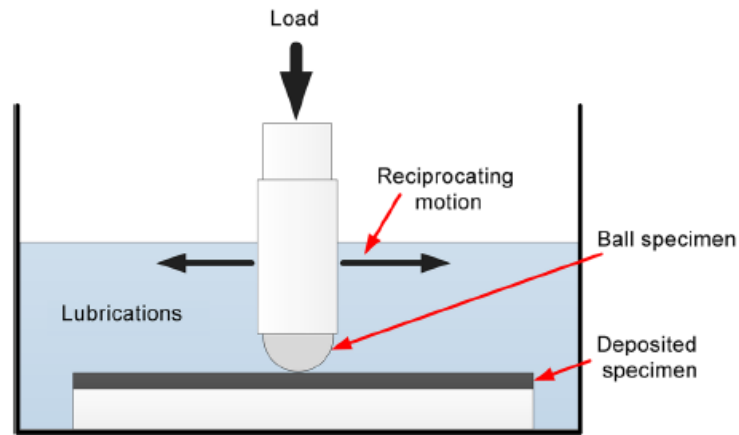


Figure 2.39: Schematics of the test setup.

Two-dimensional images of the disks and balls were acquired both before and after each test using an optical microscope (AmScope, ME300 Series and Olympus Vanox-T, Leica Microsystems B.V., Netherlands, respectively for the disks and the balls) (Figure 2.40).

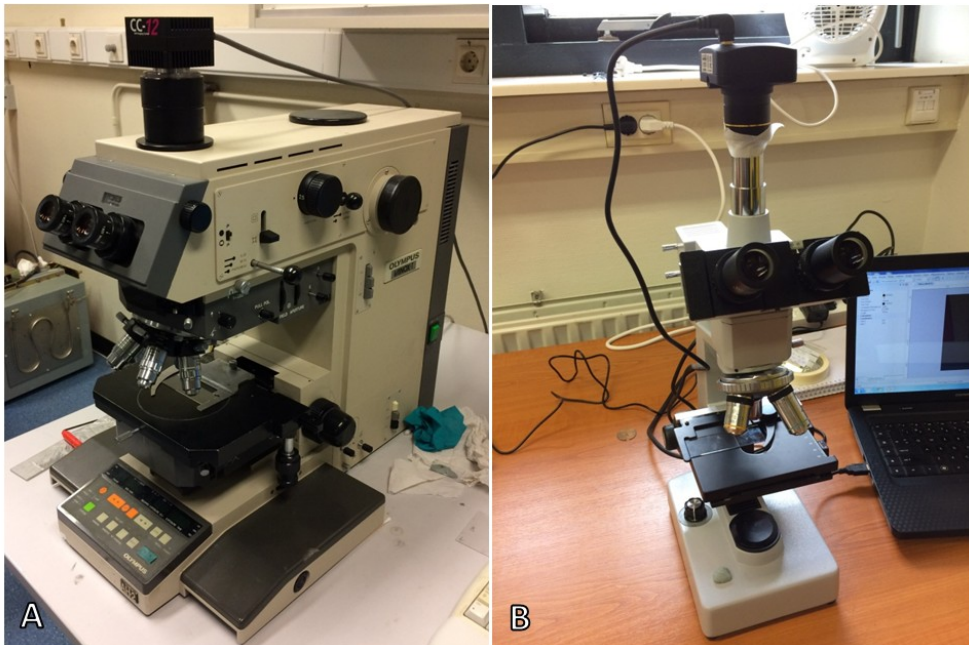


Figure 2.40: Optical microscopes, Olympus Vanox-T, Leica Microsystems B.V. (A) and AmScope, ME300 Series (B).

2.1.6 Experimental test procedure

Previously to the test, a control image of each disk and ball was taken using an optical microscope, as mentioned before.

Then the following procedure was performed for each test:

- The metal disk has been mounted on the disk holder and secured with two screws; then the sample was cleaned with ethanol.
- The zirconia ball was mounted on the ball holder and secured with two screws; then the sample was cleaned with ethanol.
- The two holders (Figure 2.41) have been fixed to the machine using the appropriate screws.

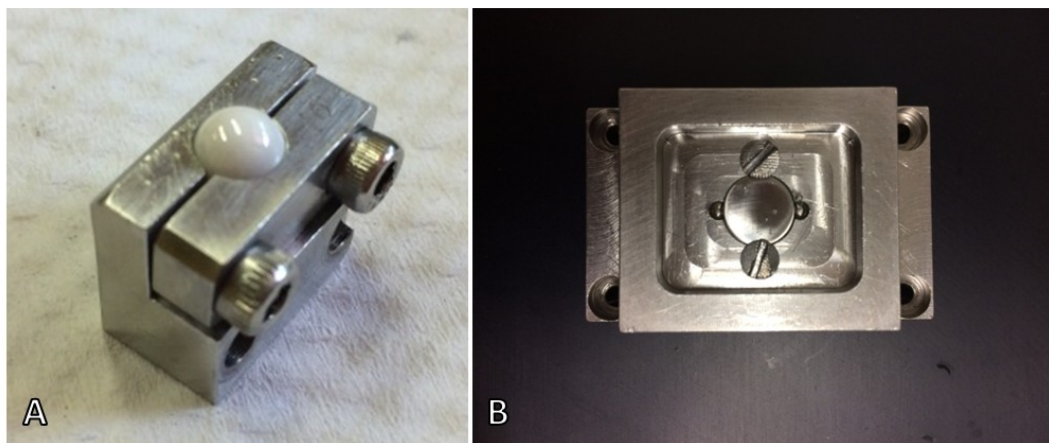


Figure 2.41: Sample holders, top specimen holder with zirconia ball (A) and bottom specimen holder with metal disk (B).

- The lubricant, or artificial saliva, was taken and measured with a syringe; then it was poured into the reservoir of the disk holder, covering the sample completely.

- The established normal load was applied manually in the appropriate seat located above the ball holder using a dead weight; in this way the zirconia ball and the metal disk come into contact (Figure 2.42).

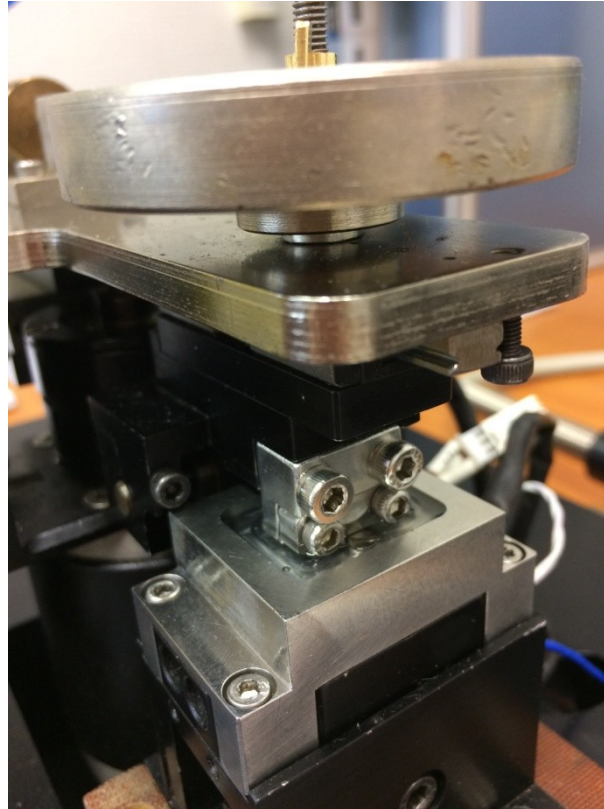


Figure 2.42: Samples in contact and completely immersed in artificial saliva after applying dead weight.

- The environmental case was closed (Figure 2.43) and the test parameters (frequency, temperature and duration) were set on the computer using the WinDucom software.

The operating parameters were fixed for all the tested materials to ensure repeatability of the tests and to significantly compare the tribological behavior of the different materials. A summary of the test parameters is reported in table 2.4.

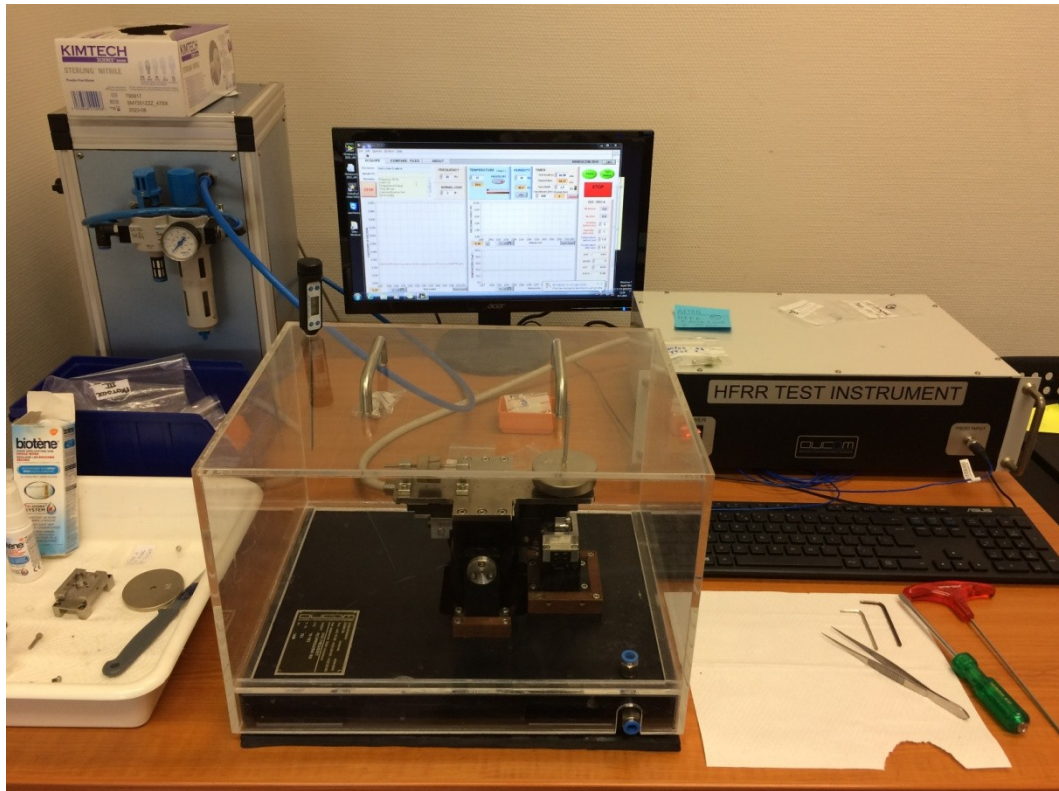


Figure 2.43: Overall view of the HFRR.

Table 2.4: Summary of the main test parameters.

Parameter	Unit	Value
Load	N	2
Frequency	Hz	30
Stroke length	mm	2
Velocity	mm/s	60
Temperature	°C	37
Duration	min	60
Lubricant volume	ml	2

Three tests were performed for each tribo-pair to ensure the repeatability of the testing procedure.

2.2 Zeta potential tests

2.2.1 Disk materials

See Chapter 2.1.1.

2.2.2 Composition of artificial saliva

See Chapter 2.1.3.

2.2.3 Sample preparation

Prior to the tests, the disks have been polished (Figure 2.44) using abrasive paper with different roughness, in particular, increasing grit values have been used (300, 600, 1000, 2500).



Figure 2.44: Grinding/polishing machine LaboPol-2, Struers.

In order to facilitate polishing, the samples were incorporated into an acrylic cold mounting resin: working under suction hood, each disk was placed in a mounting cup and the components (a large measuring cup of LevoCit Powder and a small measuring

cup of LevoCit Liquid) were then mixed thoroughly and poured over the specimen (Figure 2.45). The drying time was 30 minutes.



Figure 2.45: cold-embedded samples in the acrylic resin.

After the polishing phase, the samples were ultrasonically cleaned (Figure 2.46) in acetone for 5 minutes and in demineralized water for 10 minutes twice, then dried with compressed air.



Figure 2.46: Ultrasonic cleaner, Sonica.

Afterwards, the samples were placed in a multi-compartment container and each of them was covered with 0.5 ml of saliva (Figure 2.47). The adsorption phase lasted 1 hour at 37 ° C in the incubator (Figure 2.48). Subsequently the samples were left to air dry for 2 days.

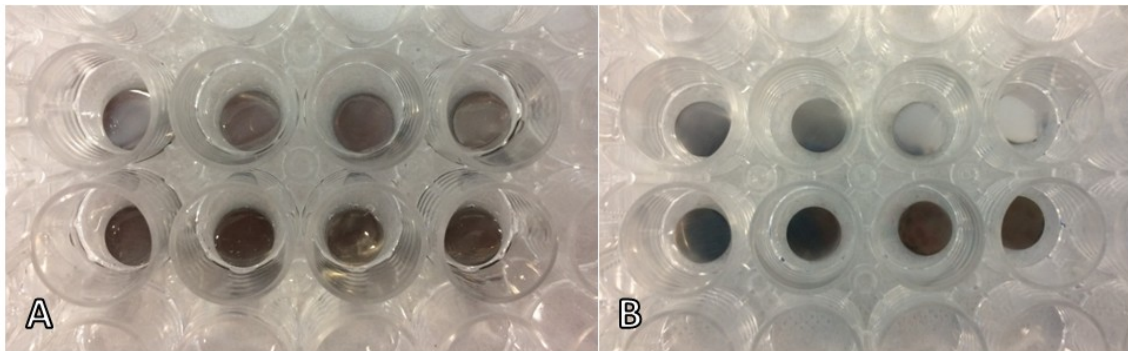


Figure 2.47: Adsorption of Biotène saliva (A) and adsorption of Bioextra saliva (B).

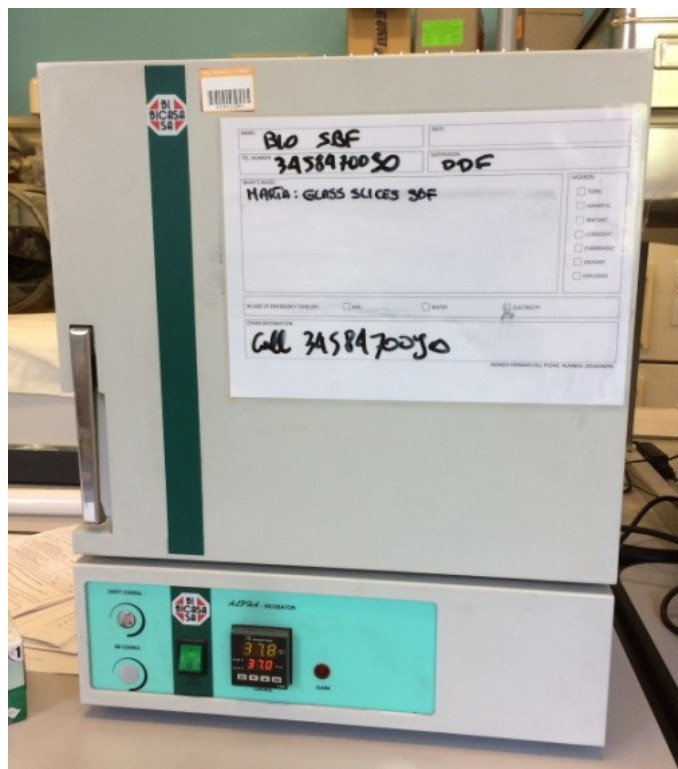


Figure 2.48: Alpha – incubator, Bicasa.

2.2.4 Instrumentation

An instrument for reliable surface zeta potential analysis requires high-end electronics, high-precision measuring cells and a pulsation free liquid circuit, as well as a deep understanding of various influences on the quality of the measured data.

The accumulated knowledge in solid surface zeta potential analysis was implemented in the most recent commercial instrument for streaming potential and streaming current measurement: SurPASS, Anton Paar GmbH, Austria (Figure 2.49). In order to calculate the zeta potential correctly according to the equations above, information about the volume flow rate of the aqueous solution is required. The SurPASS instrument determines the flow rate.

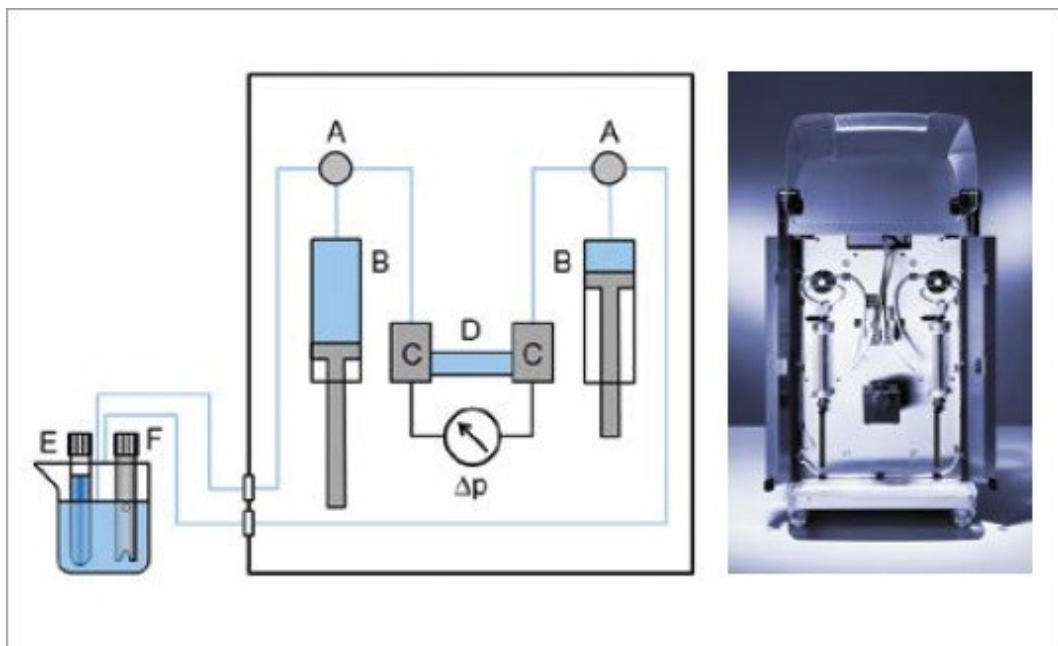


Figure 2.49: Components of the SurPASS electrokinetic analyzer (A48IB04en-B, 2013): A) 3-way valve, B) syringes for electrolyte transport, C) pressure transducers, electrodes, D) measuring cell, E) pH electrode, F) conductivity probe.



The Clamping Cell is the tool of choice used with the SurPASS for measuring planar surfaces like polymer films and sheets, metals, ceramics, glass or semiconductor wafers. Two different arrangements of planar samples are possible. In the symmetric configuration two identical surfaces are mounted and separated by a well-defined gap. The asymmetric geometry uses a reference surface and enables the non-destructive measurement of samples with different thicknesses. A proprietary mechanism guarantees a specified contact pressure and thus a highly reproducible sample mounting.

The Cylindrical Cell is mainly used for the investigation of natural or technical fibers and fabrics, granular samples and coarse particles. It combines easy sample mounting with outstanding measurement reproducibility. A unique sensor design common to all measuring cells ensures precise detection of streaming potential and streaming current, and reliable pressure measurement.

The Adjustable Gap Cell extends the range of application to small samples with a rectangular or disk shape. The smart sealing concept and the clever mechanism for adjusting the distance between sample surfaces also enables zeta potential determination for porous materials or materials which swell strongly.

With the integrated Titration Unit the zeta potential can be determined fully automatically depending on the pH value or additive concentration in the electrolyte. Two stepper motor-driven syringe pumps facilitate high-resolution dispensing of liquids such as acidic or alkaline solutions. The design of the cover for the external electrolyte beaker completes the high-precision titration system.

VisioLab for SurPASS is a Microsoft Windows®-based control and evaluation software which collects all measured parameters (Figure 2.50). It automatically calculates the zeta potential and displays the results both as graphs and tables.

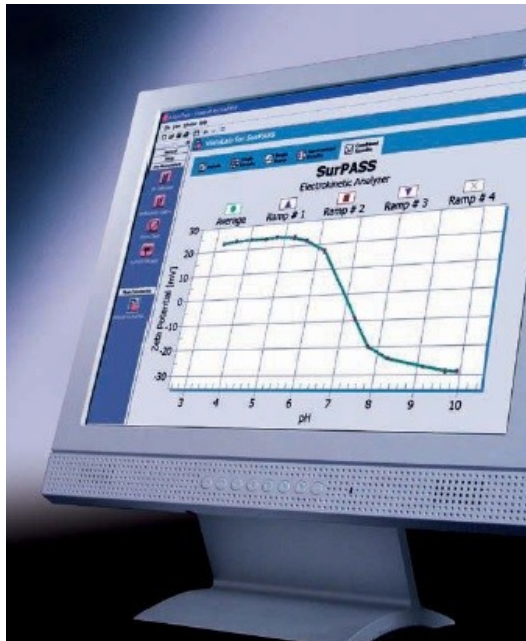


Figure 2.50: VisioLab software.

The VisioLab for SurPASS software includes features for customizing the data display in tables and diagrams, enabling complete measurement reporting. In addition, all measured results may be exported for further analysis and data processing.

2.2.5 Experimental test procedure

The adsorption of the two artificial saliva was done on four samples for both types of titanium. In fact, the tests to be carried out for each combination of material-saliva are two, one in a acidic range of pH and one in a basic range of pH, and for each test two samples are required.

After adsorption, the samples are attached to the holder with double-sided adhesive tape (Figure 2.51).

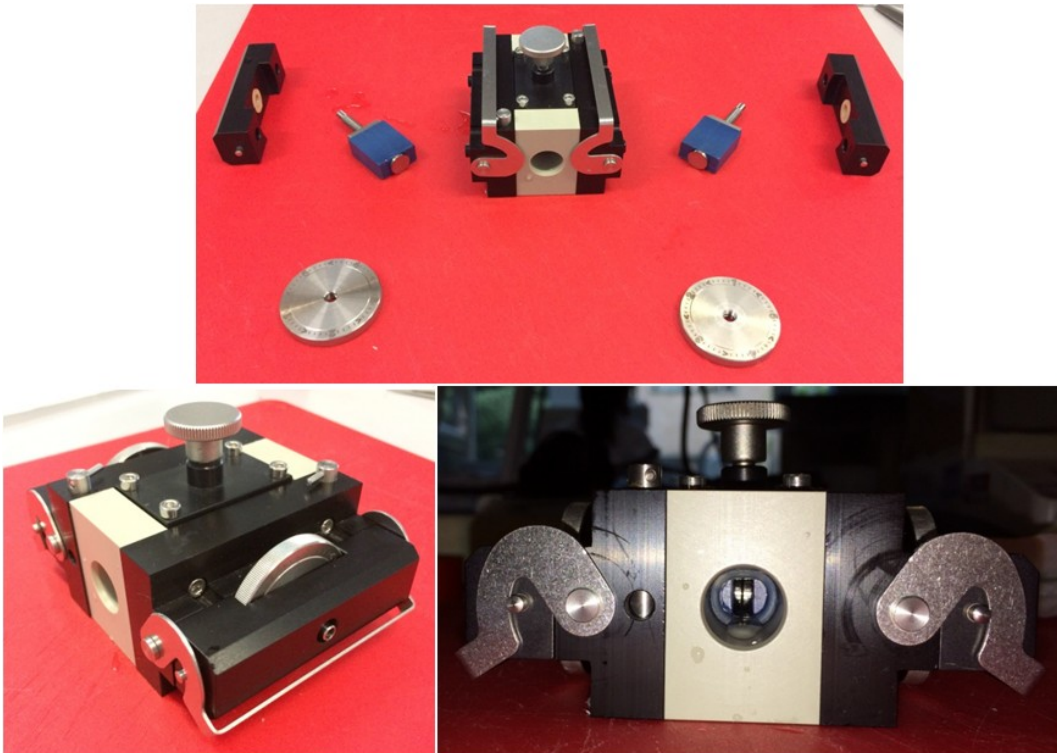


Figure 2.51: Sample holder of SurPass.

Then the holder is mounted on the machine (Figure 2.52).

It should be noted that it was decided not to use the same pair of samples both for acid titration and for basic titration to avoid artifacts related to the reactivity of surfaces in contact with acid or basic solutions.

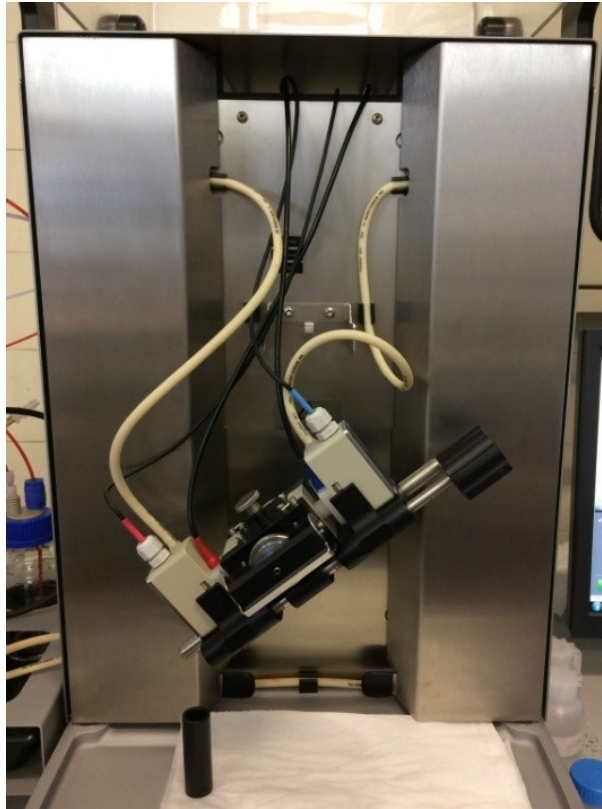


Figure 2.52: Sample holder mounted on the SurPass.

The preparation of each test consists of the following steps:

- the “clean” phase which includes two machine washes with 0.5 l of distilled water each. Conductivity becomes void at the end of the washings.
- the “fill” phase in which the electrolyte in the machine is turned in an open circuit. The pH and conductivity values are measured to check if they change in the subsequent phases.
- the "rinse" phase in which, in a closed circuit, the electrolyte is turned into the machine, until reaching the desired gap between the samples (100 μm). The gap between samples can be adjusted manually.
- the “flow check” phase in which it is checked that the flow rate as a function of pressure has a linear trend. The flow value must be 100 ml/min with a pressure of 100 mbar.



Afterward, the titration program is set:

- for the acidic pH test an HCl solution is used and a 0.1 ml step is set.
- for the basic pH test a NaOH solution is used and a step of 0.01 ml is set.

The pH range is from 2 to 9.

The duration of each test is two hours.

In summary, the electrolyte (an aqueous 0.001 mol/l KCl solution) is circulated through the measuring cell containing the solid sample, thus creating a pressure difference. A relative movement of the charges in the electrochemical double layer occurs and gives rise to the streaming potential. This streaming potential – or alternatively the streaming current – is detected by electrodes placed at both sides of the sample. The electrolyte conductivity, temperature and pH value are determined simultaneously.

The pH, in particular, is the most important parameter of the liquid phase that influences the measurement of the potential ζ ; the data of the potential measurements ζ , in fact, refer to the pH of the aqueous solution used for the analysis of the surface charge of the samples. The relationship between pH and potential ζ measured in each experiment, in turn, makes it possible to estimate the isoelectric point (IEP) of the surface under investigation; in other words, it becomes possible to identify the pH value at which the analyzed surface has a net null electric charge, and therefore a balance between the positively and negatively charged surface groups. This value can be defined by identifying the pH value for which the measured zeta potential changes sign (where, in fact, ζ takes the value of 0 mV).

2.3 Wettability tests

To perform the contact angle measurements relating to this thesis work, a specific instrument is used (KRÜSS DSA 100, KRÜSS GmbH, Hamburg, Germany)(Figure 2.53).

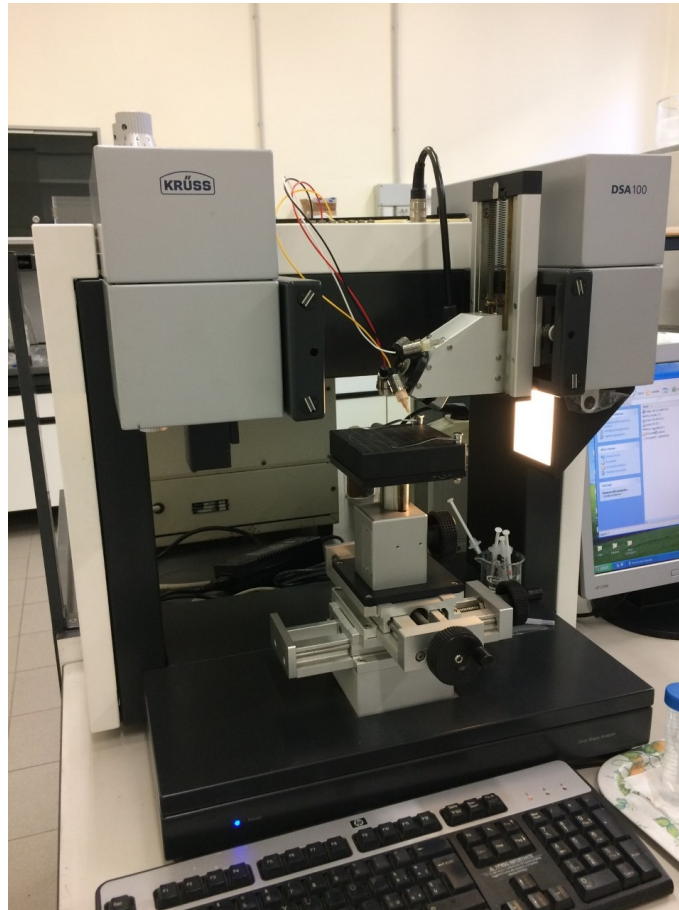


Figure 2.53: Drop Shape Analyzer DSA100.

Measurement operations are performed at room temperature. The sample is placed on the horizontal plate of the appliance. The optical apparatus of the microscope, placed in front of the sample, once set to have an adequate focus of the object of investigation, allows to acquire the images of each test. The geometry of the samples does not make possible to perform multiple measurements on the same sample. The drops of water injected on the surface, if too close together, can in fact, due to chemical / physical phenomena of molecular cohesion, coalesce and unite, making the measure



unattainable. For this reason, for each sample of each group, given the limited surface area on which to inject a (albeit limited) quantity of water, one/two measurements were conducted. On the surface of each sample, in summary, one/two droplets of 5 μ l of purified and deionized water were deposited with the aid of a micropipette; attention has been paid to making sure that these drops are deposited at a certain safety distance from each other. The shape of each drop is recorded by a camera. The contact angle measurement is performed by exploiting the capacity of a specific software dedicated to automatic image processing. This allows the static contact angle to be determined for each sample of interest.

The measurement of the contact angle with water was performed on the same group of samples used for the zeta potential measurement test.

Once the experimental data were obtained, a simple statistical analysis was carried out, determining the average value and the standard deviation of the measured contact angle for each of the groups of samples under investigation.

The rationale behind this series of investigations is to evaluate how different types of artificial saliva go to influence, and eventually modify, the surface wettability of titanium surfaces.

3. Results and discussion

3.1 Tribological tests

3.1.1 Friction

The HFRR acquired the data points for the coefficient of friction (COF) throughout the test. Using Excel, the mean and standard deviation of the COF values were calculated for each point.

The results were statistically analyzed using t-student test, with p value < 0.05 considered as statistically significant.

The graphs below show the average friction coefficient as a function of the sliding distance (m) for the four tested material/saliva combinations (Figure 3.1 and Figure 3.2).

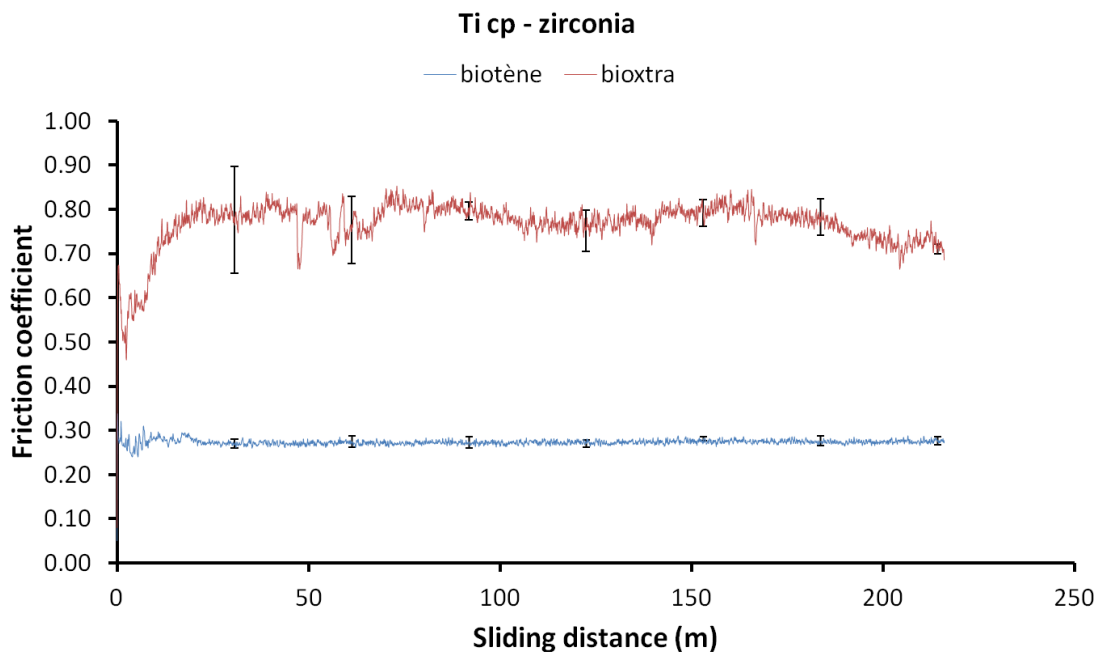


Figure 3.1: Average COF over sliding distance of commercially pure titanium disk against zirconia ball in the presence of biotène (blue) and in the presence of bioxtra (red).

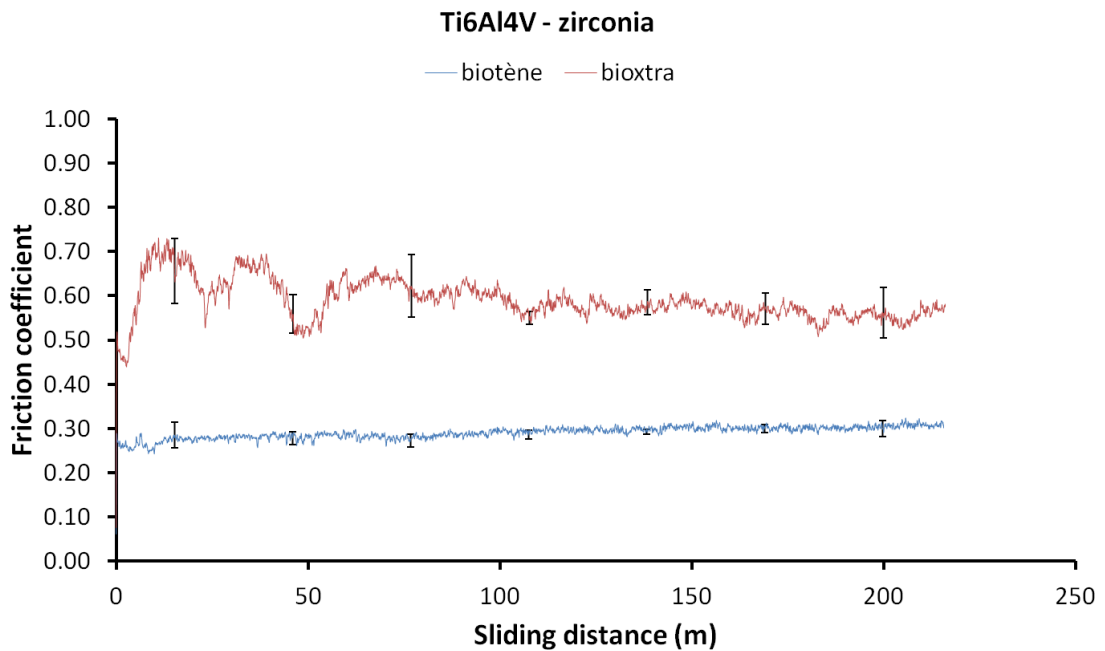


Figure 3.2: Average COF over sliding distance of Ti6Al4V alloy disk against zirconia ball in the presence of biotène (blue) and in the presence of bioxtra (red).

Compared to BioXtra saliva, the Biotène decreases the friction coefficient of both the substrates with a good lubrication action of the coating (Figure 3.3). In particular, the COF of the Ti cp is 0.27 ± 0.005 and that of the Ti6Al4V is 0.29 ± 0.011 .

As can be seen from the values shown in Table 3.1, the coefficients of friction of both materials are much lower in the presence of the Biotène and they do not differ significantly ($p > 0.05$, Student's t-test).

Table 3.1: Average friction coefficients and standard deviations of all the tested samples.

	Lubricant	Test 1	Test 2	Test 3	Average	Standard deviation
Ti cp	biotène	0.27	0.27	0.28	0.27	0.005
	bioxtra	0.73	0.76	0.80	0.77	0.033
Ti6Al4V	biotène	0.29	0.30	0.28	0.29	0.011
	bioxtra	0.58	0.59	0.60	0.59	0.009

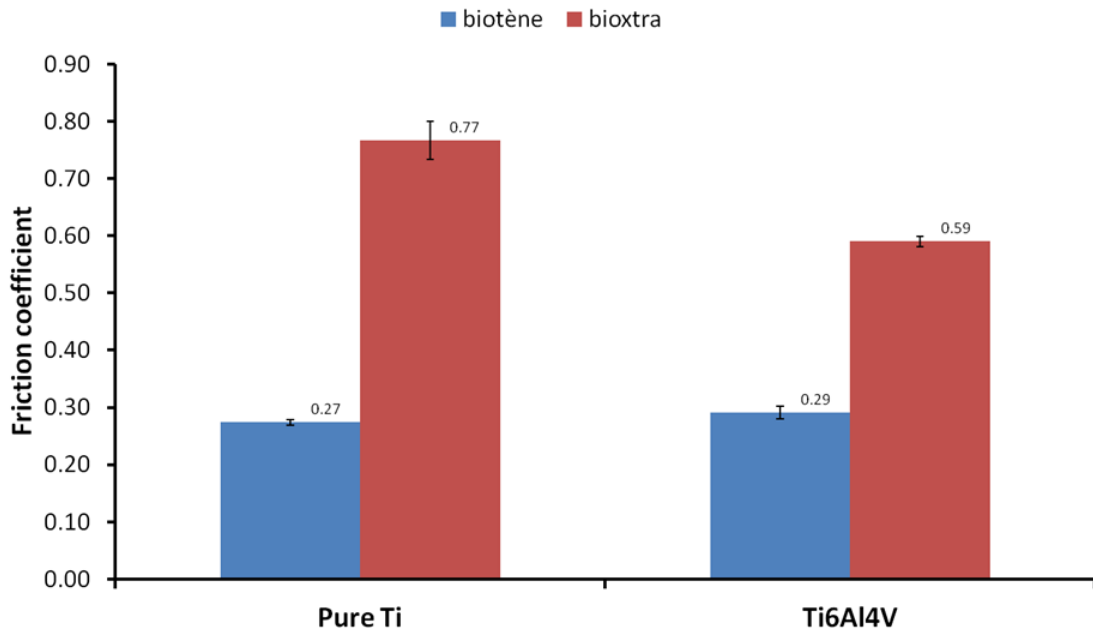


Figure 3.3: Average COF for each tribo-pair.

As for the tests carried out in the presence of BioXtra saliva, it can be seen that the values of the friction coefficient are far from each other, even if they remain higher than those with Biotène, as already mentioned. In particular, the COF of the Ti cp reaches the value of 0.77 ± 0.033 , while that of the Ti6Al4V is 0.59 ± 0.009 .

It can be said that the lowest friction occurred in the tests involving Biotène as the tested artificial saliva. Furthermore, the Biotène showed by far a lower variability in the friction coefficient. In fact, there is a clear difference in the curve trend: those of the BioXtra have an initial region in which there is a gradual increase of the COF, called the “running-in period”, much more extensive than those of the Biotène. In this region occurs an adjustment of the two contacting surfaces by crushing and smearing of the asperities [18]. Then a second region can be identified, during which the COF remains fairly stable in presence of the Biotène, while the COF of the BioXtra exhibits strong oscillations. After the running-in period, these oscillations may be attributed to the build-up and accumulation of third-body particles in the contact region [18].

3.1.2 Wear

Through an optical microscope (AmScope, ME300 Series), a picture of the wear scar on each disk was acquired. In this way, the width and the length of the wear scars was evaluated at the end of each test.

The samples were rinsed and wiped with ethanol before the imaging.

A representative set of images is reported below for each of tested materials.

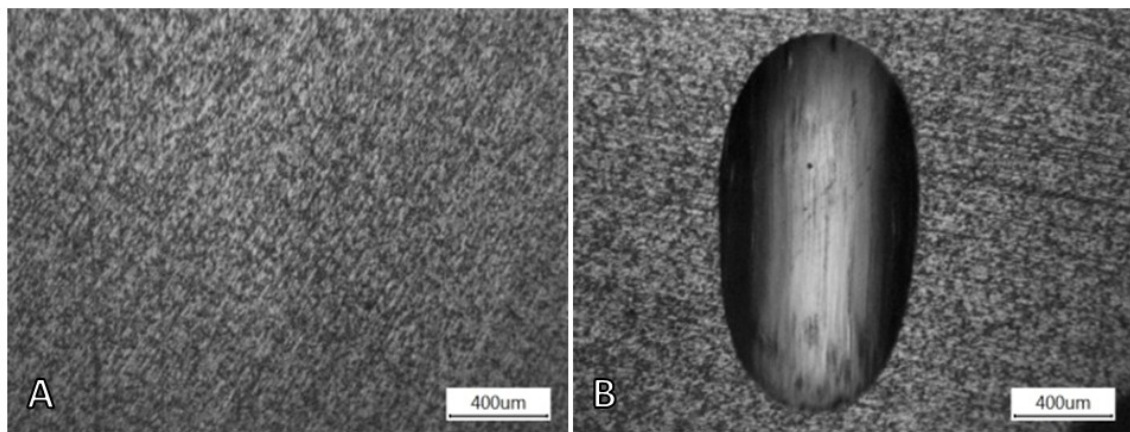


Figure 3.4: Image of Ti cp disk before the test (A) and wear scar on it with Biotène after the test (B).

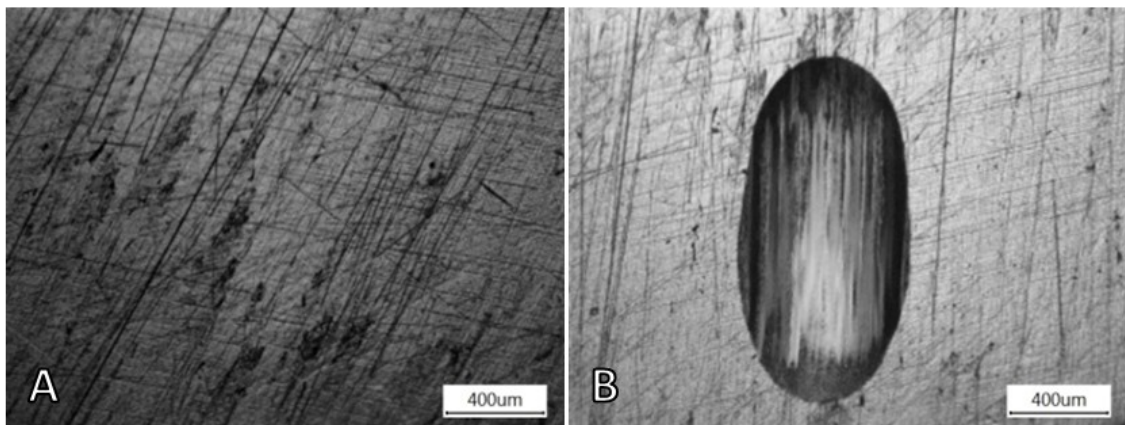


Figure 3.5: Image of Ti6Al4V disk before the test (A) and wear scar on it with Biotène after the test (B).

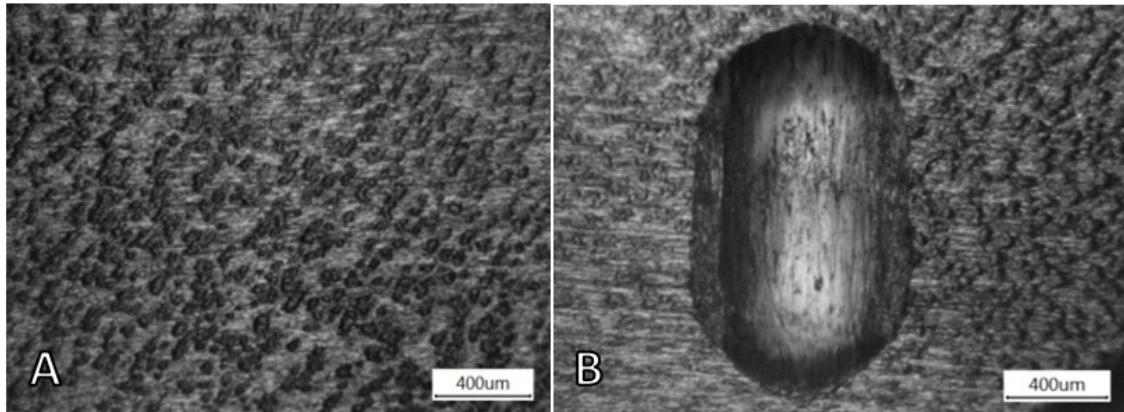


Figure 3.6: Image of Ti cp disk before the test (A) and wear scar on it with BioXtra after the test (B).

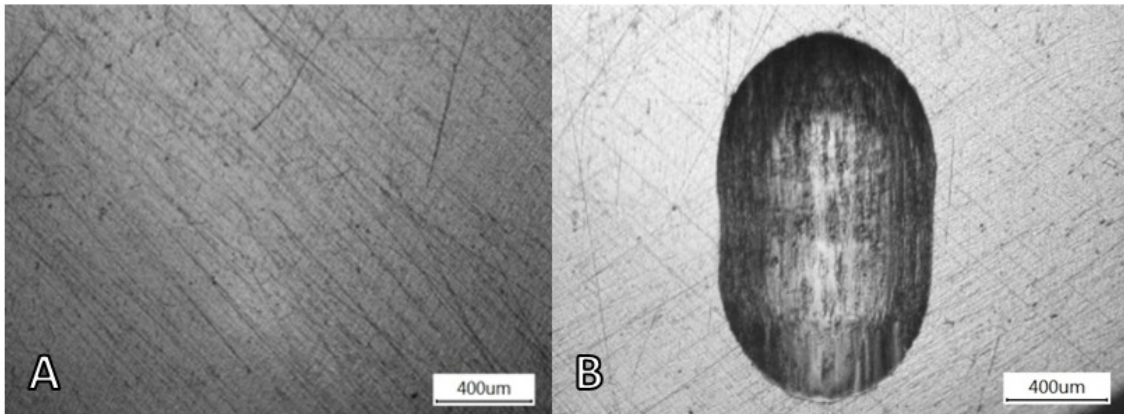


Figure 3.7: Image of Ti6Al4V disk before the test (A) and wear scar on it with BioXtra after the test (B).

In the presence of Biotène (Figure 3.4 and 3.5), the shape of the grooves on the discs of both materials is very similar and is almost a perfect ellipse. The edges are regular and well defined. The groove surface is uniform and almost free of debris.

Instead, in the presence of BioXtra (Figure 3.6 and 3.7), the grooves of the two materials result in a more irregular elliptical shape. The edges are more jagged and the surface grain of the wear scars are coarse with a considerable presence of debris.

In both cases, it can be seen that the grooves surface shows an oriented texture aligned to the sliding direction. It can be explained by third-body abrasion processes caused by the formation of metal debris, due to the ultra-hardness of zirconia.

Using the length and width measurements of the wear scars on the disks shown in table 3.2 and 3.3, the area of the grooves was calculated, assuming they are ellipses.

Table 3.2: Wear scar width (μm) of the disks after each test.

	Lubricant	Test 1	Test 2	Test 3	Average	Standard deviation
Ti cp	biotène	897.06	863.97	849.26	870.10	24.48
	bioextra	937.50	948.53	897.06	927.70	27.10
Ti6Al4V	biotène	720.59	742.65	786.76	750	33.69
	bioextra	1022.06	1044.12	900.74	988.97	77.20

Table 3.3: Wear scar length (μm) of the disks after each test.

	Lubricant	Test 1	Test 2	Test 3	Average	Standard deviation
Ti cp	biotène	1658.09	1595.59	1617.65	1623.78	31.70
	bioextra	1628.68	1694.85	1665.44	1662.99	33.15
Ti6Al4V	biotène	1448.53	1470.59	1437.50	1452.21	16.85
	bioextra	1713.24	1577.21	1621.32	1637.26	69.40

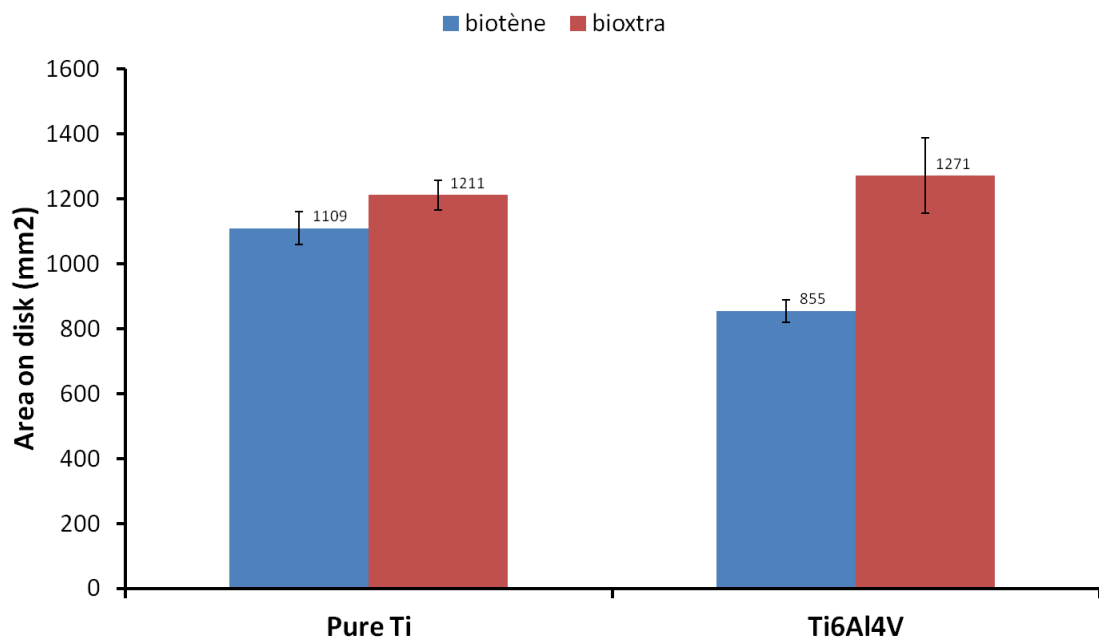


Figure 3.8: Average areas (mm^2) of the wear scars on the disks.

The areas of wear scars in the presence of Biotène are smaller than those in the presence of BioXtra (Figure 3.8), in particular, that of the titanium alloy is the lowest of all.

Table 3.4: Average areas values (mm²) of the tested samples after each test.

	Lubricant	Test 1	Test 2	Test 3	Average	Standard deviation
Ti cp	biotène	1168	1082	1078	1109	50
	bioxtra	1199	1262	1173	1211	46
Ti6Al4V	biotène	819	857	888	855	34
	bioxtra	1375	1293	1146	1271	116

It therefore appears that the Biotène decreases the wear between the tested materials: this is due first of all to the fact that the friction coefficient is lower than that of the BioXtra. Furthermore, the presence in this artificial saliva of organic corrosion inhibitors, such as the surfactants peg-60 hydrogenated castor oil, cetylpyridinium chloride and the polymer vp/va copolymer, can justify the lower tendency to wear. In fact the mechanism of action of organic corrosion inhibitors is based on the adsorption on the surface to form protective film which displace water from the metal surface and protect it against deteriorating [19].

As seen above, the friction coefficient in the presence of the BioXtra is greater than that of the Biotène, showing that a strong adhesive interaction has occurred. Hence, the predominant wear mechanism is adhesive galling. Probably the surfactants, absent in this artificial saliva, provide some protection to titanium .

An image of all the wear scars on the zirconia balls was taken at the end of each test by means of an optical microscope (Olympus Vanox-T, Leica Microsystems B.V., Netherlands).

The samples were rinsed and wiped with ethanol before the imaging.

A representative picture of the ball is reported below for each tribo-pair.

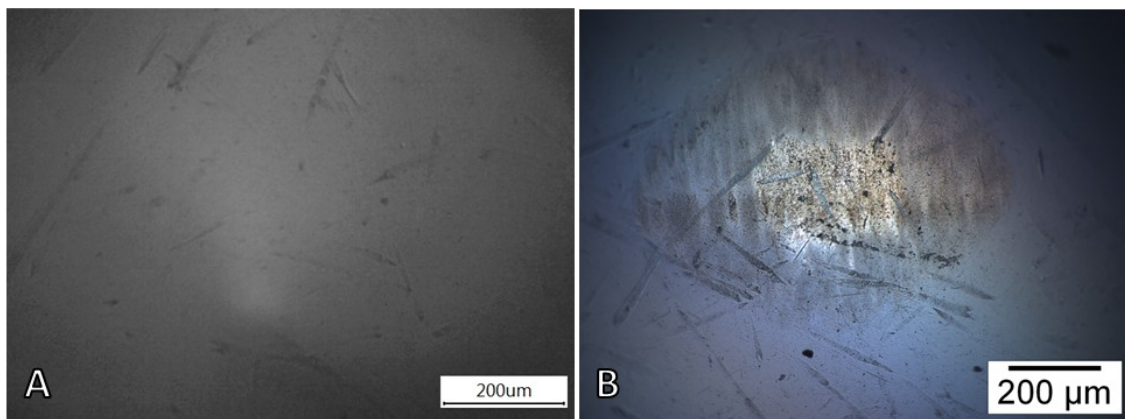


Figure 3.9: Image of a zirconia ball used against Ti cp disk before the test (A) and after the test with Biotène (B).

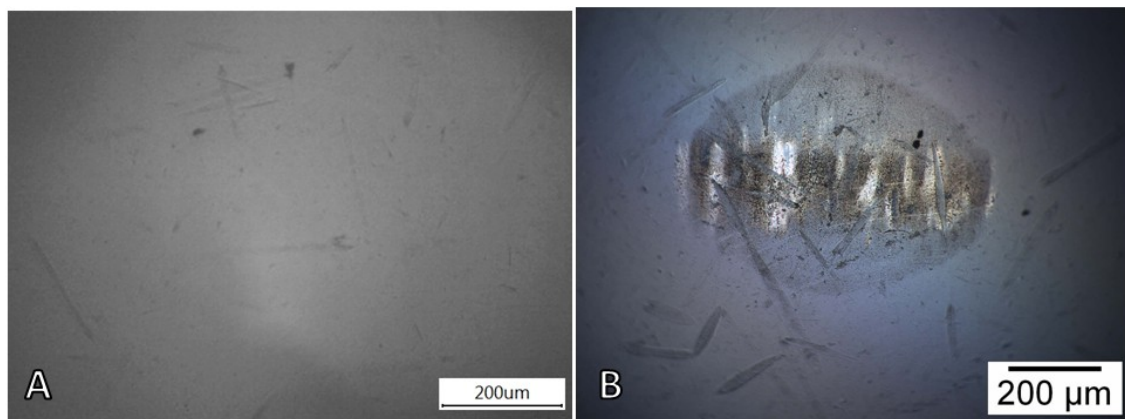


Figure 3.10: Image of a zirconia ball used against Ti6Al4V disk before the test (A) and after the test with Biotène (B).

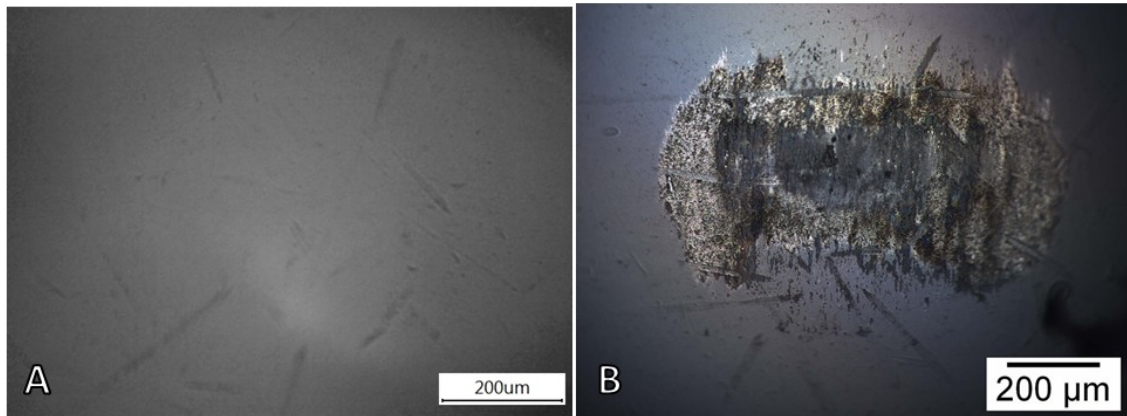


Figure 3.11: Image of a zirconia ball used against Ti cp disk before the test (A) and after the test with BioXtra (B).

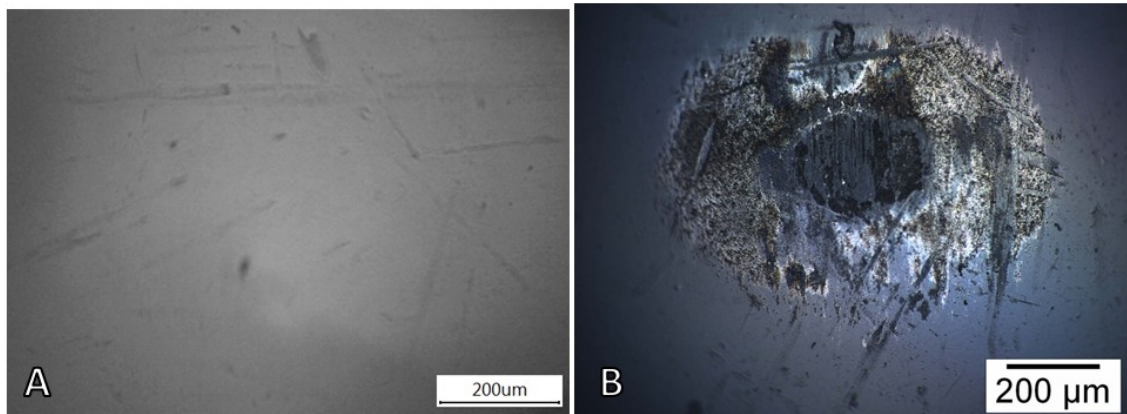


Figure 3.12: Image of a zirconia ball used against Ti6Al4V disk before the test (A) and after the test with BioXtra (B).

It can be immediately noticed that, again, the wear tracks on the zirconia balls in the presence of the Biotène have similar characteristics and so also for those tested with the BioXtra.

The occurrence of a strong adhesive interaction between the fretting surfaces lubricated with the BioXtra is supported by the higher amount of material transfer on the zirconia balls (Figure 3.11 and 3.12).

In all cases, the wear scars formed on zirconia balls have an elliptical shape similar to each other; in particular they consist of a darker, more stressed and worn-out central area, and around it a lighter area (almost a halo in tests with Biotène), less damaged.

The mean wear scar diameter (MWSD) was calculated averaging the two main diameters, a and b (Figure 3.13).

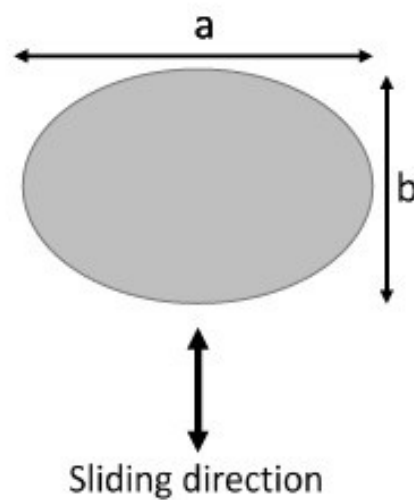


Figure 3.13: Schematics of the calculation of the mean wear scar diameter on zirconia balls.

The MWSD of the titanium alloy in the presence of Biotène was the smallest of all ($p < 0.05$, Student's t -test).

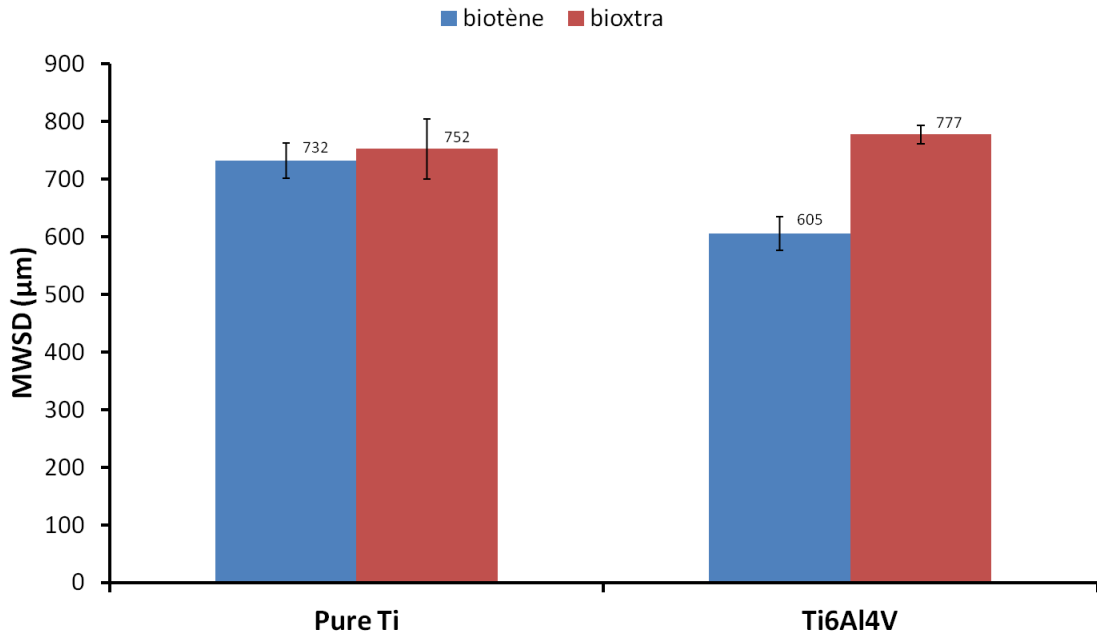


Figure 3.14: Average mean wear scar diameters (µm) on zirconia balls.

The mean wear scar diameters on the balls are reported in Table 3.5.

Table 3.5: Mean wear scar diameters (µm) on the balls used for the tests.

	Lubricant	Test 1	Test 2	Test 3	Average	Standard deviation
Ti cp	biotène	767	713	715	732	30
	bioxtra	752	804	701	752	52
Ti6Al4V	biotène	577	604	635	605	29
	bioxtra	791	781	760	777	16

At the end of the tests, the amount of metallic debris dispersed in the artificial saliva used as a lubricant can be observed: once again the difference between the two salivas is evident (Figure 3.15).

A greater quantity of residues is visible at the end of the tests carried out with the Biotène and this supports what was previously stated: the surfactants present in this

saliva form a protective film between the fretting surfaces, reducing wear and the transfer of metallic material on the balls.

The near absence of residues at the end of the tests with the BioXtra therefore indicates the greater adhesive interaction, with consequent entrapment and attachment of the metal debris between the fretting surfaces, which leads to a greater rate of wear.

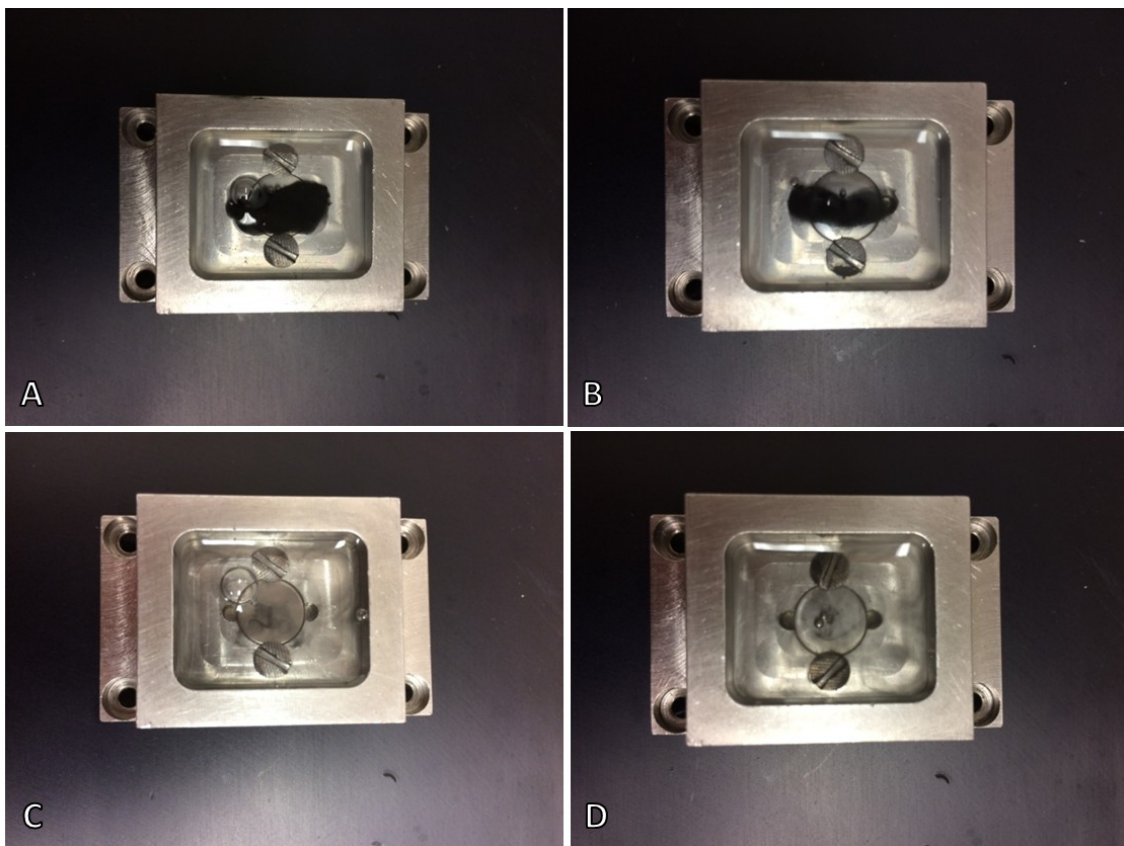


Figure 3.15: Representative images of cp Ti with Biotène (A), Ti6Al4V with Biotène (B), cp Ti with BioXtra (C) and Ti6Al4V with BioXtra (D) at the end of the tests.

3.2 Surface characterization tests

3.2.1 Zeta potential

The SurPASS carried out 4 measurements for each number of set points (about 15 for each test).

Using Excel, the mean pH values and mean and standard deviation values of the zeta potential (mV) were calculated for each point.

The graphs below show the trend of the zeta potential when the pH changes, compared by type of material and type of artificial saliva.

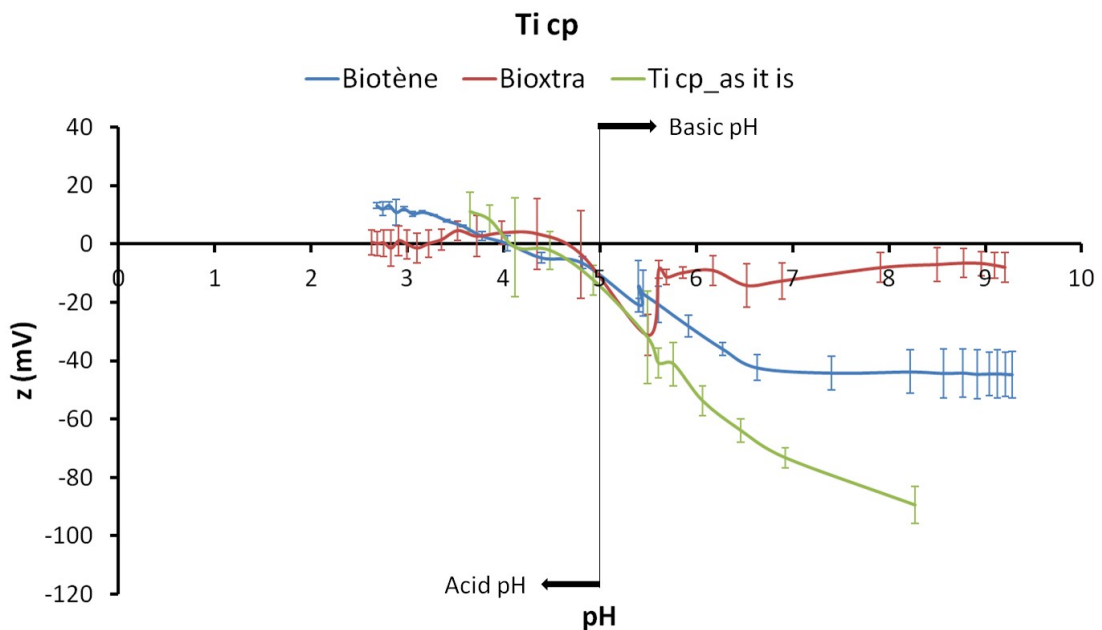


Figure 3.16: Evolution of the zeta potential according to the pH of commercially pure titanium. Green curve(Ti cp_as it is): IEP=4; blue curve(Ti cp_Biotène): IEP=4.05; red curve(Ti cp_BioXtra).

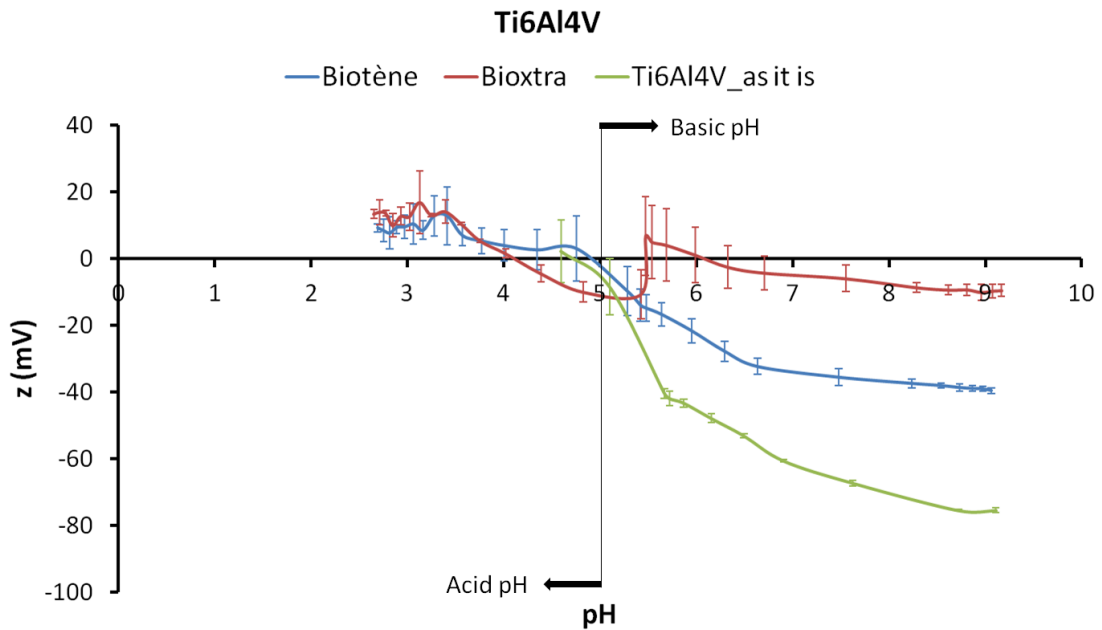


Figure 3.17: Evolution of the zeta potential according to the pH of Ti6Al4V alloy. Green curve(Ti6Al4V_as it is): IEP=4.7; blue curve(Ti6Al4V_Biotène): IEP=4.88; red curve(Ti6Al4V_BioXtra).

Observing the curves related to the adsorption of the Biotène and comparing them with the Ti cp and Ti6Al4V curves as-received (ie tested without saliva pre-adsorption) (Figure 3.16 and Figure 3.17), we note that:

- the curves obtained after adsorption are significantly different from the curves of the as-received materials: this means that adsorption of saliva compounds occurred with formation of a continuous layer.
- the slope of the titration curves after adsorption is significantly lower than that of the as-received materials: this means that the hydrophilicity of the adsorbed layer is higher than that of the bare metals.
- the presence of a plateau indicates the presence of functional groups (such as for instance -OH groups) exposed on the surface by the adsorbed compounds which are of a single specific chemical type with a specific acidic strength. They are all completely dissociated when pH is higher than 6.5.

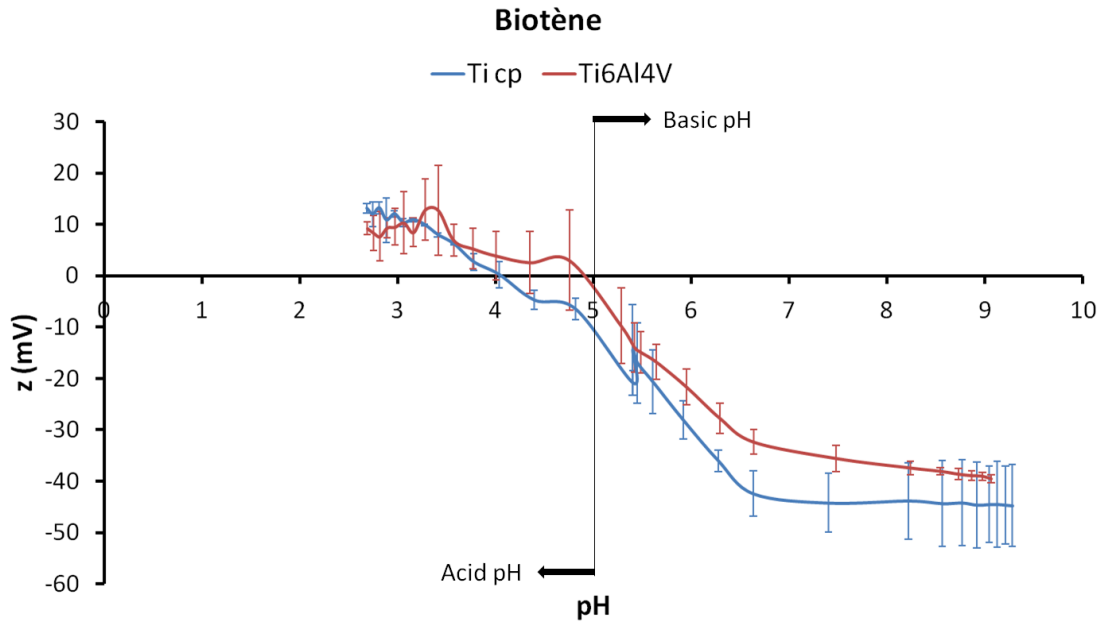


Figure 3.18: Trend of zeta potential as a function of pH with artificial saliva Biotène.

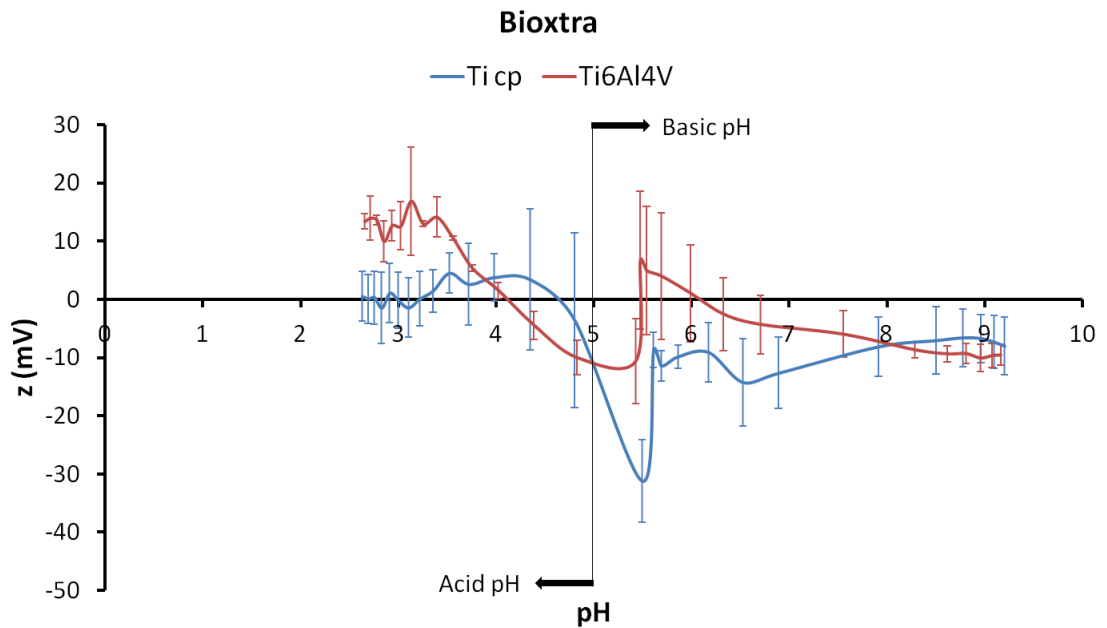


Figure 3.19: Trend of zeta potential as a function of pH with artificial saliva BioXtra.

The curves obtained after absorption of Biotène on both Ti cp and Ti6Al4V substrates (Figure 3.18) are very similar except for the isoelectric point (IEP) that is respectively close to the two different substrates. This behavior can have different explanations: uncomplete covering of the surface by the adsorbed layer, different chemistry of the adsorbed layers with a different amount of acidic groups (higher in the case of a Ti substrate).

Observing the curves related to the adsorption of the BioXtra (Figure 3.19), it can be said that:

- the curves obtained after adsorption are significantly different from the curves of the as-received materials: this means that adsorption of saliva compounds occurred with formation of a continuous layer.
- the adsorbed layer has zeta potential values not far from 0 in all the explored range with a slope of the curve near to 0: it means that the adsorbed layer does not adsorb neither OH^- or H_3O^+ instead of water molecules even if the solution is strongly basic or acidic. This behavior could be related to a super hydrophilic behavior [20].
- no plateau is observable, so no functional group with a specific acidic or basic strength is present on the surface.
- the step registered between the curves related to the basic and acidic range detected at the beginning of the measurements can be related to some instability or not perfect reproducibility of the adsorbed layer.

These results can be used for interpreting the results obtained from tribological tests. Compared to BioXtra, Biotène decreases the friction coefficient and wear of both the substrates and it allows the formation of a stable adsorbed layer with a moderate hydrophilic behavior acting as a good lubricant.

3.2.2 Wettability

The results of the wettability tests are shown in Figure 3.20.

Based on the values of the measurements obtained, both the mean and the standard deviation of the static contact angle were calculated.

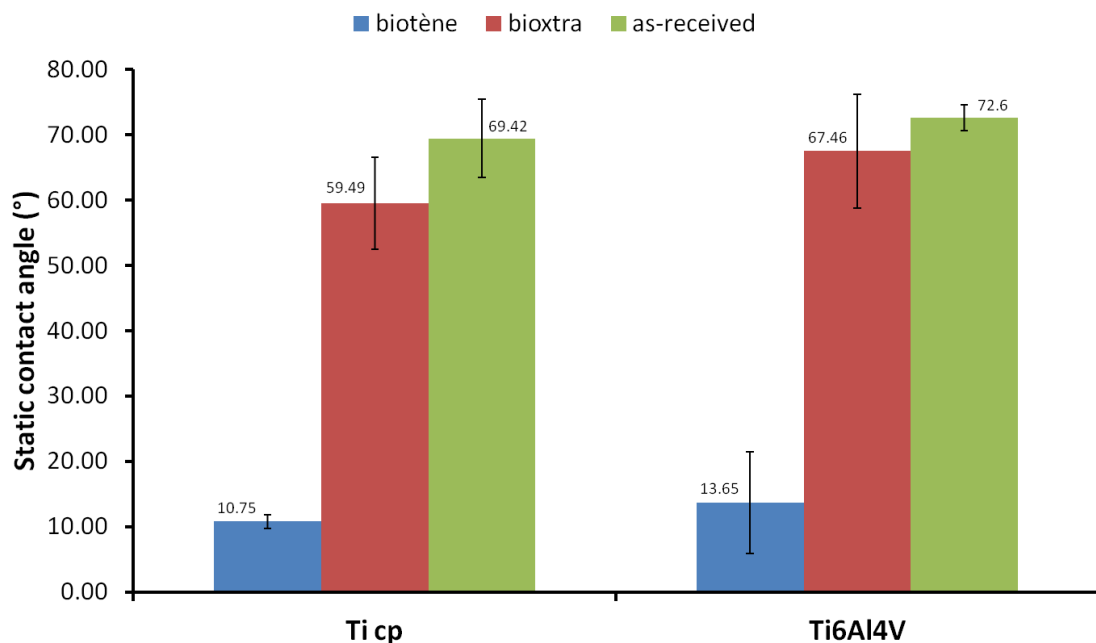


Figure 3.20: Average static contact angle (°) of cp Ti and Ti6Al4V disks after the absorption of Biotène (blue) and BioXtra (red) and as-received (green).

The values of the static contact angle on the Ti cp and Ti6Al4V samples after the adsorption of BioXtra are equal to $59.49 \pm 7.06^\circ$ and $67.46 \pm 8.75^\circ$, respectively. These values do not differ significantly from those measured on samples of the as-received material (ie tested without saliva pre-adsorption). This shows that the moderate hydrophilicity of the adsorbed layer (BioXtra) is comparable with that of the bare materials: in accordance with the results obtained in the tests on the zeta potential, the adsorption of this artificial saliva is not able to significantly modify the surface of the



substrate and consequently its wettability (absence of functional groups with a specific acidic or basic strength on the surface).

The values of the static contact angle on the Ti cp and Ti6Al4V substrates after the adsorption of Biotène are equal to $10.75 \pm 1.06^\circ$ and $13.65 \pm 7.77^\circ$, respectively. These values, on the other hand, are significantly lower than those measured on samples tested with BioXtra pre-adsorption and without saliva pre-adsorption. This means that the hydrophilicity of the adsorbed layer (Biotène) is higher than that of BioXtra and the bare metals. The adsorption of this artificial saliva is able to significantly modify the surface of the substrate and consequently to increase its wettability, because of the presence of functional groups (such as for instance -OH groups) exposed on the surface by the adsorbed compounds which are of a single specific chemical type with a specific acidic strength, in accordance with the results obtained in the tests on the zeta potential.

The results of this tests confirm that Biotène is able to form on the titanium a stable adsorbed layer with a highly hydrophilic behavior and is therefore effective in lubricating and maintaining a wet surface on dental implants and oral mucosa.

4. Conclusions

In this thesis work, tribological and surface characterization experiments were conducted on two structural materials for dental implants (Ti cp and Ti6Al4V) aimed at evaluating the different performances of two artificial saliva (Biotène and BioXtra).

For tribological tests, a sphere-plane system was used to simulate the dental implant-abutment contact, where the sphere (zirconia) simulates the abutment and the plane (Ti cp and Ti6Al4V) simulates the implant. It was possible to demonstrate that the tribological behavior of implant surfaces is influenced by the characteristics of the oral fluid used. The results show that, compared to BioXtra, the Biotène significantly reduces the friction coefficient (COF) and its variability and therefore the wear between the tested materials (in particular the lower values are reached with the Ti6Al4V alloy). This could be due to the presence in Biotène of some surfactants and polymers that act as organic corrosion inhibitors, forming a protective film between the fretting surfaces and reducing the transfer of metallic material on the balls (lower adhesive interactions); moreover, even the absence of fluorides in this saliva could positively influence the corrosion resistance of titanium. For wear evaluation, using an optical microscope, the area of wear scars on the titanium disks was measured and also the mean wear scar diameter (MWSD) of the wear scars on the zirconia balls.

On the other hand, the surface characterization tests were carried out on titanium samples. After a saliva adsorption phase on the surface of the disks, their surface electric charge was evaluated by measuring the zeta potential (ζ) and subsequently their wettability by measuring the static contact angle. The results obtained were compared also with those of the bare metals (ie tested without saliva pre-adsorption) and show that adsorption of saliva compounds occurred for both fluids with the formation of a continuous layer; but the one formed by Biotène is more stable and hydrophilic, acting as a good lubricant, in accordance with the results obtained from tribological tests.

It should be noted that there are limitations due to the nature of the testing equipment for the tribological experiments: since the sphere-plane system is simpler and less expensive than the methods that use real implants, only material specimens can be



tested and not actual implant and abutment components. Moreover, the linear movement of the tribometer is much larger and less complex than the micro-motion or fretting process that occurs between implants and abutments in a clinical setting.

It would be advisable to combine the results obtained in the present work with those of other investigation techniques, such as X-ray photoelectron spectroscopy (XPS), 3D profilometry and SEM analysis.

Furthermore, tribocorrosion tests would allow the addition of electrochemical investigation which is essential to gaining a complete understanding of the complex relationship between materials at the implant-abutment interface in the oral environment.



Appendix

Internship context

This project has been developed during some internships. In particular, the tribological tests were performed in the research department of Ducom Instruments, Groningen (The Netherlands) and the solid surface analysis was conducted in the Department of Applied Science and Technology (DISAT) of Polytechnic University of Turin, Torino (Italy).

Ducom Instruments

Founded in 1978, Ducom Instruments has led the way in designing and manufacturing advanced materials testing instruments with a specialization in tribology. Applying cutting-edge technology and strong design principles to its products, Ducom focuses on providing customers with an excellent ownership experience starting with ease of use and maintenance.

This enterprise have locations in the United States, The Netherlands and India and each one have an in-house Research & Development initiative.

As a result, Ducom holds several proprietary technologies, copyrights and patents with additional filings every year. Many of these technologies are applied to their instruments, and work in the background so users can enjoy better results and user experiences.

Their instruments use components that are manufactured in an AS9100:2009 certified “aerospace grade” manufacturing facility for excellent quality and they are operational all over the world. Research labs working on innovative technology development which requires advanced and highly configurable test systems to standardized quality control requirements which rely on highly repeatable systems to accurately monitor product quality test instruments by Ducom [1].

My internship was leaded in the Research & Development location in Groningen , the Netherlands, where Ducom have his machines and his offices in the Zernike Institute for Advanced Materials, University of Groningen.



Polytechnic of Turin

The Polytechnic University of Turin is an engineering public university based in Turin, Italy. Established in 1859, "Politecnico di Torino" is Italy's oldest technical university. The university offers several courses in the fields of Engineering, Architecture and Industrial Design.

The Politecnico is a "Research University" acknowledged as a centre of excellence in all over the world for the qualifying research areas of Architecture and Engineering. The development of the fields of excellence, the investment on frontier subjects, and also the support to the curiosity driven research allow a virtuous mix of basis and applied research.

Research activities, in particular, are structured in four macro-areas: Industrial Engineering; Information Technology; Management and Mathematical Engineering; Civil, Environmental, Architecture and Design Engineering [2].

In particular, the Department of Applied Science and Technology (DISAT) helped me with the scanning electron microscopy (SEM) of the polyethylene and metal samples before the wear testing. DISAT focuses on research and education involving the fundamental principles of matter and energy, their transformation and related engineering applications [3].

References

- [1] Instruments, D. Ducom Instruments - Company - About Us. 2015; Available from: <http://ducom.com/company/about-us-4/>.
- [2] Turin, W.-P.o. 2015; Available from: http://en.wikipedia.org/wiki/Polytechnic_University_of_Turin.
- [3] Technology, D.-D.o.A.S.a., 2015.
- [4] Bhushan, B. (2013). Introduction to tribology. Retrieved from <http://ebookcentral.proquest.com>
- [5] Zhou, Z. R., & Jin, Z. M. (2015). Biotribology: Recent progresses and future perspectives. *Biosurface and Biotribology*, 1(1), 3–24.
- [6] Gwidon Stachowiak and Andrew W. Batchelor, *Engineering Tribology*, Elsevier Inc. ; 2014.
- [7] Ananth, H., Kundapur, V., Mohammed, H. S., Anand, M., Amarnath, G. S., & Mankar, S. (2015). A review on biomaterials in dental implantology. *International Journal of Biomedical Science*, 11(3), 113–120.
- [8] Anusavice K, Shen C, Rawls HR. *Phillips' Science of Dental Materials*. 12th ed. St. Louis, Missouri 63043: Saunders; 2012.
- [9] Han, J., Zhao, J., & Shen, Z. (2017). Zirconia ceramics in metal-free implant dentistry, 6753. <https://doi.org/10.1080/17436753.2016.1264537>
- [10] Manicone, P. F., Iommetti, P. R., & Raffaelli, L. (2007). An overview of zirconia ceramics : Basic properties and clinical applications, 35, 819–826. <https://doi.org/10.1016/j.jdent.2007.07.008>
- [11] Osman, R. B., & Swain, M. V. (2015). A critical review of dental implant materials with an emphasis on titanium versus zirconia. *Materials*, 8(3), 932–958. <https://doi.org/10.3390/ma8030932>
- [12] Oshida Y. *Bioscience and Bioengineering of Titanium Materials*. 2nd ed. London, UK: Elsevier; 2012.
- [13] Fleck, C., & Eifler, D. (2010). Corrosion , fatigue and corrosion fatigue behavior of metal implant materials , especially titanium alloys. *International Journal of Fatigue*, 32(6), 929–935.
- [14] Revathi, A., Borrás, A. D., Muñoz, A. I., Richard, C., & Manivasagam, G. (2017). Degradation mechanisms and future challenges of titanium and its alloys for dental implant applications in oral environment. *Materials Science and Engineering C*, 76, 1354–1368. <https://doi.org/10.1016/j.msec.2017.02.159>
- [15] Sivakumar, B., Kumar, S., Narayanan, T. S. N. S., Sivakumar, B., Kumar, S., & Narayanan, T. S. N. S. (2013). Comparison of fretting corrosion behaviour of Ti – 6Al – 4V alloy and CP-Ti in Ringer ' s solution, 5831.
- [16] Souza, J. C. M., Henriques, M., Teughels, W., Ponthiaux, P., Celis, J. P., & Rocha, L. A. (2015). Wear and Corrosion Interactions on Titanium in Oral Environment: Literature Review. *Journal of Bio- and Tribo-Corrosion*, 1(2).
- [17] Stimmelmayer, M., Edelhoff, D., Güth, J., Erdelt, K., Happe, A., & Beuer, F. (2012). Wear at the titanium – titanium and the titanium – zirconia implant – abutment interface : A comparative in vitro study. *Dental Materials*, 28(12), 1215–1220.

- [18] Vieira, A. C., Ribeiro, A. R., Rocha, L. A., & Celis, J. P. (2006). Influence of pH and corrosion inhibitors on the tribocorrosion of titanium in artificial saliva. *Wear*, 261(9), 994–1001.
- [19] Bogumił Eugeniusz Brycki, Iwona H. Kowalczyk, Adrianna Szulc, Olga Kaczerewska and Marta Pakiet (2018). Organic Corrosion Inhibitors. <http://dx.doi.org/10.5772/intechopen.72943>
- [20] W. Shalaby, *Polymers as Biomaterials* (1984). American Chemical Society
- [21] Jost, Peter (1966). "Lubrication (Tribology) - A report on the present position and industry's needs". Department of Education and Science, H. M. Stationery Office, London, UK.
- [22] Hutchings, Ian M. (15 August 2016). "Leonardo da Vinci's studies of friction" (PDF). *Wear*. 360 (Supplement C): 51–66.
- [23] https://en.wikipedia.org/wiki/Tribology#cite_note-0-1
- [24] Amontons, G. (1699), "De la resistance causee dans les Machines," 'Memoires de l'Academic Royale, A', 257–282.
- [25] Gao, Jianping; Luedtke, W. D.; Gourdon, D.; Ruths, M.; Israelachvili, J. N.; Landman, Uzi (1 March 2004). "Frictional Forces and Amontons' Law: From the Molecular to the Macroscopic Scale". *The Journal of Physical Chemistry B*. 108 (11): 3410–3425
- [26] Coulomb, C.A. (1785), "Theorie des Machines Simples, en ayant regard au Frottement de leurs Parties, et 'a la Roideur ` des Cordages," *Mem. Math. Phys.*, X, Paris, 161–342
- [27] Dowson, D. (1998), *History of Tribology*, Second edition, Instn Mech. Engrs, London, UK.
- [28] Popova, Elena; Popov, Valentin L. (1 June 2015). "The research works of Coulomb and Amontons and generalized laws of friction". *Friction*. 3 (2): 183–190
- [29] Chaston, J. C. (1 December 1974). "Wear resistance of gold alloys for coinage". *Gold Bulletin*. 7 (4): 108–112.
- [30] Reye, Karl Theodor (1860) [1859-11-08]. Bornemann, K. R. (ed.). "Zur Theorie der Zapfenreibung" [On the theory of pivot friction]. *Der Civilingenieur - Zeitschrift für das Ingenieurwesen. Neue Folge (NF)* (in German). 6: 235–255
- [31] Archard, John Frederick (1 August 1953). "Contact and Rubbing of Flat Surfaces". *Journal of Applied Physics*. 24 (8): 981–988
- [32] Tabor, D. (1 November 1969). "Frank Philip Bowden, 1903-1968". *Biographical Memoirs of Fellows of the Royal Society*. 15: 1–38
- [33] Field, J. (2008). "David Tabor. 23 October 1913 -- 26 November 2005". *Biographical Memoirs of Fellows of the Royal Society*. 54: 425–459
- [34] Bowden, Frank Philip; Tabor, David (2001). *The Friction and Lubrication of Solids*. Oxford Classic Texts in the Physical Sciences.
- [35] Neale, Michael J. (1995). *The Tribology Handbook* (2nd Edition). Elsevier
- [36] Torbacke, Marika, et al. *Lubricants - Introduction to Properties and Performance : Introduction to Properties and Performance*, John Wiley & Sons, Incorporated, 2014.
- [37] D.Dowson, V.Wright, Bio-tribology, in: *Proceeding of the Conference on the Rheology of Lubrication*, The Institute of Petroleum, The Institution of Mechanical Engineers, and the British Society of Rheology, London, 1973, pp.81–88.

- [38] Zhou ZR, Zheng J. Tribology of dental materials: a review. *J Phys D Appl Phys.* 2008;41(11):113001
- [39] D. Upadhyay, M.A. Panchal, R.S. Dusbey, V.K. Srivastava, Corrosion of alloys used in dentistry: a review, *Mater. Sci. Eng. A432* (2006) 1–11
- [40] R. Van Noort, N. Gjerdet, A. Schedle, L. Bjökman, A. Berglund, An overview of the current status of national reporting systems for adverse reactions to dental materials, *J. Dent.* 32(2004) 351–358.
- [41] R.B. Waterhouse, *Fretting Fatigue*, Elsevier Applied Science, London, 1981
- [42] J.R. Kelly, *Ceramics in restorative and prosthetic dentistry*, *Annu. Rev. Mater. Sci.* 27(1997)443–468
- [43] L. Wang, Y. H. Liu, W. J. Si, H. L. Feng, Y. Q. Tao, Z. Z. Ma, Friction and wear behaviors of dental ceramics against natural tooth enamel, *J. Eur. Ceram. Soc.* 32 (2012) 2599–2606
- [44] G. Mitov, S. D. Heintze, S. Walz, K. Woll, F. Muecklich, P. Pospiech, Wear behavior of dental Y-TZP ceramic against natural enamel after different finishing procedures, *Dent. Mater.* 28 (2012) 909–918
- [45] V. Preis, M. Behr, G. Handel, S. Schneider-Feyrer, S. Hahnel, M. Rosentritt, Wear performance of dental ceramics after grinding and polishing treatments, *J. Mech. Behav. Biomed. Mater.* 10 (2012) 13–22.
- [46] M.J. Kim, S. H. Oh, J. H. Kim, S. W. Ju, D. G. Seo, S. H. Jun, J. S. Ahn, J. J. Ryu, Wear evaluation of the human enamel opposing different Y- TZP dental ceramics and other porcelains, *J. Dent.* 40 (2012) 979–988
- [47] P.V. DeAlmeida, A. Gregio, M. Machado, A. DeLima, L.R. Azevedo, Saliva composition and functions: a comprehensive review, *J. Contemp. Dent. Pract.* 9(2008)72–80
- [48] M. Shabaniyan, L.C. Richards, In vitro wear rates of materials under different loads and varying pH, *J. Prosthet. Dent.* 87(2002)650–656
- [49] I.C.H. Berg, M.W. Rutland, T. Arnebrant, Lubricating properties of the initial salivary pellicle – an AFM study, *Biofouling* 19(6)(2003) 365–369
- [50] L. Macakova, G.E. Yakubov, M.A. Plunkett, J.R. Stokes, Influence of ionic strength changes on the structure of pre-adsorbed salivary films. A response of a natural multi-component layer, *Colloids Surf. B: Biointerfaces* 77(2010)31–39
- [51] Y. Zhang, J. Zheng, L. Zheng, X. Shi, L. Qian, Z. Zhou, Effect of adsorption time on the lubricating properties of the salivary pellicle on human tooth enamel, *Wear* 301(2013)300–307
- [52] L. Macakova, G.E. Yakubov, M.A. Plunkett, J.R. Stokes, Influence of ionic strength on the tribological properties of pre-adsorbed salivary films, *Tribol. Int.* 44(2011)956–962.
- [53] I.E. Svendsen, L. Lindh, The composition of enamel salivary films is different from the ones formed on dental materials, *Biofouling* 25(2009) 255–261
- [54] M. Shabaniyan, L. C. Richards, In vitro wear rates of materials under different loads and varying pH, *J. Prosthet. Dent.* 87 (2002) 650–656
- [55] *Dental implant prosthetics: Carl E. Misch: 3rd edition*
- [56] Malvin ER. *Dentistry, An illustrated history.* Chapter 3: 32-33.
- [57] https://www.google.it/search?q=Endosteal+implant&source=lnms&tbm=isch&sa=X&ved=0ahUKewirua70xefiAhUCDuwKHaw9DSIQ_AUIECgB&cshid=1560466300616837&biw=1366&bih=625#imgrc=isDhCVc7MtoPKM

- [58] Buddy D. Ratner, Allan S. Hoffman, Frederick J. Schoen, Jack E. Lemons, *Biomaterials Science: An Introduction to Materials in Medicine*, 3rd edition, 2013, Elsevier Inc.
- [59] https://www.google.it/search?biw=1366&bih=625&tbm=isch&sa=1&ei=ftMCXZGyEo6kaaSgk_AO&q=Subperiosteal+implant+&oq=Subperiosteal+implant+&gs_l=img.3..0i30j0i8i30.2600291.2600291..2601499...0.0..0.76.76.1.....0....2j1..gws-wiz-img.3mxKmCdYPEQ
- [60] https://www.google.it/search?biw=1366&bih=625&tbm=isch&sa=1&ei=qN0CXZ7GM4LekgXHmonwCQ&q=Transosteal+implant+&oq=Transosteal+implant+&gs_l=img.3..0i1914j0i8i30i19.169029.169029..170696...0.0..0.108.108.0j1....0....2j1..gws-wiz-img.0I-ulTHSat4
- [61] https://www.google.it/search?biw=1366&bih=625&tbm=isch&sa=1&ei=Vd4CXfXSA8TUaFlq4yAAw&q=Epithelial+or+intramucosal+implant+&oq=Epithelial+or+intramucosal+implant+&gs_l=img.3...201923.201923..202796...0.0..0.98.98.1.....0....2j1..gws-wiz-img.J6rcvy66sFE
- [62] https://www.google.it/search?q=types+of+wear&source=lnms&tbm=isch&sa=X&ved=0ahUKEwj92-bq0-viAhWCY1AKHaEtBWcQ_AUIECgB&biw=1366&bih=625#imgrc=
- [63] https://www.google.it/search?biw=1366&bih=625&tbm=isch&sa=1&ei=6foEXbe5DIGXlwT-lor4Dw&q=human+tooth&oq=human+tooth&gs_l=img.3..0i19110.113778.116909..117887...0.0..0.115.1020.9j2.....0....1..gws-wiz-img.....0.WGo9UeRsnow
- [64] T. Albrektsson, P.-I. Brånemark, H.-A. Hansson & J. Lindström (1981) *Osseointegrated Titanium Implants: Requirements for Ensuring a Long-Lasting, Direct Bone-to-Implant Anchorage in Man*, *Acta Orthopaedica Scandinavica*, 52:2, 155-170, DOI: 10.3109/17453678108991776
- [65] Schnitman PA1, Wohrle PS, Rubenstein JE. Immediate fixed interim prostheses supported by two-stage threaded implants: methodology and results. *J Oral Implantol.* 1990;16(2):96-105
- [66] BRÅNEMARK, P. Osseointegrated implants in the treatment of the edentulous jaw. *Scand J Plast Reconstr Surg.* 1977;11. <http://ci.nii.ac.jp/naid/10005288551/en/>
- [67] Hunter, John. "Of Diseases, Supposed to Be Venereal, Produced by Transplanted Teeth." *The London medical journal* vol. 7, Pt 2 (1786): 205-216
- [68] "Implant biomaterials: A comprehensive review", Cases, C. (2015). *World Journal of Clinical Cases* © 2015, 3(1). <https://doi.org/10.12998/wjcc.v3.i1.52>
- [69] Crin, A. anN., Schnitman, P. A., Rabkin, M. , Dennison, T. and Onesto, E. J. (1975), Alumina and zirconia coated vitallium oral endosteal implants in beagles. *J. Biomed. Mater. Res.*, 9: 257-262.
- [70] Abi CBE. Toughening mechanisms in dental composites. Qin Q, Ye J, eds. *Toughening Mech Compos Mater.* 2015:321-337. doi:<https://doi.org/10.1016/B978-1-78242-279-2.00012-3>.
- [71] https://www.google.it/search?q=Schematics+of+the+transformation+toughening+mechanism+of+zirconia.&source=lnms&tbm=isch&sa=X&ved=0ahUKEwiFp7y9_6vjAhXDZ1AKHV_iAWcQ_AUIECgB&biw=1366&bih=625
- [72] https://www.google.it/search?biw=1366&bih=625&tbm=isch&sa=1&ei=m7YmXZ_BCJmDhbIP8rGNmAE&q=Schematics+of+low+thermal+degradation+mechanism+of+zirconia+&oq=Schematics+of+low+thermal+degradation+mechanis

- [m+of+zirconia+&gs_l=img.3...697872.697872..698834...0.0..0.125.125.0j1.....0...2j1..gws-wiz-img.Di2cgk7Qqxc](#)
- [73] Duraccio, D., Mussano, F., & Giulia, M. (2015). Biomaterials for dental implants : current and future trends. *Journal of Materials Science*, 50(14), 4779–4812. <https://doi.org/10.1007/s10853-015-9056-3>
- [74] Jokstad, A., Braegger, U., Brunski, J.B., Carr, A.B., Naert, I., Wennerberg, A., 2003. Quality of dental implants. *Int. Dent. J.* 53 (6 Suppl 2), S409–S443.
- [75] Jung, R.E., Zembic, A., Pjetursson, B.E., Zwahlen, M., Thoma, D.S., 2012. Systematic review of the survival rate and the incidence of biological, technical, and aesthetic complications of single crowns on implants reported in longitudinal studies with a mean follow-up of 5 years. *Clin. Oral Implant. Res.* 23 (Suppl 6), S2–S21.
- [76] Maló, P., de Araújo Nobre, M., Lopes, A., Ferro, A., Gravito, I., 2015. Single-tooth rehabilitations supported by dental implants used in an immediateprovisionalization protocol: report on long-term outcome with retrospective follow- Up. *Clin. Implant Dent. Relat. Res.* 17 (2), e511–e519.
- [77] Saadoun, A.P., Le Gall, M.G., Touati, B., 2004. Current trends in implantology: part II – treatment planning, aesthetic considerations, and tissue regeneration. *Pract. Proced. Aesthet. Dent.* 16 (10), 707–714.
- [78] Tischler, M., 2004. Dental implants in the esthetic zone. Considerations for form and function. *NY State Dent. J.* 70 (3), 22–26.
- [79] Linkevicius, T., Apse, P., 2008. Influence of abutment material on stability of periimplant tissues: a systematic review. *Int. J. Oral Maxillofac. Implant.* 23 (3), 449–456.
- [80] Bidra, A.S., Rungruanganunt, P., 2013. Clinical outcomes of implant abutments in the anterior region: a systematic review. *J. Esthet. Restor. Dent.* 25 (3), 159–176.
- [81] Bishti, S., Strub, J.R., Att, W., 2014. Effect of the implant-abutment interface on periimplant tissues: a systematic review. *Acta Odontol. Scand.* 72 (1), 13–25.
- [82] Sailer, I., Zembic, A., Jung, R.E., Hämmerle, C.H., Mattioli, A., 2007. Single-tooth implant reconstructions: esthetic factors influencing the decision between titanium and zirconia abutments in anterior regions. *Eur. J. Esthet. Dent.* 2 (3), 296–310.
- [83] Carrillo de Albornoz, A., Vignoletti, F., Ferrantino, L., Cardenas, E., De Sanctis, M., Sanz, M., 2014. A randomized trial on the aesthetic outcomes of implant-supported restorations with zirconia or titanium abutments. *J. Clin. Periodontol.* 41 (12), 1161–1169.
- [84] Foong, J. K. W., Judge, R. B., Palamara, J. E., & Michael, V. (n.d.). Fracture resistance of titanium and zirconia abutments : An in vitro study. *The Journal of Prosthetic Dentistry*, 109(5), 304–312. [https://doi.org/10.1016/S0022-3913\(13\)60306-6](https://doi.org/10.1016/S0022-3913(13)60306-6)
- [85] Sui, X., Wei, H., Wang, D., Han, Y., Deng, J., Wang, Y., ... Yang, J. (2014). ScienceDirect Experimental research on the relationship between fit accuracy and fracture resistance of zirconia abutments. *Journal of Dentistry*, 42(10), 1353–1359. <https://doi.org/10.1016/j.jdent.2014.02.008>
- [86] Brodbeck U. The ZiReal post: a new ceramic implant abutment. *J Esthet Restor Dent.* 2003;15(1):10–24.



- [87] Alsahhaf, A., Christopher, B., Vach, K., Kohal, R., & Cam, C. A. D. (2017). Journal of the Mechanical Behavior of Biomedical Materials Fracture resistance of zirconia-based implant abutments after artificial long-term aging, *66*(September 2016), 224–232. <https://doi.org/10.1016/j.jmbbm.2016.11.018>
- [88] Truninger TC, Stawarczyk B, Leutert CR, et al. Bending moments of zirconia and titanium abutments with internal and external implant-abutment connections after aging and chewing simulation. *Clin Oral Implant Res.* 2012;23(1):12–18.
- [89] Sailer I, Sailer T, Stawarczyk B, et al. In vitro study of the influence of the type of connection on the fracture load of zirconia abutments with internal and external implant-abutment connections. *Int J Oral Maxillofac Implants.* 2009;24(5):850–858.
- [90] Yilmaz B, Salaita LG, Seidt JD, et al. Load to failure of different zirconia abutments for an internal hexagon implant. *J Prosthet Dent.* 2015;114(3):373–377.
- [91] Zembic A, Philipp AO, Hammerle CH, et al. Eleven year follow-up of a prospective study of zirconia implant abutments supporting single all-ceramic crowns in anterior and premolar regions. *Clin Implant Dent Relat Res.* 2015;17(Suppl 2): e417–426.
- [92] Nothdurft FP, Nonhoff J, Pospiech PR. Pre-fabricated zirconium dioxide implant abutments for single tooth replacement in the posterior region: success and failure after 3 years of function. *Acta Odontol Scand.* 2014;72(5):392–400.
- [93] Gehrke P, Alius J, Fischer C, et al. Retentive strength of two-piece CAD/CAM zirconia implant abutments. *Clin Implant Dent Relat Res.* 2014;16(6):920–925.
- [94] Rosentritt M, Rembs A, Behr M, et al. In vitro performance of implant-supported monolithic zirconia crowns: Influence of patient-specific tooth-coloured abutments with titanium adhesive bases. *J Dent.* 2015;43(7):839–845.
- [95] Maeda Y, Satoh T, Sogo M. In vitro differences of stress concentrations for internal and external hex implant-abutment connections: a short communication. *J Oral Rehabil.* 2006;33(1):75–78.
- [96] Passos SP, Linke B, Larjava H, et al. Performance of zirconia abutments for implant-supported singletooth crowns in esthetic areas: a retrospective study up to 12-year follow-up. *Clin Oral Implant Res.* 2016;27(1):47–54.
- [97] Lazzara RJ, Porter SS, Platform Switching: a new concept in implant dentistry for controlling postrestorative crestal bone levels, *Int J Periodontics Restorative Dent* 2006 Feb; 26(1):9-17.
- [98] Gardner DM, Platform switching as a means to achieving implant esthetics: a case study, *NY State Dent J* 2005 Apr; 71(3):34-7.
- [99] Alqahtani F, Flinton R. Postfatigue fracture resistance of modified prefabricated zirconia implant abutments. *J Prosthet Dent.* 2014;112(2):299–305.
- [100] Hjerpe J, Lassila LV, Rakkolainen T, et al. Loadbearing capacity of custom-made versus prefabricated commercially available zirconia abutments. *Int J Oral Maxillofac Implants.* 2011;26(1):132–138.
- [101] Gibbs CH, Anusavice KJ, Young HM, et al. Maximum clenching force of patients with moderate loss of posterior tooth support: a pilot study. *J Prosthet Dent.* 2002;88(5):498–502.
- [102] Park JI, Lee Y, Lee JH, et al. Comparison of fracture resistance and fit accuracy of customized zirconia abutments with prefabricated zirconia abutments in internal hexagonal implants. *Clin Implant Dent Relat Res.* 2013;15(5):769–778.

- [103] Baixe S, Fauxpoint G, Arntz Y, et al. Microgap between zirconia abutments and titanium implants. *Int J Oral Maxillofac Implants*. 2010;25(3):455–460.
- [104] Alikhasi M, Monzavi A, Bassir SH, et al. A comparison of precision of fit, rotational freedom, and torque loss with copy-milled zirconia and prefabricated titanium abutments. *Int J Oral Maxillofac Implants*. 2013;28(4):996–1002.
- [105] Abdelhamed MI, Galley JD, Bailey MT, et al. A comparison of zirconia and titanium abutments for microleakage. *Clin Implant Dent Relat Res*. 2015;17 (Suppl. 2):e643–651.
- [106] Smith NA, Turkyilmaz I. Evaluation of the sealing capability of implants to titanium and zirconia abutments against *Porphyromonas gingivalis*, *Prevotella intermedia*, and *Fusobacterium nucleatum* under different screw torque values. *J Prosthet Dent*. 2014;112(3):561–567.
- [107] Sui X, Wei H, Wang D, et al. Experimental research on the relationship between fit accuracy and fracture resistance of zirconia abutments. *J Dent*. 2014;42 (10):1353–1359.
- [108] Carrillo de Albornoz A, Vignoletti F, Ferrantino L, et al. A randomized trial on the aesthetic outcomes of implant-supported restorations with zirconia or titanium abutments. *J Clin Periodontol*. 2014;41 (12):1161–1169.
- [109] Yang J, Wang K, Liu G, et al. Fracture resistance of inter-joined zirconia abutment of dental implant system with injection molding technique. *Clin Oral Implant Res*. 2013;24(11):1247–1250.
- [110] Pedersen, A. M. L., Sørensen, C. E., Proctor, G. B., & Carpenter, G. H. (2018). Salivary functions in mastication , taste and textural perception , swallowing and initial digestion, (April), 1399–1416. <https://doi.org/10.1111/odi.12867>
- [111] Guindy JS, Schiel H, Schmidli F, Wirz J (2004) Corrosion at the marginal gap of implant-supported suprastructures and implant failure. *Int J Oral Maxillofac Implants* 19:826–831
- [112] Mabileau G, Bourdon S, Joly-Guilou ML, Filmon R, Basle´ MF, Chappard (2006) Influence of fluoride, hydrogen peroxide and lactic acid on the corrosion resistance of commercially pure titanium. *Acta Biomater* 2:121–129
- [113] Souza JCM, Barbosa SL, Ariza E, Ponthiaux P, Henriques M, Teughels W, Celis J-P, Rocha LA (2015) How do titanium and Ti6Al4V corrode in fluoridated medium as found in the oral cavity? An in vitro study. *J Mater Sci Eng C* 47:384–393
- [114] Nakagawa M, Matsuya S, Shiraishi T, Ohta M (1999) Effect of fluoride concentration and pH on corrosion behavior of titanium for dental use. *J Dent Res* 78:1568–1572
- [115] Mabileau G, Bourdon S, Joly-Guilou ML, Filmon R, Basle´ MF, Chappard (2006) Influence of fluoride, hydrogen peroxide and lactic acid on the corrosion resistance of commercially pure titanium. *Acta Biomater* 2:121–129
- [116] Barril S, MischlerS Landolt D (2005) Electrochemical effects on the fretting corrosion behaviour of Ti6Al4 V in 0.9 % sodium chloride solution. *Wear* 259:282–291
- [117] Brogginini N, McManus LM, Hermann JS, Medina R, Schenk RK, Buser D, Cochran DL (2006) Peri-implant inflammation defined by the implant-abutment interface. *J Dent Res* 85:473–478



- [118] Broggin N, McManus LM, Hermann JS, Medina RU, Oates TW, Schenk RK, Buser D, Mellonig JT, Cochran DL (2003) Persistent acute inflammation at the implant-abutment interface. *J Dent Res* 82:232
- [119] Hallab NJ, Jacobs JJ, Skipor A, Black J, Mikecz K, Galante JO (2000) Systemic metal-protein binding associated with total joint replacement arthroplasty. *J Biomed Mater Res* 49:353–361
- [120] Goodman SB (2007) Wear particles, periprosthetic osteolysis and the immune system. *Biomaterials* 28:5044–5048
- [121] Ozakaki Y (2001) A New Ti–15Zr–4Nb–4Ta alloy for medical applications. *Curr Opin Sol St Mater Sci* 5:45–53
- [122] Manaranche C, Hornberger H (2007) A proposal for the classification of dental alloys according to their resistance to corrosion. *Dent Mater* 23:1428–1437
- [123] Garabrant DH, Fine LJ, Oliver C, Bernstein L, Peters JM (1987) Abnormalities of pulmonary function and pleural disease among titanium metal production workers. *Scand J Work Environ Health* 13:47–51
- [124] Wang JJ, Sanderson BJS, Wang H (2007) Cyto- and genotoxicity of ultrafine TiO₂ particles in cultured human lymphoblastoid cells. *Mutat Res* 628:99–106
- [125] «tecnologia farmaceutica: sospensioni». Available at: <http://dctf.uniroma1.it/galenotech/potzeta.htm>.
- [126] Večeřa, Jan & Čech, Jan & Mikulášek, Petr & Šulcová, Petra. (2013). The study of rutile pigments Ti_{1–3x} Cr_x M_{2x} O₂. *Central European Journal of Chemistry*. 11. 10.2478/s11532-013-0287-3.
- [127] «Surfaces, Interfaces, and Colloids: Principles and Applications, 2nd Edition», Wiley.com. Available at: <https://www.wiley.com/enus/Surfaces%2C+Interfaces%2C+and+Colloids%3A+Principles+and+Applications%2C+2nd+Edition-p-9780471330608>.
- [128] «Fenomeni elettrocinetici.pdf», Enciclopedia Treccani, vol. 5.
- [129] A. M. Gallardo-Moreno, V. Vadillo-Rodríguez, J. Perera-Núñez, J. M. Bruque, e M. L. González-Martín, «The zeta potential of extended dielectrics and conductors in terms of streaming potential and streaming current measurements», *Phys. Chem. Chem. Phys.*, vol. 14, n. 27, pag. 9758, 2012.
- [130] «The ZETA Guide :: Anton-Paar.com», Anton Paar. Available at: <https://www.anton-paar.com/it-it/the-zeta-guide/>.
- [131] https://www.google.it/search?biw=1366&bih=625&tbm=isch&sa=1&ei=ZVoyXe6-NYv6kwXqpKOoBQ&q=contact+angle&oq=contact+a&gs_l=img.1.0.0j0i3019.5777228.5780517..5782575...0.0..0.92.651.9.....0....1..gws-wiz-img.....0i67j0i10.vLflKVM-QjU#imgrc=-VfjWifbddJJBM:
- [132] D. M. Brunette, P. Tengvall, M. Textor, e P. Thomsen, Titanium in medicine: material science, surface science, engineering, biological responses and medical applications. Springer Science & Business Media, 2012.
- [133] «TOGWT: Surface Energy». [In linea]. Available at: <http://togwt1980.blogspot.it/2015/06/surface-energy.html>.